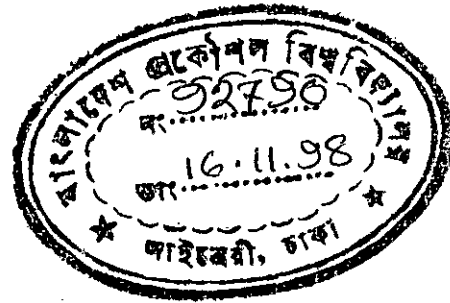
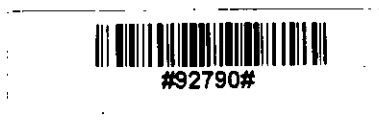


**THEORETICAL INVESTIGATION OF PERFORMANCE CHARACTERISTICS AND
DESIGN OF VAWT WITH PITCHING**

**BY
MAZHARUL ISLAM**



**A THESIS
SUBMITTED TO THE
DEPARTMENT OF MECHANICAL ENGINEERING
IN PARTIAL FULFILLMENT OF THE REQUIREMENTS
FOR THE DEGREE
OF
MASTER OF SCIENCE IN ENGINEERING (MECHANICAL)**

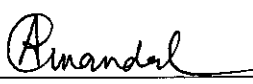
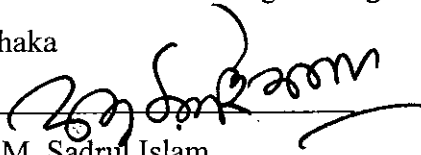
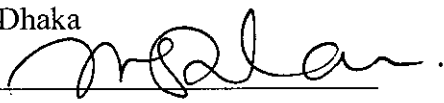
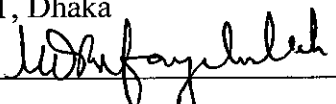


**DEPARTMENT OF MECHANICAL ENGINEERING
BANGLADESH UNIVERSITY OF ENGINEERING AND TECHNOLOGY
DHAKA, BANGLADESH**

OCTOBER, 1998

The thesis titled "Theoretical Investigation of Performance Characteristics and Design of VAWT With Pitching" submitted by Mazharul Islam, Roll No. 931052P, Registration No. 93778 of M. Sc. Engineering (Mechanical) has been accepted as satisfactory in partial fulfillment of the Master of Science in Engineering (Mechanical).

BOARD OF EXAMINERS

1. 
Dr. A. C. Mandal
Professor & Dean
Department of Mechanical Engineering
BUET, Dhaka
Chairman
(Supervisor)
2. 
Dr. A. K. M. Sadrul Islam
Professor & Head
Department of Mechanical Engineering
BUET, Dhaka
Member
(Ex-officio)
3. 
Dr. Md. Quamrul Islam
Professor
Department of Mechanical Engineering
BUET, Dhaka
Member
4. 
Dr. Md. Refayet Ullah
Professor & Head
Department of Naval Arch. & Marine Engineering
BUET, Dhaka
Member
(External)

Acknowledgement

I would like to thank my thesis supervisor Dr. Amalesh Chandra Mandal, Professor, Department of Mechanical Engineering, BUET for his consistent supervision, patient guidance and astute suggestions throughout the research work.

I am grateful to my wife and mother for supporting me in different ways.

I am also grateful to Bangladesh Power Development Board for granting me the permission of doing the M. Sc. Engineering (Mechanical) degree.

I browsed the Internet extensively for information regarding straight-bladed Darrieus wind turbine and I was benefited greatly. I wrote to different researchers in this field and most of them gave me a kind response. Especially Mr. Brian Kirke of Griffith University, Australia, who is working on VAWT for a long time, gave me useful suggestions and views for which I am grateful to him.

Abstract

Performance prediction and design of a straight-bladed vertical-axis Darrieus Wind Turbine is done with the cascade theory. In this prediction model the effect of dynamic stall and flow curvature is taken into consideration with blade pitching.

For dynamic stall consideration, Boeing-Vertol stall model with modification is taken into account. An empirical relation is used to determine the drag characteristics. In the prestall condition, the ECN stall model is followed to calculate the lift characteristics.

For the flow curvature effect the lift values are corrected only by a factor that is determined using the thin airfoil theory. However, the drag values are modified for the effect of chord-radius ratio, thus further correction of them due to the effect of flow curvature is not necessary. The finite aspect ratio effect is also incorporated in the prediction model.

Incorporation of blade pitching with dynamic stall and flow curvature effects in the performance prediction model is the prime objective of the thesis. Different important parameters, like normal and tangential forces, power coefficients, torque coefficients, drag coefficients etc. at different fixed pitch angles are obtained in this investigation and they are presented in graphical form.

Also design of a 1 KW straight-bladed vertical axis Darrieus wind turbine is done with mean wind velocity for the coastal regions of Bangladesh. The design wind speed is taken as 5 m/s and cutout wind speed as 15 m/s. The effect of dynamic stall and flow curvature is taken into consideration with fixed and variable blade pitching.

CONTENTS

ACKNOWLEDGEMENT	III
ABSTRACT	IV
CONTENTS	V
LIST OF SYMBOLS	VII
CHAPTER 1: INTRODUCTION	1
1.1 GLOBAL WIND ENERGY UTILIZATION SCENARIO	1
1.2 ADVANTAGES AND DISADVANTAGES OF VAWT	1
1.3 VAWT AROUND THE WORLD	2
1.4 AIM OF THE THESIS	4
1.5 SCOPE OF THE THESIS	5
CHAPTER 2: REVIEW OF EXISTING THEORIES	7
2.1 MOMENTUM MODEL	7
2.2 VORTEX MODEL	10
2.3 CASCADE MODEL	11
CHAPTER 3: CASCADE THEORY	12
3.1 BASIC ASSUMPTIONS	12
3.2 BLADE ELEMENT ANGLES AND VELOCITIES	12
3.3 AERODYNAMIC FORCES	14
3.4 VELOCITY CONTRIBUTED BY CIRCULATION	16
3.5 TOTAL PRESSURE LOSS TERM	18
3.6 VELOCITY RATIOS	19
3.7 ROTOR POWER COEFFICIENT	21
CHAPTER 4: DYNAMIC STALL	23
4.1 INTRODUCTION	23
4.2 DYNAMIC STALL MODEL	23

CHAPTER 5: FLOW CURVATURE	25
5.1 INTRODUCTION	25
5.2 FLOW CURVATURE MODEL	25
CHAPTER 6: BLADE PITCHING	28
6.1 INTRODUCTION	28
6.2 PITCHING MODEL	28
CHAPTER 7: RESULTS AND DISCUSSIONS	29
7.1 CALCULATED RESULTS	29
7.2 COMPARISON OF CALCULATED AND EXPERIMENTAL RESULTS	31
CHAPTER 8: DESIGN OF TURBINES	32
8.1 1 KW STRAIGHT-BLADED DARRIEUS TURBINE	33
8.2 COMPARISON BETWEEN OVERHANG AND SIMPLE SUPPORTED VAWT	34
CHAPTER 9: CONCLUSIONS AND RECOMMENDATIONS	35
9.1 CONCLUSIONS	35
9.2 RECOMMENDATIONS FOR FURTHER RESEARCHES	36
REFERENCES	37
FIGURES	43
APPENDICES	80
APPENDIX-A : FLOW DIAGRAM OF COMPUTATIONAL METHOD	81
APPENDIX-B : FLOW DIAGRAM OF DESIGN PROCEDURE	84
APPENDIX-C : ZERO-LIFT-DRAG COEFFICIENT	86
APPENDIX-D : FINITE ASPECT RATIO	89
APPENDIX-E : AIRFOIL CHARACTERISTIC	91
APPENDIX-F : DERIVATION OF MOMENT OF INERTIA OF BLADE AIRFOIL SECTION	92
APPENDIX-G : DERIVATION OF BENDING MOMENT AND BENDING STRESS	96

LIST OF SYMBOLS

A	projected frontal area of turbine
A_b	total blade sectional area
A_r	area of blade rib
A_s	area of blade skin
AR	aspect ratio = H / C
b	a factor
C	blade chord
C_1	distance along chord from leading edge point to blade fixing point
C_2	distance along chord from trailing edge point to blade fixing point
C_d	blade drag coefficient
C_{dd}	blade drag coefficient due to dynamic stall effect
C_{di}	induced drag coefficient
C_{do}	zero-lift-drag coefficient/section drag coefficient for infinite aspect ratio
C_{doc}	zero-lift-drag coefficient corrected for chord radius ratio
C_{dor}	reference zero-lift-drag coefficient
C_D	turbine overall drag coefficient = $F_D / \frac{1}{2} \rho A V_\infty^2$
C_{DD}	rotor drag coefficient = $F_D / \frac{1}{2} \rho A V_\infty^2$
C_l	blade lift coefficient
C_m	blade pitching moment coefficient
C_n	normal force coefficient
C_P	turbine overall power coefficient = $P_o / \frac{1}{2} \rho A V_\infty^3$
C_Q	turbine overall torque coefficient = $Q / \frac{1}{2} \rho A V_\infty^2 R$
C_t	tangential force coefficient
D	blade drag force
f	maximum camber of imaginary circular arc
F	force on blade airfoil
F_{cf}	centrifugal force
F_D	turbine overall drag force

F_f	a factor for lift correction due to flow curvature
F_n	normal force (in radial direction)
F_{net}	net normal force (in radial direction)
F_{nid}	force appearing in frictionless flow
F_{nv}	force due to pressure loss
F_n^+	non-dimensional normal force = $C_n(W/V_\infty)^2$
F_t	tangential force
F_{ta}	average tangential force
F_t	non-dimensional tangential force = $C_t(W/V_\infty)^2$
g	acceleration due to gravity
h_d	rotor height diameter ratio = H/D
H	height of turbine
I	area moment of inertia
\bar{I}	centroidal area moment of inertia
I_r	moment of inertia of blade rib
I_s	moment of inertia of blade skin
k_1	an empirical constant
k_c	a constant
k_i	exponent in the induced velocity relation
K	factor to include dynamic stall
L	blade lift force
L_{id}	lift force appearing in frictionless flow
L_v	lift force contributed by pressure loss
\dot{m}	mass flow rate
m_b	blade mass per unit length
M	blade pitching moment
M_{bn}	bending moment due to net normal force in Nm
M_{bt}	bending moment due to net tangential force in Nm
n	an exponent
N	number of blade
p	static pressure

P_f	a factor in prestall condition
P_o	overall power
P_∞	atmospheric pressure
Q	overall torque
Q_s	starting torque
rpm	turbine speed in revolutions per minute
R	turbine radius
Re	local Reynolds number = WC/ν
Re_r	reference Reynolds number corresponding to C_{dor}
Re_t	turbine speed Reynolds number = $R\omega C/\nu$
Re_w	wind speed Reynolds number = $V_\infty C/\nu$
S_a	allowable stress in N/mm^2
S_{bn}	bending stress due to net normal force in N/mm^2
S_{bt}	bending stress due to tangential force in N/mm^2
S_m	maximum value of blade stress in each revolution in N/mm^2
	sign of rate of change of angle of attack
t	blade spacing = $(2\pi R/N)$
t_c	maximum blade thickness as a fraction of chord
t_s	blade skin thickness
V	centre line velocity along freestream velocity direction
V_a	induced velocity
\vec{V}_c	chordal velocity component
V_{cut}	cutout speed
V_c	wake velocity in upstream side
V_n	normal velocity component
V_r	radial velocity component
V_w	wake velocity in downstream side
V_Γ	velocity contributed by circulation
V_∞	wind velocity
W	relative flow velocity

α	effective blade angle/angle of attack for finite wing
$\dot{\alpha}$	instantaneous rate of change of α
α_c	incidence correction angle due to flow curvature
α_i	induced angle of attack
α_m	modified angle of attack due to dynamic stall
α_o	angle of attack for infinite wing
α_s	stalling angle
β	$(\alpha_e - \alpha_i)$
γ	an empirical constant
γ_p	blade pitch angle
Γ	circulation per unit length
δ	correction factor for induced drag
Δp_{ov}	total pressure loss term (total cascade loss)
ε	$= D/L$
θ	azimuth angle
λ	tip speed ratio $= R\omega/V_\infty$
ν	kinematic viscosity
ρ	fluid density
σ	solidity $= NC/R$
τ	correction factor for induced angle
ω	angular velocity of turbine in rad/s

SUBSCRIPTS

d	downstream side / design point
e	trailing edge point
eq	equivalent condition due to flow curvature
i	leading edge point
u	upstream side
x	x-axis
y	y-axis
1	cascade inlet
2	cascade outlet

CHAPTER 1

INTRODUCTION

INTRODUCTION



In the present day civilization, energy has become synonymous with progress. Various types of energy, like oil, hydro, coal, natural gas, nuclear etc., are used as fuels for different activities all around the world. Among these conventional fuels, only hydro is renewable in nature and the other sources are major causes of air pollution and greenhouse effect. Replacing the conventional fuels with renewable ones may offer one solution to environmental problems in a reasonable amount. Renewable energy sources include wind energy, solar (photovoltaic) systems, solar thermal systems, biomass energy (wood and other plant fuels), geothermal energy, fuel cell, municipal waste etc. The costs of many of these technologies have come down considerably in recent years, particularly wind energy, which is now competitive with conventional power sources in regions with strong winds

Wind energy has become very lucrative now-a-day due to its reliability. According to a projection by American Wind Energy Association (AWEA) - wind turbine installation in the world through the end of 2006 will be 6,950 MW, in which Asia will have 5,970 MW; and Other 2,495 MW. By the end of the decade, it added, 38 countries should have at least 50 MW of wind capacity in place compared with just 10 MW today.

1.1 Global Wind Energy Utilization Scenario

In 1997, wind turbines installed all around the world generated about 13 trillion watt-hour of energy; the installed capacity was 7500 MW. The current growth rate of wind energy is 1,500 MW/year.

According to AWEA, Europe will continue to dominate worldwide installations over the next 10 years, erecting 14,310 MW of additional wind capacity, or nearly half of the 30,000 MW projected for the world. European countries--in particularly Germany, Denmark, Spain, and the United Kingdom- have very strong and consistent domestic market supports in place for atleast several years. While those supports are being reduced in many markets, the European wind industry now has enough momentum and investment that rapid growth is expected to continue into the indefinite future.

1.2 Advantages and Disadvantages of VAWT

The basic theoretical advantages of vertical axis wind turbines are-

- 1) they are omnidirectional i.e. they accept the wind from any direction
- 2) the generator, gearbox etc. can be placed on the ground.

The basic disadvantages are-

- 1) The machine may not be self-starting.
- 2) The machine may need guy wires to hold it up, but guy wires are impractical in heavily farmed areas.

1.3 VAWT Around The World

Most of the present VAWT of egg-beater type are operating in California, USA.

Among all types of vertical axis wind turbines, the egg-beater like Darrieus and S-rotor type or Savonius type systems, have proven to be more expensive. That is why different organizations of different countries are carrying out research work on straight-bladed Darrieus wind turbine on models, prototypes and computational methods. Some of the VAWT models and prototypes are described below:

3 KW Kirke-Lazauskas VAWT, Australia

This prototype, situated at Molendinar, Gold Coast, Queensland, Australia, is a research work of Brian Kirke of Griffith University, Australia. The airfoil of this straight-bladed Darrieus turbine is NACA 0018. The diameter of the turbine is 6m, the swept area is 18 m^2 and the chord is 0.4 m. This is passive variable pitch turbine i.e. pitch is determined by the interaction of inertial and aerodynamic forces, not by conventional cams. Mr. Kirke has plan to replace the existing NACA 0018 blades with fixed pitch S1210 blades and higher aspect ratio, possibly 0.3 m chord and 3 or 4 m long.

WS-4, Island in Archipelago of coast, Finland

A Finnish company, Oy Windside Production Ltd, has developed a new vertical-axis wind turbine. The Windside-turbine has two spiral vanes and is able to take advantage of very low winds. The wind direction is not important because some part of the spiral vanes always face the wind at right angles. No automatic yawing mechanisms are needed.

Windside-turbines can be used for battery charging, lighting, water pumping and electric systems in country cottages and boats and for measuring systems and control units.

In 1989 one Windside WS-4 turbine was installed on an island off the coast of Finland for the Finnish Defense Forces. In 1989-91 the Defense Forces made a continuous, 450-day test with WS-4. Measurements showed that Windside produces 50% more electricity a year than traditional wind turbines with the same swept area. The result was based on the ability to take advantage of wind speeds as low as 2 m/s.

The Windside WS-4 wind turbine produced energy every day during 200 continuous days. Measurements were made by computer with 8 different values being taken every second.

The turbine is storm-proof with no ice build-up while spinning in arctic conditions. It produces about 50% more electricity at low-speed winds than traditional horizontal-axis turbines with the same swept area.

Shrouded vertical axis wind turbine, Greece

The machine acts like an aerodynamic lens. Twin concentric flow achieved by a particular arrangement of guide vanes and rotor blades for maximum efficiency and power production, otherwise unattainable. Reduces noise and no moving parts are seen in open space, self regulating overspeed adjustment in severe weather conditions, compactness, the capability of being built in much bigger scale than the existing ones. This turbine is designed for power generation.

V-VAWT Wind Turbine, UK

The V-type vertical axis wind turbine (V-VAWT) is a novel wind turbine design devised by Dr Derek Taylor. This turbine resembles a helicopter rotor with its blades inclined 45 degrees in the form of a letter 'V'. It has a number of advantages over existing wind turbines.

The Engineering and Physical Sciences Research Council has funded an ongoing program of tests on the prototype V-turbine and also funded research into a second generation one-bladed derivative of the turbine (the Mono V-Turbine) which has been successfully completed.

The Mono V-Turbine includes a number of innovations to improve its operation. These include a one-bladed rotor and novel balance weight combination which means that the rotor is both statically and dynamically balanced even though it is able to teeter ('see-saw') freely to relieve the wind loads. Wind tunnel tests on an instrumented model have demonstrated that such a design is both practical and stable at both low and high rotational speeds.

As it has only one blade and a relatively short tower it is expected that the capital and installation costs should be competitive with conventional designs and that maintenance should be easier as all the electrical equipment would be at ground level. In addition the blade can be easily lowered to ground level for inspection or parking during calm spells. This feature considerably reduces its visibility. Dr Taylor is currently designing a full scale prototype and a bid to EPSRC for further research is in preparation.

FLOWIND EHD, USA

Flowind's 300 KW EHD (Extended Height/Diameter ratio) is a Darrieus (egg beater-shaped) vertical-axis wind turbine. Its three blades spin about an axis perpendicular to the ground, capturing energy from winds blowing from all directions. The drive train and generator are located under the rotor near the ground for easy maintenance and inspection.

The EHD series will use tall, high-performance 17 to 21 m rotors incorporating advanced airfoils designed specifically for the series. Flowind's prototype turbine rotor, which has a height to diameter ratio of 2.78, is taller and thinner than the 19-m rotor on Flowind's existing vertical-axis turbines. The shape allows the larger rotor to be placed upon existing turbine bases, if desired.

This design also makes it easier to bend the turbine blades into the desired shape and makes better (and more profitable) use of available sites in a wind power plant.

The EHD's low-cost blades are manufactured using a new, automated pultrusion technique, in which fiber-resin blades are pulled through a die. The blades incorporate natural laminar flow airfoils developed at Sandia National Laboratories to keep air flowing smoothly over the blades and increase energy capture. The rotor should effectively double the annual energy output of Flowind's current vertical-axis turbines that use aluminum blades and are about half as tall.

For 2000, the hypothesized VAWT will almost certainly retain one aspect of its current strength: simplicity. The key to future success with this configuration, however, will be cost-effective manufacturing techniques (primarily for blade production) that will produce significantly less expensive blades, based on cost per unit length. VAWT blades are not geometrically complex (e.g., no twist or taper), thus making manufacturing processes such as extrusion and pultrusion viable candidates to reduce costs. In addition, the inherent advantage of the VAWT configuration, having all drive train and generator parts at ground level, creates opportunities for using components with high weight or large physical size. Of recent interest in this regard is the direct- or linear-drive generator, which eliminates the need for a gearbox and provides the advantages of variable-speed operation at a very competitive price.

Apart from these turbines, research work on straight-bladed Darrieus turbine is going on different universities and organizations. Like in University of Naples, Italy by Domenico Coiro, in University of Calgary, Canada by Dr. Kentfield and in Melbourne University, Australia by Dr. Ken Brown. Mr. Domenico coiro is working on a prototype of straight-bladed VAWT. The diameter of the prototype is 1.5 m, the height is 0.8 m and the length of chord is 0.15 m. The airfoil is NACA 0018 and the test wind speed is between 10 to 15 m/sec.

1.4 Aim Of The Thesis

There are three theories such as momentum, vortex and cascade currently available for performance prediction of Vertical Axis Wind Turbines. Of them, the Cascade theory, proposed by Hirsch & Mandal in 1987, gives reasonable correlation with the experimental data available. The problem of convergence associated with the momentum and vortex theories can be eliminated mostly by using the cascade theory. In 1989, Muniruzzaman [Muniruzzaman and Mandal, 1993] included the effect of Dynamic Stall with Cascade theory that gives improved correlation. Finally in 1994, Mandal & Burton [Mandal & Burton, 1994] carried out further work with the effect of dynamic stall including flow curvature that gives better prediction.

The effect of blade pitching is quite important for self-starting and for better performance prediction of Straight Bladed Vertical Axis Darrieus Wind Turbine. From the previous work it has been observed that the consideration of dynamic stalling effect gives better correlation with the experimental data. But the effect of blade pitching was not considered with dynamic stalling which is also important for improved performance. The aim of the thesis is to consider the effect of Dynamic stalling and flow curvature with blade pitching by cascade theory for performance prediction of straight-bladed vertical-axis Darrieus wind turbine. In addition, design of a straight-

bladed Darrieus wind turbine was carried out with dynamic stalling and flow curvature effects including blade pitching.

1.5 Scope of the Thesis

In this thesis, a theoretical investigation of the aerodynamic performance and design of a vertical-axis Darrieus wind turbines is presented. Blade pitching with the dynamic stalling and flow curvature effects is added to the cascade theory introduced by Hirsch and Mandal (Hirsch and Mandal, 1987).

In Chapter 1, the general introduction about wind energy utilization with special emphasis on vertical axis wind turbines (VAWT) is given.

Chapter 2 presents short description of the various existing aerodynamic theories and their extension works so far introduced by different researchers of different countries. The advantages and disadvantages of the theories are also discussed briefly.

Chapter 3 describes the mathematical model of the existing cascade theory that is considered for the determination of the aerodynamic performance in this thesis work.

The cascade theory cannot predict the instantaneous aerodynamic forces properly unless the dynamic stall and flow curvature effects are added to it. In the chapter 4, the theory of dynamic stall that is added to the cascade model described in the chapter 3 is described. The existing Boeing-Vertol stall model (Gormont, 1973) with modification is added in this chapter.

The dynamic stalling effect is very important at the lower tip speed ratio since angle of attack in the low tip speed ratio is high. When the angle of attack remains constant or varies slowly with time, the turbine encounters the static stall. But when the angle of attack changes rapidly with time, the turbine experiences the dynamic stall. There are substantial differences between the characteristics of the static and dynamic stalls. The dynamic stall is a complex and unsteady flow phenomena. Aerodynamic forces due to the dynamic stall may be much higher than those due to the static stall. As a result, for the performance prediction of Darrieus turbines, especially for the local forces, there appear substantial differences between the experimental data and the calculated values unless the dynamic stalling effect is added.

To simplify the analysis and eliminate the deficiency associated with this method, some modifications are done with the Boeing-Vertol method: one for lift characteristics in the prestall condition and another for the drag characteristics.

Chapter 5 describes simplified flow curvature model added with the cascade model for better prediction. For the high chord-radius ratio Darrieus wind turbines, the flow on the blade aerofoil appears to be of curvilinear nature. The relative flow velocity direction varies continuously along the blade chord. A simple analytical method developed by Dr A.C Mandal (Mandal, 1994) is used to take into account of the curvilinear nature of flow. According to this method, the effect of curvilinear nature of flow is considered in the calculation by making a correction of the lift

coefficient. Correction of lift coefficient due to the effect of flow curvature is done after correcting it due to the dynamic stall effect.

Chapter 6 shows the blade pitching model used with the cascade theory. The angle of attack correction due to dynamic stalling effect is done after the blade pitching consideration.

Chapter 7 presents the calculated results and comparison of the turbine performance at different fixed pitch angles.

Chapter 8 presents a design method of 1 KW straight-bladed vertical-axis Darrieus wind turbine. Design at variable turbine speed condition is done.

Finally in the Chapter 9, general conclusions are given and few recommendations for the future works are presented.

CHAPTER 2

REVIEW OF EXISTING THEORY

REVIEW OF EXISTING THEORIES

For the performance prediction of Darrieus wind turbines, many computational models, based on different theories, have been given by researchers of different countries. These models can be broadly classified into three categories- (1) Momentum model, (2) Vortex model and (3) Cascade model.

Description of these models are given below-

2.1 Momentum Model

2.1.1 Single Streamtube Model

In 1974 Dr. Templin proposed the single streamtube model which is the first and most simple prediction method for the calculation of the performance characteristics of a Darrieus wind turbine. In this model the whole turbine is assumed to be enclosed within the single streamtube. The concept of windmill actuator disc theory was first incorporated into the analytical prediction model of a Darrieus wind turbine. In the actuator disc theory the induced velocity (rotor axial flow velocity) is assumed to be constant throughout the disc and is obtained by equating the streamwise drag with the change in axial momentum. In the assumption, the actuator disc is considered as the surface of the imaginary body of revolution. It is assumed that the flow velocity is constant throughout the upstream and downstream faces of the swept volume. This theory takes into account the curved blade shape and the effect of airfoil stalling on the performance characteristics. The blade shape is approximated by a parabola. The effects of geometric variables such as blade solidity and rotor height-diameter ratio have been included in the analysis. The effect of zero-lift-drag coefficient on the performance characteristics has also been included. Wind shear effect cannot be incorporated into the model.

This model can predict the overall performance of a lightly loaded wind turbine but according to the inquest, it always predicts higher power than the experimental results. It does not predicts the wind velocity variations across the rotor. These variations gradually increase with the increase of the blade solidity and tip speed ratio.

In 1980, Noll and Ham presented an analytical method for the performance prediction of a cyclically pitched straight bladed vertical-axis wind turbine using the single streamtube model. They added the effect of strut drag, turbulent wake state and dynamic stall to their analytical method.

2.1.2 Multiple Streamtube Model

Wilson and Lissaman, in 1974, introduced Multiple streamtube model which was an improvement to single streamtube model. In this model the swept volume of the turbine is divided into a series

of adjacent, aerodynamically independent parallel streamtubes. The blade element and momentum theories are then employed for each streamtube. In their model they considered the flow as inviscid and incompressible for the calculation of the induced velocity through the streamtube. As a result, there appears only the lift force in the calculation of the induced velocity. Wilson et al considered the theoretical lift for their calculation. The induced velocity varies over the frontal disc area both in the vertical and horizontal directions. Atmospheric wind shear can be included in the multiple streamtube model. Multiple streamtube model is still inadequate in its description of flow field. Wilson's model can be applied only for a fast running lightly loaded wind turbine.

In 1975, Strickland (Strickland, 1975) in his paper presented his multiple streamtube model for a vertical axis Darrieus wind turbine. In this model, induced velocity is found by equating the blade elemental forces (including airfoil drag) and the change in the momentum along each streamtube. The basic difference between Wilson's and Strickland's models is that Wilson used the theoretical lift force only in the calculation of induced velocity while Strickland added the effect of drag force as well for the similar calculation. Among these two model, Wilson's model gives fast convergence while Strickland's model gives slow convergence. There appears relatively higher convergence problem with Strickland's model. Wind shear effects have been included in the calculation of the model. This model predicts the overall performance of a Darrieus wind turbine reasonably, especially when the rotor is lightly loaded. It displays improvement over the single streamtube model.

In 1976, the streamtube models with both the uniform and non-uniform velocity distributions were presented by Shankar (Shankar, 1976). In his uniform velocity distribution model, the axial-flow velocity in the vertical and horizontal directions of the rotor frontal area and both in the upwind and downwind sides of the rotor is assumed to be constant. So, this model is similar to the single streamtube model (Templin, 1974). Shankar's non-uniform velocity distribution model is actually the multiple streamtube model where the axial-flow velocity varies both in the vertical and horizontal directions, but in each streamtube it remains constant throughout the upwind and downwind sides. Shankar worked out this model independently but this is identical to that given by Strickland (Strickland, 1975). In the calculation of Shankar, he applied the lift-drag characteristics independent of Reynolds number like that of Strickland.

In 1977, Sharpe (Sharpe, 1977) gave an elaborate description of the multiple streamtube model in a report. The principal idea of his model is similar to Strickland's model. Additionally, he incorporated the effect of Reynolds number into the calculation and he used analytical expressions for the Troposkien shape.

In 1980, an improved version of the multiple streamtube model was presented by Read and Sharpe (Read and Sharpe, 1980) for vertical-axis Darrieus wind turbines. In their model the parallel streamtube concept is dispensed with and the expansion of the streamtube is included. It is strictly applicable to low solidity lightly loaded wind turbines with large aspect ratio. It can predict the instantaneous aerodynamic blade forces and the induced velocities better than those by the conventional multiple streamtube model. But the prediction of overall power coefficients cannot be made with reasonable accuracy. It usually gives lower power than that obtained experimentally.

2.1.3 Double Multiple Streamtube Model

In 1981, Paraschivoiu (Paraschivoiu, 1981) introduced double multiple streamtube theory for the performance prediction of a Darrieus wind turbine. In this model the calculation is done separately for the upstream and downstream half cycles of the turbine. At each level of the rotor, the upstream and downstream induced velocities are obtained using the principle of two actuator discs in tandem. The concept of the two actuator discs in tandem for a Darrieus wind turbine was originally given by Lapin (Lapin, 1975). For both the upstream and downstream half cycles vertical variation of the induced velocity (like that in the multiple stream tube model) is considered while in the horizontal direction induced velocity is assumed to be constant (like that of a single streamtube model). According to his results, he observed better correlation between the calculated and experimental results, especially for the local aerodynamic blade forces than with the multiple streamtube model. This model gives over prediction of power for a high solidity turbine and there appears convergence problem for the same type of turbine especially in the downstream side and at the higher tip speed ratio.

The double multiple streamtube model with constant and variable interference factors (induced velocity ratios), including secondary effects for a Darrieus wind rotor was examined by Paraschivoiu, Delclaux, Fraunie and Beguier (Paraschivoiu et al, 1983). They found relatively significant influence of the secondary effects, namely, the blade geometry and profile type, the rotating tower and the presence of struts and aerodynamically spoilers, especially at high tip speed ratios. They considered the variation of the induced velocity as a function of azimuth angle that gives a more accurate calculation of the aerodynamic loads.

In the paper presented by Paraschivoiu and Delclaux (Paraschivoiu and Delclaux, 1983), they made improvements in the double multiple streamtube model. They considered the induced velocity variation as a function of the azimuth angle for each streamtube. They added a new formulation for an approximate Troposkien shape by considering the effect of gravitational field and a semi-empirical dynamic stall model.

In 1985, Paraschivoiu, Fraunie and Beguier (Paraschivoiu et al, 1985) introduced the expansion effects of the streamtubes through the rotor in their paper and these effects were included with double multiple streamtube model. With the measured and predicted data they observed that the streamtube expansion effects are relatively significant at high tip speed ratios.

A theory based on the multiple streamtube model including the effects of airfoil geometry, support struts, blade aspect ratio, turbine solidity, blade interference and curved flow was presented by Muraca, Stephens and Dagenhart (Muraca et al, 1975). The effect of flow curvature is evaluated by considering the flow over a flat plate. They derived an expression of lift distribution on the plate with the variable angle of attack from the leading to the trailing edge points of the flat plate and averaged the distributed lift force over the whole surface of the flat plate. According to them, the effect of flow curvature on the performance characteristics is insignificant for a low chord to radius ratio. They considered flow curvature effect for a straight-bladed wind turbine only.

In 1980, Migliore and Wolfe (Migliore and Wolfe, 1980) performed an elaborate study of the flow curvature effect on the performance characteristics of a straight-bladed Darrieus wind turbine. In

their method they considered the curved flow consisting of concentric streamlines pattern on the turbine blade airfoils (geometric airfoils). By conformal mapping techniques the geometric airfoil is transformed into a virtual airfoil with change in camber and incidence angle appearing in the rectilinear flow. They observed strong influence of the flow curvature on the performance characteristics of a Darrieus wind turbine especially when the chord-radius ratio is high. They found experimentally that the minimum value of the drag coefficient depends on the chord-radius ratio. They also noted that under most circumstances the flow curvature effect has a detrimental influence on the blade aerodynamic efficiency. However, when properly considered, the virtual aerodynamics may be used advantageously to enhance the turbine performance. In addition they described the effect of centrifugal forces on the flow pattern of the blade airfoils of the turbine.

In 1984, Cardona (Cardona, 1984) incorporated the effect of flow curvature following the method given by Migliore and Wolfe (Migliore and Wolfe, 1980) into the original aerodynamic vortex model presented by Strickland (Strickland et al, 1979). He also added a modified form of the dynamic stall effects. He found an improved correlation with the calculated and experimental results for the instantaneous aerodynamic blade forces and the overall power coefficients.

2.2 Vortex Model

In 1975, Larsen (Larsen, 1975) first introduced the idea of vortex model. He used his vortex model for the performance prediction of a cyclogiro windmill. His model is a two-dimensional one but if the vortex trailing from the rotor blade tips is considered it may not be said strictly two-dimensional. However, in his model angle of attack is assumed small, as a result, the stall effect is neglected.

Fanucci and Walters (Fanucci and Walters, 1976) presented a two-dimensional vortex model applicable to a straight bladed wind turbine. In their analysis they considered the angle of attack very small which eliminates the stall effect.

Holme (Holme, 1976) presented a vortex model for a fast running vertical-axis wind turbine having a large number of straight, very narrow blades and a high height-diameter ratio (in order to make a two dimensional flow assumption). The analysis is valid for a lightly loaded wind turbine only.

Wilson (Wilson, 1978) also introduced a two dimensional vortex analysis to predict the performance of a giromill. In his method he did not take the stall effect into account, because the angle of attack was assumed to be small.

A vortex model applicable to a curved-bladed Darrieus wind turbine was presented by Strickland, Webster and Nguyen (Strickland et al, 1979). It is simply the extensions of the previous vortex models. This vortex model is a three dimensional one and the aerodynamic stall is incorporated into the model. They presented the experimental results for a series of two dimensional rotor configurations. Their calculated values show more or less good correlation with the experimental results for the instantaneous blade forces and the near wake flow behind the rotor. The disadvantage of this model is that it takes too much computation time.

Strickland, Smith and Sun (Strickland et al, 1981) made improvements on the prior vortex model (quasi-steady vortex model) of Strickland et al. The latest model is termed as the dynamic vortex model, since, in this model the dynamic effects are included. The improvements over the prior model are that it includes the dynamic stall effect, pitching circulation and added mass effect. They repeated the experiment with the test model as is mentioned in the reference (Strickland et al, 1979) and found appreciable variations with the prior results. The correlation with their calculated values by the dynamic vortex model and the latest experimental results of the local blade forces and wake velocities are seemed to be reasonable in some cases.

2.3 Cascade Model

Hirsch and Mandal (Hirsch and Mandal, 1987) introduced the cascade model for the performance prediction of vertical-axis Darrieus wind turbines. This theory acts on the cascade principle, hence the name is the cascade theory. To make the theory applicable for the performance prediction, analytical expressions of wake and induced velocities are introduced.

In the cascade model, the blade airfoils of a turbine are assumed to be positioned in a plane surface (termed as the cascade) with the blade interspace equal to the turbine circumferential distance divided by the number of blades. The relationship between the wake velocity and the freestream velocity is established by using Bernoulli's equation while the induced velocity is related to the wake velocity through a particular assumed analytical expression.

The cascade model can predict the overall values of both low and high solidity turbines quite well. It takes reasonable computation time. It does not make any convergence problem even at the high tip speed ratio and high solidity. Though the calculated instantaneous blade forces by this model show improved correlation in comparison to that by the conventional momentum model, yet some shortcomings are always observed.

Based on all considerations, this theory is considered to be suitable for the analytical solution in this report. To eliminate the shortcomings of this model, two important effects of the dynamic stall and flow curvature with blade pitching are taken into account. The theory already incorporates the effect of the zero-lift-drag coefficient and finite aspect ratio in the calculation.

Since, the cascade model is applied for the calculation, the mathematical model of this theory is given in detail in the following chapter.

CHAPTER 3

CASCADE THEORY

CASCADE THEORY

3.1 Basic Assumptions

To apply the cascade theory for the determination of the performance prediction of a straight-bladed Darrieus wind turbine, the following assumptions are made in order to simplify the analysis:

- 1) The blades on the cylindrical surface are assumed to be developed into a plane surface and this configuration is known as the rectilinear cascade.
- 2) As the turbine blade rotates in a circular path, the flow velocity on the blade continuously varies; as a result, at any instant each of the turbine blades faces flow conditions different from those on the others. In the analysis, one of the blades is considered as the reference blade and at any instant power is calculated with the supposition that each of the blades sees the same flow and produces the same power as those of the reference blade. This process is continued at every station with the reference blade for one complete revolution of the turbine. Later the average power is obtained.
- 3) The wake velocity of the upstream side is supposed to act in the axial direction and behaves as the freestream velocity on the downstream blade that is positioned behind the upstream blade. The pressure in the wake region of the upstream side is assumed equal to the atmospheric pressure.
- 4) While finding the wake velocity, the flow is assumed to be steady, one-dimensional, incompressible and rotationally symmetric.

3.2 Blade Element Angles and Velocities

The flow velocities in the upstream and downstream sides of the Darrieus turbine are not constant which can be seen in Figure 3.1. From this Figure one can observe that the flow is considered to occur in the axial direction. The chordal velocity component V_{cu} and the normal velocity component V_{nu} are respectively obtained from the following expressions,

$$V_{cu} = R\omega + V_{au} \cos \theta \quad (3.1)$$

$$V_{nu} = V_{au} \sin \theta \quad (3.2)$$

Referring to Figure 3.2, the angle of attack α_u for the upstream side can be expressed as,

$$\alpha_u = \tan^{-1}\left(\frac{V_{nu}}{V_{cu}}\right) \quad (3.3)$$

Introducing the values of V_{nu} and V_{cu} and non-dimensionalizing,

$$\alpha_u = \tan^{-1}\left[\frac{\sin\theta}{\left(\frac{R\omega}{V_\infty} / \frac{V_{au}}{V_\infty}\right) + \cos\theta}\right] \quad (3.4)$$

The relative flow velocity W_u for the upstream side is obtained as (Figure 3.2),

$$W_u = \sqrt{V_{cu}^2 + V_{nu}^2} \quad (3.5)$$

Inserting the values of V_{cu} and V_{nu} in the equation (3.5), and non-dimensionalizing, one can find,

$$\frac{W_u}{V_\infty} = \frac{W_u}{V_{au}} \cdot \frac{V_{au}}{V_\infty} = \frac{V_{au}}{V_\infty} \sqrt{\left[\left(\frac{R\omega}{V_\infty} / \frac{V_{au}}{V_\infty}\right) + \cos\theta\right]^2 + \sin^2\theta} \quad (3.6)$$

Following the same procedure, similar expressions are obtained for the downstream side. Hence, to determine the angle of attack α_d and the relative flow velocity W_d for the downstream side, subscript u is replaced by d in the equation (3.4) and (3.6) respectively.

After determination of the local relative flow velocity and the angle of attack, the Darrieus turbine is developed into a cascade configuration that is shown in Figure 3.3. the cascade is considered in a plane normal to the turbine axis. If the blade represented by ① at an azimuth angle θ is considered as the reference blade, the flow conditions on the other two blades represented by ② and ③, are assumed to be equal to those of the reference blade. This process is continued for one complete revolution of the reference blade with a step of $\delta\theta$.

In the following analysis, the general mathematical expressions are derived for the upstream and downstream sides by omitting the subscripts u and d. These general expressions can be applied for both the upstream and downstream sides by subscripting the variable parameters (dependent of sides of turbine) with u for upstream and d for downstream.

Figure 3.4 show the velocity diagram on the reference blade of the cascade configuration for a straight-bladed Darrieus turbine. To perform the analysis a control surface is chosen as shown in this Figure. The control surface consists of two parallel lines to the cascade front and two identical streamlines having interspace t . This figure also shows velocities in reference to the blade in the cascade. Referring to Figure 3.4, the expressions of these velocities are obtained as,

$$\frac{W_y}{V_\infty} = \frac{W}{V_\infty} \cos\alpha \quad (3.7)$$

$$\frac{W_x}{V_\infty} = \frac{W}{V_\infty} \sin \alpha \quad (3.8)$$

$$\frac{W_1^2}{V_\infty^2} = \frac{W_x^2}{V_\infty^2} + \frac{(W_y - V_\Gamma)^2}{V_\infty^2} \quad (3.9)$$

$$\frac{W_2^2}{V_\infty^2} = \frac{W_x^2}{V_\infty^2} + \frac{(W_y + V_\Gamma)^2}{V_\infty^2} \quad (3.10)$$

$$\text{where, } V_\Gamma = \frac{\Gamma H}{2t} = \frac{N\Gamma H}{4\pi R} \quad (3.11)$$

W_x and W_y the components of the relative flow velocity W , in the x- and y- directions respectively where x is chosen along the perpendicular direction and y is chosen along the parallel direction of the cascade front (Figure 3.4). W_1 and W_2 are the relative flow velocities respectively at the cascade inlet and outlet. The blade airfoil upstream and downstream sides are termed as the cascade inlet and outlet respectively. V_Γ is the velocity contributed by circulation ΓH . $t=2\pi R/N$ is the blade spacing. The angles of attack at the cascade inlet α_1 and outlet α_2 are respectively expressed as,

$$\alpha_1 = \tan^{-1} \left[\frac{W_x / V_\infty}{(W_y - V_\Gamma) / V_\infty} \right] \quad (3.12)$$

$$\alpha_2 = \tan^{-1} \left[\frac{W_x / V_\infty}{(W_y + V_\Gamma) / V_\infty} \right] \quad (3.13)$$

3.3 Aerodynamic Forces

Along the bounding streamlines (Figure 3.4) the pressure forces are cancelled; viscous forces can be neglected outside of the boundary layers. There exists only the momentum flux through the straight lines parallel to the cascade front. So, the force in the tangential direction due to the rate of change of momentum is obtained as,

$$F_t = \dot{m}(W_2 \cos \alpha_2 - W_1 \cos \alpha_1) \quad (3.14)$$

Applying the continuity equation, the mass flow rate \dot{m} can be determined as,

$$\dot{m} = \rho H t W_1 \sin \alpha_1 = \rho H t W_2 \sin \alpha_2 = \rho H t W_x \quad (3.15)$$

From the equation (3.14) and (3.15), one can obtain the expression of F_t as,

$$F_t = \rho H t (W_2^2 \sin \alpha_2 \cos \alpha_2 - W_1^2 \sin \alpha_1 \cos \alpha_1) \quad (3.16)$$

The force in the normal direction to the cascade can be found as,

$$F_n = \dot{m} (W_1 \sin \alpha_1 - W_2 \sin \alpha_2) + H t (p_1 - p_2) \quad (3.17)$$

where p_1 and p_2 are respectively the pressures at the cascade inlet and outlet. Introducing the value of \dot{m} from the equation (3.15), the equation (3.17) can be written as,

$$F_n = \rho H t (W_1^2 \sin^2 \alpha_1 - W_2^2 \sin^2 \alpha_2) + H t (p_1 - p_2) \quad (3.18)$$

Considering the total cascade loss by a total pressure loss term ΔP_{ov} and using Bernoulli's equation between the cascade inlet and outlet, one finds,

$$\frac{p_1}{\rho g} + \frac{W_1^2}{2g} = \frac{p_2}{\rho g} + \frac{W_2^2}{2g} + \frac{\Delta P_{ov}}{\rho g} \quad (3.19)$$

Rearranging,

$$p_1 - p_2 = \frac{\rho}{2} (W_2^2 - W_1^2) + \Delta P_{ov} \quad (3.20)$$

Introducing $W_1 \sin \alpha_1 = W_2 \sin \alpha_2$ (Figure 3.4), one can obtain the expression of normal force from the equations (3.18) and (3.20) as,

$$F_n = \frac{\rho H t}{2} (W_2^2 - W_1^2) + H t \Delta P_{ov} \quad (3.21)$$

The expressions of the normal force coefficient C_n and the tangential force coefficient C_t are written as,

$$C_n = C_1 \cos \alpha + C_d \sin \alpha \quad (3.22)$$

$$C_t = C_1 \sin \alpha - C_d \cos \alpha \quad (3.23)$$

The non-dimensional tangential force coefficient F_t^+ and normal force coefficient F_n^+ can be defined as,

$$F_t^+ = \frac{F_t}{\frac{1}{2} \rho C H V_\infty^2} \quad (3.24)$$

$$F_n^+ = \frac{F_n}{\frac{1}{2}\rho CHV_\infty^2} \quad (3.25)$$

The tangential and normal forces can be defined as,

$$F_t = C_t \frac{1}{2}\rho CHW^2 \quad (3.26)$$

$$F_n = C_n \frac{1}{2}\rho CHW^2 \quad (3.27)$$

Now from the equations (3.24), (3.25), (3.26) and (3.27), one can obtain,

$$F_t^+ = C_t \frac{W^2}{V_\infty^2} \quad (3.28)$$

$$F_n^+ = C_n \frac{W^2}{V_\infty^2} \quad (3.29)$$

3.4 Velocity Contributed by Circulation

The circulation about the blade profile is defined by,

$$\Gamma = \oint_s \vec{W} d\vec{s} \quad (3.30)$$

Its contribution along the streamlines is cancelled by virtue of the opposing directions of s , while the contribution along the parallel direction of the cascade front is retained. As a result, the circulation becomes,

$$\Gamma = t(W_2 \cos \alpha_2 - W_1 \cos \alpha_1) \quad (3.31)$$

From the equations (3.14), (3.15) and (3.31), one can obtain,

$$F_t = \rho HW_x \Gamma \quad (3.32)$$

Referring to the Figure 3.5, the lift force can be written as,

$$L = L_{id} + L_v \quad (3.33)$$

Where, L_{id} and L_v are respectively the lift force appearing in the frictionless flow and the lift force due to pressure loss. According to Figure 3.5, L_{id} and L_v can be expressed as,

$$L_{id} = \frac{F_t}{\sin \alpha} \quad (3.34)$$

$$L_v = D \cot \alpha \quad (3.35)$$

where, D is the drag force on the blade airfoil.

From the equations (3.33), (3.34) and (3.35), one can find,

$$L = \frac{F_t}{\sin \alpha + D \cot \alpha} \quad (3.36)$$

Dividing both sides of the equation (3.36) by L, introducing $\varepsilon = D/L$ and arranging,

$$\frac{F_t}{L \sin \alpha} = (1 - \varepsilon \cot \alpha) \quad (3.37)$$

Rearranging,

$$L = \frac{F_t}{\sin \alpha} \frac{1}{(1 - \varepsilon \cot \alpha)} \quad (3.38)$$

Introducing the value of F_t from the equation (3.32), the lift force L becomes,

$$L = \frac{\rho H W_x}{\sin \alpha} \frac{\Gamma}{(1 - \varepsilon \cot \alpha)} \quad (3.39)$$

Since $W_x = W \sin \alpha$ according to the Figure 3.4, so, the lift force can be expressed as ,

$$L = \rho H W \frac{\Gamma}{(1 - \varepsilon \cot \alpha)} \quad (3.40)$$

The lift force L is defined as,

$$L = \frac{1}{2} C_l \rho W^2 C H \quad (3.41)$$

From the above two equations (3.40) and (3.41), the expression of the circulation is obtained as,

$$\Gamma = \frac{1}{2} C_l C W (1 - \varepsilon \cot \alpha) \quad (3.42)$$

One obtain the expression of $V \Gamma$ from the equations (3.11) and (3.42) as,

$$V_r = \frac{1}{8\pi} C_l \frac{NC}{R} W(1 - \varepsilon \cot \alpha) H \quad (3.43)$$

Non-dimensionalizing,

$$\frac{V_r}{V_\infty} = \frac{1}{8\pi} C_l \frac{NC}{R} \frac{W}{V_\infty} (1 - \varepsilon \cot \alpha) H \quad (3.44)$$

3.5 Total Pressure Loss Term

From Figure 3.5, the normal force can be expressed as,

$$F_n = F_{nid} + F_{nv} \quad (3.45)$$

Where F_{nid} is the force appearing in the frictionless flow and F_{nv} is the force due to pressure loss. Referring to the Figure 3.5, F_{nv} can be expressed as,

$$F_{nv} = \frac{D}{\sin \alpha} \quad (3.46)$$

The force F_{nv} can also be expressed as,

$$F_{nv} = tH\Delta P_{ov} \quad (3.47)$$

From the equations (3.46) and (3.47), one obtains,

$$\Delta P_{ov} = \frac{D}{tH \sin \alpha} \quad (3.48)$$

The drag force D is defined as,

$$D = \frac{1}{2} C_d \rho W^2 CH \quad (3.49)$$

As a result, one can find the pressure loss term from the equations (3.48) and (3.49) as,

$$\Delta P_{ov} = \frac{\rho}{2} \frac{C_d}{\sin \alpha} \frac{C}{t} W^2 \quad (3.50)$$

$$\text{where, } \frac{C}{t} = \frac{NC}{2\pi R} = \frac{1}{2\pi} \frac{NC}{R} \quad (3.51)$$

Now from the above two equations, one obtains,

$$\Delta P_{ov} = \frac{\rho}{2} \frac{C_d}{\sin \alpha} \frac{1}{2\pi} \frac{NC}{R} W^3 \quad (3.52)$$

In the non-dimensionalized form,

$$\frac{\Delta P_{ov}}{\rho V_\infty^2} = \frac{1}{4\pi} \frac{C_d}{\sin \alpha} \frac{1}{2\pi} \frac{NC}{R} \frac{W^2}{V_\infty^2} \quad (3.53)$$

3.6 Velocity Ratios

Applying Bernoulli's equation with absolute velocity in front and behind the cascade, one obtains for the upstream side,

$$\frac{V_\infty^2}{2g} + \frac{p_\infty}{\rho g} = \frac{V_{au}^2}{2g} + \frac{p_{1u}}{\rho g} \quad (3.54)$$

$$\frac{V_e^2}{2g} + \frac{p_\infty}{\rho g} = \frac{V_{au}^2}{2g} + \frac{p_{2u}}{\rho g} \quad (3.55)$$

where V_{au} and V_e are respectively the induced velocity and the wake velocity for the upstream side. p_{1u} and p_{2u} are the static pressures respectively at the cascade inlet and outlet for the upstream side. In the wake region of the upstream side with the velocity V_e , the pressure is assumed equal to the atmospheric pressure (Figure 3.1). Subtracting the above two equations (3.54) and (3.55), one finds,

$$\frac{V_\infty^2}{2g} - \frac{V_e^2}{2g} = \frac{p_{1u}}{\rho g} - \frac{p_{2u}}{\rho g} \quad (3.56)$$

After rearranging,

$$(p_{1u} - p_{2u}) = \frac{\rho}{2} (V_\infty^2 - V_e^2) \quad (3.57)$$

Now subscripting the variable parameters in the equation (3.20) by u for the upstream side and balancing with the equation (3.57), one obtains,

$$\frac{\rho}{2} (V_\infty^2 - V_e^2) = \frac{\rho}{2} (W_{2u}^2 - W_{1u}^2) + \Delta P_{ov_u} \quad (3.58)$$

Again subscripting the variable parameters in the equation (3.52) by u for the upstream side, introducing in the equation (3.58) and dividing throughout by $\rho/2$, one can find,

$$V_{\infty}^2 - V_e^2 = (W_{2u}^2 - W_{1u}^2) + \frac{1}{2\pi} \frac{NC}{R} \frac{C_{d_u}}{\sin \alpha_u} W_u^2 \quad (3.59)$$

From the equation (3.59), the expression of the wake velocity in the non-dimensionalized form for the upstream side can be written as,

$$\frac{V_e}{V_{\infty}} = \sqrt{1 - (W_{2u}^2 - W_{1u}^2) - \frac{1}{2\pi} \frac{NC}{R} \frac{C_{d_u}}{\sin \alpha_u} \frac{W_u^2}{V_{\infty}^2}} \quad (3.60)$$

Similarly, the expression of the wake velocity in the non-dimensionalized form for the downstream side can be found as,

$$\frac{V_w}{V_e} = \sqrt{1 - \left(\frac{W_{2d}^2}{V_e^2} - \frac{W_{1d}^2}{V_e^2} \right) - \frac{1}{2\pi} \frac{NC}{R} \frac{C_{d_d}}{\sin \alpha_d} \frac{W_d^2}{V_e^2}} \quad (3.61)$$

The wake velocity ratio for the downstream side can be related as,

$$\frac{V_w}{V_{\infty}} = \frac{V_w}{V_e} \frac{V_e}{V_{\infty}} \quad (3.62)$$

In the cascade model to find the induced velocity a relationship between the wake velocity and the induced velocity is introduced. For the upstream side this is expressed as,

$$\frac{V_{au}}{V_{\infty}} = \left(\frac{V_e}{V_{\infty}} \right)^{k_i} \quad (3.63)$$

and for the downstreamside, this is expressed as,

$$\frac{V_{ad}}{V_e} = \left(\frac{V_w}{V_e} \right)^{k_i} \quad (3.64)$$

The value of the exponent k_i is found from a fit of experimental results. The induced velocity ratio for the downstream side can be written in the form,

$$\frac{V_{ad}}{V_{\infty}} = \frac{V_{ad}}{V_e} \frac{V_e}{V_{\infty}} = \frac{V_e}{V_{\infty}} \left(\frac{V_w}{V_e} \right)^{k_i} \quad (3.65)$$

The expression of the exponent k_i is written in accordance with reference (Hirsch and Mandal, 1987) as,

$$k_i = (.425 + .332\sigma) \quad (3.66)$$

$$\text{Where, } \sigma = \frac{NC}{R}$$

3.7 Rotor Power Coefficient

General expressions are given in this section for the upstream and downstream sides thereby omitting the subscripts u and d. The same expressions can be used for the upstream and downstream sides by subscripting the variable parameters with u (upstream) and d (downstream).

The equations (3.16) and (3.21) are expressed in the following forms inserting $t=2\pi R/N$.

$$F_t(\theta) = \frac{2\pi}{N} \rho R^2 \frac{H}{R} (W_2^2 \sin \alpha_2 \cos \alpha_2 - W_1^2 \sin \alpha_1 \cos \alpha_1) \quad (3.67)$$

$$F_n(\theta) = \frac{\pi}{N} \rho R^2 \frac{H}{R} (W_2^2 - W_1^2) + \frac{2\pi}{N} R^2 \frac{H}{R} \Delta P_{ov} \quad (3.68)$$

Since, the tangential and normal forces represented by the equations (3.67) and (3.68) are for any azimuthal position, so, they are considered as the function of azimuth angle θ . Average tangential force on one blade can be expressed as,

$$F_{ta} = \frac{1}{2\pi} \int_0^{2\pi} F_t(\theta) d\theta \quad (3.69)$$

The torque for the number of blades N is obtained as,

$$Q = NF_{ta}R \quad (3.70)$$

From the equations (3.67), (3.69) and (3.70), one can find,

$$Q = \rho R^3 \frac{H}{R} \int_0^{2\pi} (W_2^2 \sin \alpha_2 \cos \alpha_2 - W_1^2 \sin \alpha_1 \cos \alpha_1) d\theta \quad (3.71)$$

The turbine torque coefficient is defined by,

$$C_Q = \frac{Q}{\frac{1}{2}AV_\infty^2 R} \quad (3.72)$$

Inserting $A=2RH$, from the above two equations (3.71) and (3.72), the expression of torque coefficient becomes,

$$C_Q = \int_0^{2\pi} \left(\frac{W_2^2}{V_\infty^2} \sin \alpha_2 \cos \alpha_2 - \frac{W_1^2}{V_\infty^2} \sin \alpha_1 \cos \alpha_1 \right) d\theta \quad (3.73)$$

The turbine overall power coefficient is obtained from the expression,

$$C_p = C_Q \cdot \lambda \quad (3.74)$$

where, $\lambda = \frac{R\omega}{V_\infty}$ is the tip speed ratio

In order to determine the turbine overall torque coefficient, numerical integration is performed by the help of Simpson's rule.

CHAPTER 4

DYNAMIC STALL

DYNAMIC STALL

4.1 Introduction

Several experimental works have been done in the field of dynamic stall, but most of them are in relation to the helicopter rotor aerofoils (Ericsson and Reding, 1978), (Mc Crosky and Pucci, 1982). The retreating side of this rotor aerofoils encounters higher angle of attack, but in the advancing side, nominal angles are seen. The experimental values shows that loads on the aerofoil oscillating harmonically differ from those of non-pitching at the same angle of attack.

In the case of Darrieus turbines, as the turbine blades rotate, the local angle of attack changes continuously with time. At the lower tip speed ratio the angle of attack exceeds the stalling angle in most of the stations, thus the dynamic stalling effect is needed to be considered in the analysis (Ham, 1968). To include the effect of dynamic stall in the analysis, Boeing-Vertol stall model (Gormont, 1973) is applied with a view to determining the lift characteristics.

4.2 Dynamic Stall Model

In the model of Boeing-Vertol, the blade angle is modified. The modified angle of attack α_m is determined from the following relation,

$$\alpha_m = \alpha - \gamma \cdot k_1 \left(\sqrt{\frac{C \dot{\alpha}}{2W}} \right) S_{\dot{\alpha}} \quad (4.1)$$

Where α is the effective blade angle of attack, γ and k_1 are the empirical constants, $\dot{\alpha}$ denotes the instantaneous rate of change of α , $S_{\dot{\alpha}}$ is the sign of $\dot{\alpha}$ and W is the relative flow velocity.

This modified angle of attack is used to calculate the lift coefficient due to the dynamic stalling effect (C_{ld}) in the following manner,

$$C_{ld} = \left(\frac{\alpha}{\alpha_m} \right) C_l(\alpha_m) \quad (4.2)$$

Where $C_l(\alpha_m)$ is the lift value chosen corresponding to the modified angle of attack α_m and the value is taken from the two-dimensional lift characteristics with static stall conditions (Jacob and Sherman, 1937), (Sheldahl and Blackwell, 1976), (Willmer, 1979).

For low Mach numbers and for aerofoil thickness to chord ratios greater than 0.1, the value of γ is,

$$\gamma = 1.4 - 6(0.06 - t_c) \quad (4.3)$$

Where t_c is the maximum aerofoil thickness ratio. The k_1 value changes with the sign of the effective angle of attack and this is obtained from the relation,

$$k_1 = 0.75 + 0.25xS_\alpha \quad (4.4)$$

This formulation is applied (Gormont, 1900) when the angle of attack α is greater than the static stall angle or when the angle of attack is decreasing after having been above the stall angle. The Boeing-Vertol stall is turned off when the angle of attack is below the stall angle and increasing. In the present analysis in the prestall condition, the dynamic stalling effect is also encountered from $\alpha=5$ degree up to the stall angle in the similar manner as that of ECN (Bulteel, 1987-88). The dynamic lift C_{ld} is calculated by using the Boeing-Vertol model and according to ECN, the lift coefficient in the prestall condition is obtained from the relation,

$$C_{lp} = P_f C_{ld}(\alpha_m) + (1 - P_f) C_l(\alpha) \quad (4.5)$$

Where the factor P_f is determined from the following linear equation,

$$P_f = \frac{\alpha - 5}{\alpha_s - 5} \quad (4.6)$$

where α_s is the stalling angle. This equation vividly shows that at $\alpha=5$ degree, $P_f = 0$ and at $\alpha = \alpha_s$, $P_f = 1.0$, which means that at $\alpha=5$ degree, the contribution of C_{ld} is zero while that at $\alpha = \alpha_s$ it is full.

In the analysis to consider the effect of drag characteristics due to the dynamic stall, an empirical relation (Muniruzzaman and Mandal, 1993) is used which is written in the form,

$$C_{dd} = \frac{C_{ld}}{C_l(\alpha)} C_d(\alpha) K \quad (4.7)$$

where K is a factor. K is chosen as 1.0 in the expression. The equation (4.7) signifies that, the dynamic drag characteristic is proportional to the dynamic lift characteristic. Due to lack of experimental drag values, the calculated dynamic drag characteristics cannot be verified at the moment. However, the nature of this equation more or less follows that presented by Mc Crosky (Mc Crosky et al, 1982) and opposes the nature which is given by Mehta, (Mehta, 1977). Mc Crosky considered the viscous flow while Mehta considered the ideal flow in their analyses.

CHAPTER 5

FLOW CURVATURE

FLOW CURVATURE

5.1 Introduction

When the wind turbine blades, made up of airfoil, rotates in a circular path, the direction of rotational velocity ($r\omega$) varies continuously along the chord making the flow over the blade airfoil like that of curvilinear nature. This fact can be observed from Figure 5.1 for a high chord-radius ratio Darrieus turbine, there is continuous variation of the direction of the instantaneous relative flow velocity along the chord of the turbine blade indicating the curvilinear nature. As a result, the angle of incidence is not constant along the chord-wise direction. This phenomenon is called flow curvature effect that has significant influence on the lift-drag characteristics of the blade airfoil of Darrieus turbines. So, it affects the aerodynamic performance of Darrieus wind turbines appreciably. With the help of a simplified method this phenomenon is taken into consideration and its mathematical model is described in detail in the following section.

5.2 Flow Curvature Model

In the present analysis, to take into account of the flow curvature effect, the aerofoil is assumed to be of cambered nature and the lift is corrected but the relative flow velocity is preserved. In order to take its effect the thin aerofoil theory is applied on an equivalent cambered aerofoil having a mean camber line like that of the shape of a circular arc as shown in Figure 5.2. The equivalent cambered aerofoil is found from the difference of the relative incidence angles between the leading and trailing edge points.

$$\text{Let, } \beta = (\alpha_o - \alpha_i) \quad (5.1)$$

Where α_i and α_o are respectively the incidence angles in reference to the blade leading and trailing edge points.

From Figure 5.2, one can obtain,

$$R_1 = \frac{C/2}{\sin(\beta/2)} \quad (5.2)$$

$$h_1 = \frac{C/2}{\tan(\beta/2)} \quad (5.3)$$

Where R_1 is the radius of the circular arc and h_1 is the maximum distance between the chord and the centre of the circular arc. The maximum camber of the circular arc f is found as,

$$f = R_1 - h_1 \quad (5.4)$$

From the equations (5.2), (5.3) and (5.4), one can find the following expression,

$$\frac{2f}{C} = \frac{1 - \cos(\beta/2)}{\sin(\beta/2)} \quad (5.5)$$

The incidence correction angle is,

$$\alpha_c = \tan^{-1}\left(\frac{2f}{C}\right) \quad (5.6)$$

Introducing the value of $(2f/C)$ from the equation (5.5), one can find,

$$\alpha_c = \tan^{-1}\left[\frac{1 - \cos(\beta/2)}{\sin(\beta/2)}\right] \quad (5.7)$$

According to the thin aerofoil theory, the lift characteristic of such a circular arc aerofoil can be obtained from the equation,

$$C_{lc} = 2\pi \sin(\alpha + \alpha_c) = 2\pi(\alpha + \alpha_c) \quad (5.8)$$

The lift characteristic of a thin aerofoil with zero camber is determined from,

$$C_l = 2\pi \sin \alpha \approx 2\pi\alpha \quad (5.9)$$

It is obvious from the above two equations that due to the effect of the flow curvature, the lift need to be corrected by a factor that is obtained from,

$$F_f = \frac{C_{lc}}{C_l} = \frac{(\alpha + \alpha_c)}{\alpha} \quad (5.10)$$

In the present analysis, the static lift is first corrected for the dynamic stalling effect, later this dynamic lift is corrected due to the flow curvature effect with the multiplying factor F_f . For the upstream side of the turbine, $F_f > 1.0$ and for the downstream side $F_f < 1.0$, since α_c is positive for the upstream side and negative for the downstream side.

The lift coefficient is corrected in order to take into account the effect of flow curvature while drag coefficient is unaltered. However, the drag coefficient is modified due to the effect of chord-radius ratio that is responsible for the flow curvature. Thus, further correction of the drag coefficient due to the flow curvature effect is not necessary.

The flow curvature method developed by Migliore (Migliore et al, 1980) gives deteriorating power coefficients. As the solidity increases there appear appreciable difference between the

experimental and calculated results (Hirsch and Mandal, 1984). On the other hand, using the model of Hirsch and Mandal (Hirsch and Mandal, 1984) with the cascade theory, higher power coefficients than the experimental results are predicted especially for high solidity turbines. So, some modifications in the model of Hirsch and Mandal are done with a view to finding suitable result. It is noted that adding Muraca's model (Muraca et al, 1975) with the cascade theory, no significant improvement is found.

CHAPTER 6

BLADE PITCHING

BLADE PITCHING

6.1 Introduction

Blade pitching mostly used to reduce the turbine overspeed thereby preventing structural failure of the turbine at high wind speeds. The pitching mechanism may be of various types: fixed pitching, sinusoidal pitching, combination of fixed and sinusoidal pitching etc. Pitching controls the performance of a turbine significantly.

6.2 Pitching Model

Figure 6.1 shows the velocities and the forces acting on the blade airfoil with pitching.

In this analysis pitching is considered to be positive for the blade airfoil nose rotating in the outward direction from the blade flight path as a result for the upstream side the angle of attack becomes,

$$\alpha_u = \alpha_{ou} - \gamma_{pu} \quad (6.1)$$

and for the downstream side the angle of attack becomes,

$$\alpha_d = \alpha_{od} + \gamma_{pd} \quad (6.2)$$

where γ_{pu} and γ_{pd} are the pitch angles in the upstream and downstream sides respectively. Now the lift and drag characteristics are taken corresponding to the α_u (upstream) and α_d (downstream). The parameters shown in the Figure 6.1 have not been subscripted to make them generalized. Subscript u and d are used with the parameters for the upstream and downstream sides respectively.

CHAPTER 7

RESULTS AND DISCUSSIONS

RESULTS AND DISCUSSIONS

In this chapter the calculated results are presented in graphical form. The effects of different parameters like blade pitching, dynamic stall, flow-curvature etc. on the performance characteristics of straight-bladed vertical-axis wind turbines are discussed.

In the present analysis aerofoil blade sections of NACA 0015 and NACA 0012 are considered. Two-dimensional aerodynamic lift-drag characteristics used in the analysis are shown in graphical form in Appendix-E.

In the present analysis pitching is said to be positive for the blade nose rotating in outward direction from the blade flight path. The effects of dynamic stall and flow-curvature are incorporated in the analysis.

7.1 Calculated Results

Performance characteristics of straight-bladed Darrieus wind turbines with fixed blade pitching have been presented in the figures. These figures present results employing pitching with the West Virginia University outdoor test model (Migliore et al, 1980).

7.1.1 Variation of Overall Power, Torque and Drag Coefficients

In the Figures 7.1, 7.2 and 7.3, the variation of overall power coefficient (C_P), overall torque coefficient (C_Q) and overall drag coefficient (C_d) with different tip speed ratios are shown.

From the Figure 7.1, it is observed that with the application of fixed blade pitching, the overall power coefficient initially increases slightly then decreases at subsequent increase in fixed pitching angle in general. It is also observed from this figure that with employing the dynamic stall and flow curvature effects, the prediction model developed in this thesis predicts higher overall power coefficients at different pitch angles.

From the Figure 7.2, it is seen that the overall torque coefficient (like the overall power coefficient) initially increases and then decreases at higher pitch angles. It is also observed from this figure that with employing the dynamic stall and flow curvature effects, the prediction model predicts higher overall torque coefficients at different pitch angles.

In the Figure 7.3, it is found that the overall drag coefficients at different fixed pitch angles do not vary much. But if the effects of dynamic stall and flow curvature are taken into consideration, the drag coefficients are slightly higher at lower tip speed ratios and slightly lower at higher tip speed ratios.

7.1.2 Variation of Non-dimensional Normal and Tangential Forces

The Figure 7.4 and 7.5 show the results of non-dimensional normal and tangential forces at different pitch angles for tip speed ratio of 1.5. It is observed from these figures that due to the effect of dynamic stall and flow curvature the magnitude of normal and tangential forces increases in both the upstream and downstream sides. From these figures it is further observed that due to the effect of pitching, the magnitude of normal force increases in the upstream and decreases in the downstream side while magnitude of tangential force increases at both the upstream and downstream sides. At low tip speed ratio, the variation as mentioned above is due to the effect of dynamic stall mainly.

The non-dimensional normal and tangential forces at high tip speed ratio ($\lambda=5.0$) are shown in the Figures 7.6 and 7.7. It is vivid from these figures that due to the effect of pitching, the magnitude of both normal and tangential forces decreases in the upstream side and increases in the downstream side in general. However, it is observed that the magnitude of both the normal and tangential force increases in the upstream side and decreases in the downstream side due to the effect of dynamic stall and flow curvature.

The effect of tip speed ratio on non-dimensional normal and tangential forces are shown in the Figures 7.8 and 7.9 respectively. One can observe from the Figure 7.8 that the magnitude of normal force increases both in the upstream and downstream sides with tip speed ratio. While from the Figure 7.9 it is observed that the tangential force does not follow any regular pattern due to the effect of tip speed ratio.

7.1.3 Variation of Local Angle of Attack

In the Figures 7.10 and 7.11, variations of local angle of attack (effective blade angle) with azimuth angles at different fixed blade pitchings and tip speed ratios respectively with dynamic stall and flow curvature effects are shown.

From Figure 7.10, it is seen that as the pitch angle increases, the angle of attack decreases in the upstream side and increases at the down stream side.

In the Figure 7.11, variation of angle of attack with azimuth angles at different tip speed ratios for fixed pitch angle of 2 degree is shown. It is observed from this figure that as the tip speed ratio increases the angle of attack decrease at both the upstream and downstream sides.

7.1.4 Variation of Local Induced Velocity

In the Figure 7.12, variation of induced velocities with azimuth angles at different fixed blade pitchings is shown. It is found from this figure that as the fixed blade pitching increases, the local induced velocity decreases at the upstream side. While at the down stream side, the effect of blade pitching is negligible.

7.1.5 Variation of Local Reynolds Number

In the Figure 7.13, variation of local Reynolds numbers with azimuth angles at different fixed blade pitchings is shown. From this figure, it is seen that the local Reynolds number does not vary much with fixed blade pitching.

7.2 Comparison of Calculated and Experimental Results

Figure 7.14 shows the comparisons of the calculated values and the experimental data of the VUB wind tunnel test model (Decleyre et al, 1981). The model test was conducted at the constant wind speed of 7.28 m/s. From this figure it can be observed that there have been some increase of overall power coefficient values in the lower tip speed ratios while in the higher tip speed ratios, some decrease in values is observed for adding the dynamic stall and flow curvature effects. In the lower tip speed ratios, mainly for the dynamic lift values and in the higher tip speed ratios for the flow curvature effect such changes have occurred. It is also found from this figure that at the higher tip speed ratio side, there has been some improvement of correlation while at the lower tip speed ratio side there has been some over prediction.

In the Figure 7.15, the comparison of the calculated values by the present prediction model and the experimental data from the Reading University (Mays and Musgrove, 1979) is shown. The running speed of the turbine varies from 3 to 7 m/s. So, in the present calculation the mean wind speed Reynolds number of 138000 is considered for this turbine with solidity of 1.185. Very few experimental data are available for their turbine and in addition these are scattered. It is seen from this figure that the correlation has improved much with the cascade model including dynamic stall and flow curvature effects.

In the Figure 7.16, the comparison of calculated values by cascade theory with and without the effects of dynamic stall and flow curvature and experimental data is shown. These experimental data are presented by Migliore et al [Migliore et al, 1980] for the outdoor test model of West Virginia University. It is observed from this figure that the correlation rather deteriorates a little in the lower tip speed ratio side if the dynamic stall and flow curvature effects are added to the cascade theory.

From the Figures 7.17 to 7.20, comparisons of calculated values by cascade theory with and without the effects of dynamic stall and flow curvature and experimental data are shown. The experimental data is obtained from the Sandia Tow Tank model (Strickland et al, 1981). It is seen from these figures that the correlation between the calculated values with the effects of dynamic stall and flow curvature is quite good.

Though there are deviations of calculated values including the effects of dynamic stall and flow curvature with the experimental data at several cases, but unless the comparison is made with a good number of experimental data, it will be unjustified at the moment to pass proper comment concerning the calculated values by the present analytical method.

CHAPTER 8

DESIGN OF TURBINES

DESIGN OF TURBINES

In this chapter, a simplified form of design method is presented for straight-bladed vertical-axis Darrieus wind turbine. The design is done at variable turbine speed condition. A number of parameters such as solidity, design power, design wind speed, cutout speed, blade stress (in other words blade material), number of blades, airfoil shape, blade supporting type (simple/overhang/cantilever) etc. control the design of turbines. Considering all the above mentioned variable parameters and the effect of dynamic stall and flow curvature, the present design method gives directions for optimum turbine configurations at variable turbine speed.

Design of a vertical-axis Darrieus wind turbine at variable turbine speed condition is generally done with a view to serving the following purposes:

1. It may be applied for water pumping for irrigation
2. It may be used in the DC generator/regulator/storage battery combination for generation of electricity in the remote areas.

The design method at variable turbine speed differs slightly than that at constant turbine speed. The flow diagrams of both the constant and variable speed design approaches have been given in the appendix-B.

For the design with variable turbine speed there appear many variable parameters. Few of them are considered to be fixed before conducting the design analysis. These are number of blades, cutout speed, blade supporting type, the blade material (aluminum alloy) and blade pitching.

Number of Blade: In this design, the number of blade is chosen as three. A turbine with three blades is better due to smooth running because of lower fluctuations of energy in each revolution.

Cutout Speed: The cutout speed is chosen as 15 m/s.

Blade Material: In this design blade material is chosen as aluminum alloy where allowable stress is chosen as 100 N/mm^2 .

Blade Support: The blades are assumed to be supported like that of the overhang types which is shown in the Figure 8.1.

In the present design analysis, the variable speed design is carried out at constant tip speed ratio. In other words, the load characteristic curve is assumed in such a way that the tip speed ratio remains constant. The constant tip speed ratio design may approximately follow the load characteristic curve of either a positive displacement pump or a centrifugal pump. However, to make the accuracy of the design, actual pump characteristic curve is necessary to be encountered. In the present design method, emphasis is given on finding a general design approach of a variable speed turbine rather than to study a particular problem.

8.1 1 kW straight-bladed Darrieus turbine

In this section design of a 1kw straight-bladed Darrieus turbine is described. The mean wind velocity of the turbine is chosen as 5 m/s that is prevailing at the coastal region of Bangladesh for most of the months of the year. The support of the turbine is chosen as overhang type because of certain advantages. Detail comparison between the overhang and simple supported type VAWT is given in the next section. For designing this turbine, the effect of dynamic stall and flow curvature with blade pitching is taken into consideration with the cascade theory for the first time.

Design configurations of variable speed turbines at various solidities are shown in the Figure 8.2 and 8.3. It is observed in the Figure 8.2 that with the increase of solidities the height increases significantly while chord of the turbine increases slightly. It is further observed that the diameter of the turbine decreases with solidity. It has also been seen that if the effect of dynamic stall and flow curvature is considered, the height and diameter of the turbine increases and decreases respectively in the high solidity range only. However, the dimensions of the chord and skin thickness do not vary with or without the effects of dynamic stall and flow curvature.

In the Figure 8.3 other design configurations with different solidities are shown. The starting torques are calculated at a wind speed of 4 m/sec. It is found from this figure that with the increase of solidities the starting torque increases significantly. It is further observed that the design tip speed ratio and rpm of the turbine decreases with solidity. It has also been seen that the design power coefficient does not vary much with solidity. It is found from this figure that if the effect of dynamic stall and flow curvature is considered, the aspect ratio and the design tip speed ratio of the turbine increases while the starting torque and rpm decreases. However, the design power coefficient do not vary with or without the effects of dynamic stall and flow curvature.

In the Figures 8.4 and 8.5, the variations of the overall power and torque coefficients with different tip speed ratio are shown respectively with or without the effect of dynamic stall and flow curvature. From the comparison it is seen that in the low tip speed ratio, the dynamic stall and flow curvature effects gives higher value of C_p and C_q , whereas in the high tip speed region they are lower. In the Figure 8.4, the value of power coefficient at the design tip speed ratio is also shown.

In the Figures 8.6, 8.7 and 8.8 the distributions of centrifugal, normal and net normal forces with azimuth angle are presented. From the figures 8.6 and 8.7, it can be observed that the contribution of the centrifugal force in comparison to the normal force is very high. It is also observed from the Figure 8.6 that due to the effects of dynamic stall and flow curvature, the magnitude of the centrifugal force drops remarkably while there is negligible variation of normal forces with or without dynamic stall and flow curvature effects which can be seen from the Figure 8.7

There appears the starting problem especially for the variable speed design where the wind turbine is directly coupled with a pump. The starting can be done in many ways. One possible way of starting may be achieved by employing variable pitching. The Figure 8.9 shows that with the increase of the variable pitching the starting torque increases significantly. Fixed pitching makes negligible change in the starting torque. It can be seen further from this figure that there is insignificant variation of starting torques with or without dynamic stall and flow curvature effects.

At cutout speed, the variations of bending moments with azimuth angle are presented in the Figures 8.10 and 8.11. The Figure 8.10 shows the bending moments due to the net normal forces while the Figure 8.11 shows the bending moments due to the tangential forces. It is seen from the figures that with dynamic stall and flow curvature effects, the bending moments due to normal forces are reasonable lower in comparison to those without dynamic stall and flow curvature effects. It can also be seen from the Figure 8.11 that there is insignificant variation of bending moment due to tangential force if dynamic stall and flow curvature effects are included. It is also seen from these figures that the contribution of bending moment due tangential forces is negligible compared to that due to normal forces. That is why the design analysis is performed based on the moment due to the net normal forces only.

The Figures 8.12 and 8.13 show respectively the variations of bending stresses due to normal and tangential forces. The variation of these with azimuth angle are similar to those of bending moments due to normal and tangential forces (Figure 8.10 and 8.11).

The variation of maximum blade stress with blade skin thickness is shown in the Figure 8.14. The skin thickness which corresponds to the lowest value of the maximum blade stress (allowable blade stress) is chosen as the design skin thickness.

8.2 Comparison Between Overhang And Simple Supported VAWT

Design configurations of variable speed turbines at various wind speeds for simple and overhang are shown in the Figures 8.15 and 8.16. The solidity is chosen as 0.5 while the design power 1 kW. It is observed in the Figure 8.15 that with the increase of wind speed, the height, diameter and chord of the turbine decreases in general. It is observed that for overhang type support the diameter of the turbine drops while the height increases significantly in comparison to those of the simple support type. The variation of chord is negligible for type of supports.

In the Figure 8.16, variations of starting torque, aspect ratio, design rpm, design tip speed ratio and overall design power coefficients with respect to different wind speeds are shown. From this figure, it is found that the starting torque and design tip speed ratio of simple supported turbines are slightly higher than those of overhang supported turbines. Whereas the design rpm and aspect ratio of overhang supported turbine are remarkably higher than those of simple supported turbines. However, the overall power coefficient is almost same for both kind of turbines.

CHAPTER 9

CONCLUSIONS AND RECOMMENDATIONS

CONCLUSIONS AND RECOMMENDATIONS

In this chapter general conclusions are drawn for the present development works on the cascade theory with blade pitching including dynamic stall and flow curvature effects and the design methods of straight-bladed Darrieus turbines. Few recommendations are also given for the future works.

9.1 Conclusions

- 1) The cascade theory with blade pitching including dynamic stall and flow curvature effects predicts higher overall power, torque and drag coefficients than those without the effects of dynamic stall and flow curvature at each fixed pitch angle.
- 2) The cascade theory including dynamic stall and flow curvature effects predicts the instantaneous blade forces remarkably.
- 3) The cascade theory with blade pitching including dynamic stall and flow curvature effects does not make convergence problem for any practical range of tip speed ratio and solidity.
- 4) The cascade theory with blade pitching including dynamic stall and flow curvature effects takes higher computational time than that by the cascade theory without blade pitching including dynamic stall and flow curvature effects.
- 5) The present analytical prediction model has no mathematical complication, as a result, the method of calculation is simple.
- 6) At present due to lack of experimental data, the calculated values of different parameters at different fixed blade pitch angles could not be compared with experimental data. But it is expected that the calculated values will not deviate much from the experimental data as it holds good with zero pitch angle.
- 7) The design of a straight-bladed vertical-axis Darrieus wind turbine using the cascade theory including dynamic stall and flow curvature effects shall be reasonable as this method can predict the local blade forces quite well.
- 8) In the present design method, design point is chosen in the higher tip speed ratio side from that corresponding to peak power coefficient. This is done because the region after the peak power coefficient is relatively stable and suitable for smooth operation. For a high solidity turbine, the power coefficient curve near the peak is not flat, as a result design with peak power coefficient is not good because with a slight shifting of tip speed ratio towards the lower value, there may appear stalling in some of the stations. As such, for normal operation of turbine it is avoided.

- 9) In the present design, the blade pitching is considered as zero for normal operation of turbine. Fixed blade pitching (either positive or negative) always gives reduced power. On the other hand, variable blade pitching may give higher power but control of variable pitching is difficult especially at high turbine speeds.
- 10) The overhang type support reduces the overall dimensions of the turbines reasonably in comparison to those of the simple supported turbines.

9.2 Recommendations for Further Researches

- 1) Wind shear has not been considered in the calculation, which is important especially when the turbine is placed close to the ground. It may be included in the calculation to see the effect on the turbine performance.
- 2) During designing the turbine, the blades are assumed to be overhang supported. Other types of support like cantilever can be considered for designing of a similar turbine.
- 3) Design work has been done with the aluminium blade. The same design may be performed for the overhang blade support applying wood with skins of aluminium as a blade material which is easily available in our country.
- 4) Natural frequency of wind turbine rotation has not been determined in the present work. It can be taken into consideration as well.
- 5) In the present design work, airfoil NACA 0015 is chosen for the turbine blade. Other airfoils like NACA 0012, NACA 0018 and S1210 can be used for comparative study.

REFERENCES

- [1] Cardona, Jose, L., "Flow Curvature and Dynamic Stall Simulated with an Aerodynamic Free-Vortex Model for VAWT", *Wind Engineering*, Vol. 8, No. 3, pp. 135-143, UK, 1984.
- [2] Dhar, N.R., "Performance and Design Optimization of Vertical Axis Straight-bladed Darrieus Wind Turbine", M.Sc. Thesis, Department of Mechanical Engineering, BUET, Dhaka, Bangladesh, September 1987.
- [3] Decleyre W, Aerschot D V and Hirsch Ir. Ch, "The Effects of Reynolds Number on The Performance Characteristics of Darrieus Windmills with Troposkien and Straight-Blades", *Proceedings of the International Colloquium on wind energy*, Brighton, UK, 243-248, 1981.
- [4] Ericsson L E and Reding J P, "Engineering Analysis of Dynamic Stall", *Proceedings of the ASME winter annual meeting*, San Francisco, California, USA, 117-123, 1978.
- [5] Fanucci J B and Walter R E, "Innovative Wind Machines : The Theoretical Performance of a Vertical-axis Wind Turbine", *Proceedings of the vertical-axis wind turbine technology workshop*, Sandia laboratories, SAND 76-5586, iii-61-95, USA, 1976.
- [6] Gormont R E, "A Mathematical Model of Unsteady Aerodynamics and Radial Flow for Application to Helicopter Rotors", U.S. Army air mobility R&D laboratory, Vertol Division, Philadelphia, USA, 1973.
- [7] Ham, N D, "Aerodynamic Loading on a Two Dimensional Airfoil during Dynamic Stall", *AIAA Journal*, Vol. 6 (10), pp. 1927-1934, 1968.
- [8] Hirsch, Ch. and Mandal, A. C., "Flow Curvature Effect on Vertical Axis Darrieus Wind Turbine having High Chord-Radius Ratio", *European Wind Energy Conf*, 22-26 Oct. 1984, Hamburg, FRG, pp. 405-410, 1984.

- [9] Hirsch, H. and Mandal, A. C., "A Cascade Theory for the Aerodynamic Performance of Darrieus Wind Turbines", *Wind Engineering*, Vol. 11, No. 3, pp. 164-175, 1987.
- [10] Holme, O., A, "Contribution to the Aerodynamic Theory of the Vertical Axis Wind Turbine", *Int. Symp. on Wind Energy Systems*, Sept. 7th-9th, Cambridge, England, C4-55-71, 1976.
- [11] Jacob E N and Sherman A, "Airfoil Characteristics as Affected by Variations of the Reynolds Number", *NACA-TR-586*, 1937.
- [12] Lapin E E, "Theoretical Performance of Vertical Axis Wind Turbines", *ASME paper, 75-WA/Ener-1*, The winter annual meeting, Houston, Texas, USA, 1975.
- [13] Larsen H C, "Summary of a Vortex Theory for the Cyclogiro" *Proceedings of the second U.S. National Conferences on wind engineering research, Colorado state university, V-8-1-3*, 1975.
- [14] Mandal, A.C. "Aerodynamics and Design Analysis of Vertical Axis Darrieus Wind Turbines" *Ph. D. Thesis, Vrije Universiteit, Brussel, Belgium*, 1986.
- [15] Mandal, A.C. and J.D. Burton, "The Effects of Dynamic Stall and Flow Curvature on the Aerodynamics of Darrieus Turbines Applying the Cascade Model", *Wind Engineering, UK, Vol 18 NO. 6* 1994.
- [16] Mandal, A.C., "The Effects of Dynamic Stall And Flow Curvature on the Aerodynamics of Darrieus Turbines Applying the Cascade Model", *A Report on Post Doctoral Research In the Renewable Energy and the Environment, Department of Engineering, University of Reading, UK*, 1994.

- [17] Mays I D and Musgrove P J, "Performance of the Variable Geometry Vertical Axis Wind Turbine at High and Low Solidities", Proceedings of the 1st wind energy association workshop, 48-56, 1979.
- [18] Mehta U B, "Dynamic Stall on an Oscillating Airfoil", proceeding of AGARD fluid dynamics panel symposium on unsteady aerodynamics, AGARD CPP-227, 1977.
- [19] Migliore, P. G. and Wolfe, W. P., "The Effect of Flow Curvature on the Aerodynamics of Darrieus Wind Turbines", Department of Aerospace Engineering, WVU, Morgantown, USA, 1980.
- [20] Migliore, P. G., Wolfe, W. P. and Fanucci, J. B., "Flow Curvature Effects on Darrieus Turbine Blade Aerodynamics", J. Energy, Vol. 4, No. 2, pp. 49-55, 1980.
- [21] Milne Thompson L M, "Theoretical Aerodynamics", 4th edition, Dover Publications Inc., New York, USA, 1973.
- [22] Muniruzzaman, M., "Prediction of A Darrieus Turbine Performance Considering Dynamic Stall", M.Sc. Thesis, Department of Mechanical Engineering, BUET, Dhaka, Bangladesh, December 1989.
- [23] Muraca R J, Stephens M V and Dagenhart J R, "Theoretical Performance of Cross-wind Axis Turbines with Results for a Catenary Vertical Axis Configuration", NASA TMX-72662, USA, 1975.
- [24] Musgrove P J and Mays I D, "Development of the Variable Geometry Vertical-axis Windmill", Proceedings of the second international symposium on wind energy systems, Amsterdam, Netherlands, E4-39-60, 1978.

- [25] Noll, R. B. and Ham, N. D., "Analytical Evaluation of the Aerodynamic Performance of a high-reliability Vertical-axis Wind Turbine", Proceedings of AWEA National conference, USA, 1980.
- [26] Paraschivoiu, I., Delclaux, F., Fraunie, P. and Beguier, C., "Aerodynamic Analysis of the Darrieus Rotor Including Secondary Effects", J. Energy, Vol. 7, No. 5, pp. 416-421, 1983.
- [27] Paraschivoiu, Ion, "Aerodynamic Loads and Performance of the Darrieus Rotor", J. Energy, Vol. 6, No. 6, pp. 406-412, Nov-Dec 1982,.
- [28] Paraschivoiu, Ion and Delclaux, Francois, "Double Multiple Streamtube Model with Recent Improvements", J. Energy, Vol. 7, pp. 250-255, May-Jun 1983.
- [29] Paraschivoiu, Ion, "Predicted and Experimental Aerodynamic Forces on the Darrieus Rotor", J. Energy, Vol. 7, No. 6, pp. 610-615, Nov-Dec 1983.
- [30] Read, S. and Sharpe, D. J., "An Extended Multiple Streamtube Theory for Vertical Axis Wind Turbines", 2nd BWEA Workshop, Cranfield, UK, Apr. 1980, pp. 65-72.
- [31] Shankar P N, "On the Aerodynamic Performance of a Class of Vertical Shaft Windmills", Proceedings of the Royal Society of London, UK, Series A, Vol. 349, 35-51, 1976.
- [32] Sharpe, D. J., "Experiments with a Darrieus Turbine", Wind Power in the UK Symposium, pp. 8-20, UK, July 1978.
- [33] Sharpe, D. J., "Refinements and Developments of the Multiple Streamtube Theory for the Aerodynamic Performance of Vertical Axis Wind Turbines", 1984.
- [34] Sheldahl R E and Blackwell B F, "Aerodynamic Characteristics of Four Symmetrical Airfoil Sections Through 180 Degrees Angle of Attack at Low Reynolds Number",

Proceedings of the vertical-axis wind turbine technology workshop, Sandia laboratories, SAND76-5586, II-73-106, USA, 1976.

- [35] Strickland, J. H., "A Performance Prediction Model for the Darrieus Turbine", Int. Symp. on Wind Energy Systems, Cambridge, UK, pp. C3-39-C3-54, Sept. 7-9, 1976.
- [36] Templin, R. J., "Aerodynamic Performance Theory for the NRC Vertical- Axis Wind Turbine", NRC Lab. Report LTR-LA-190, pp. 29, June 1974.
- [37] Vittecoq, P. and Laneville, A., "The Aerodynamic Forces for a Darrieus Rotor with Straight Blades: Wind Tunnel Measurements", J. Wind Engineering and Industrial Aerodynamics, pp. 381-388, 1983.
- [38] Willmer A C, "Low Reynolds Number Tests on the NACA 0015 section", Proceedings of the 1st British wind energy association workshop, 109-116, UK, 1979.
- [39] Wilson, R. E., "Darrieus Rotor Aerodynamics", 3rd Wind Energy Workshop, Proceedings: 3rd Biennial Conf./Workshop on WECS, Washington D.C., USA, pp. 584-594, Sept. 19-21, 1977.
- [40] Wilson, R. E. and McKie, W. R., "A Comparison of Aerodynamic Analyses for the Darrieus Rotor", 2nd Int. Symp. on Wind Energy Systems, Oct. 3rd-6th 1978.
- [41] Wilson, R. E., "Wind-Turbine Aerodynamics", J. Wind Engineering and Industrial Aerodynamics, pp. 357-372, 1980.
- [42] Wilson, R. E., Lissaman, P. B. S., James, M. and McKie, W. R., "Aerodynamic Loads on a Darrieus Rotor Blade", J. Fluids Engineering, Vol. 105, pp. 53-58, Mar. 1983.

- [43] Walters, R.E.; Migliore, P.G.; Wolfe, W.P. (West Virginia University), "Innovative Wind Turbines: The Circulation Control Vertical Axis Wind Turbine". SERI/STR-217-1755. Golden, CO: Solar Energy Research Institute; 81 pp, Sept. 1985.

FIGURES

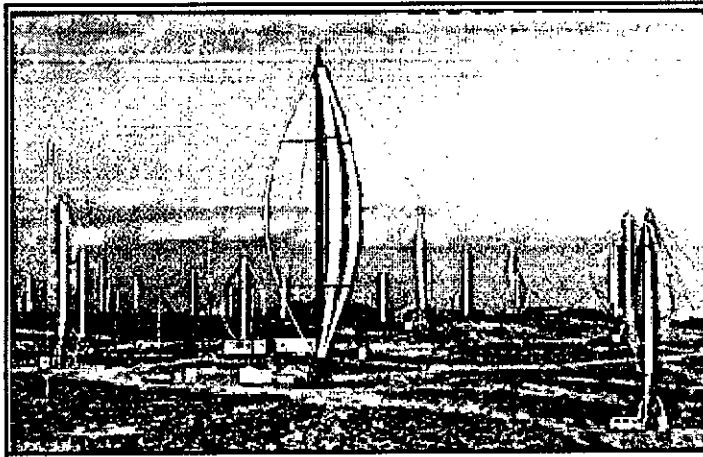


Figure 1.1: Egg-beater Darrieus turbines at California, USA

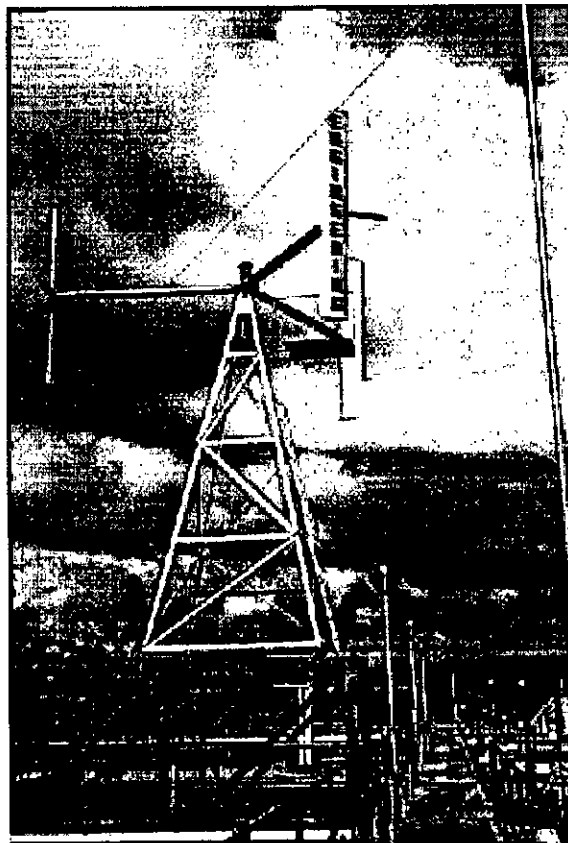


Figure 1.2: A 3kW Kirke-Lazauskas VAWT

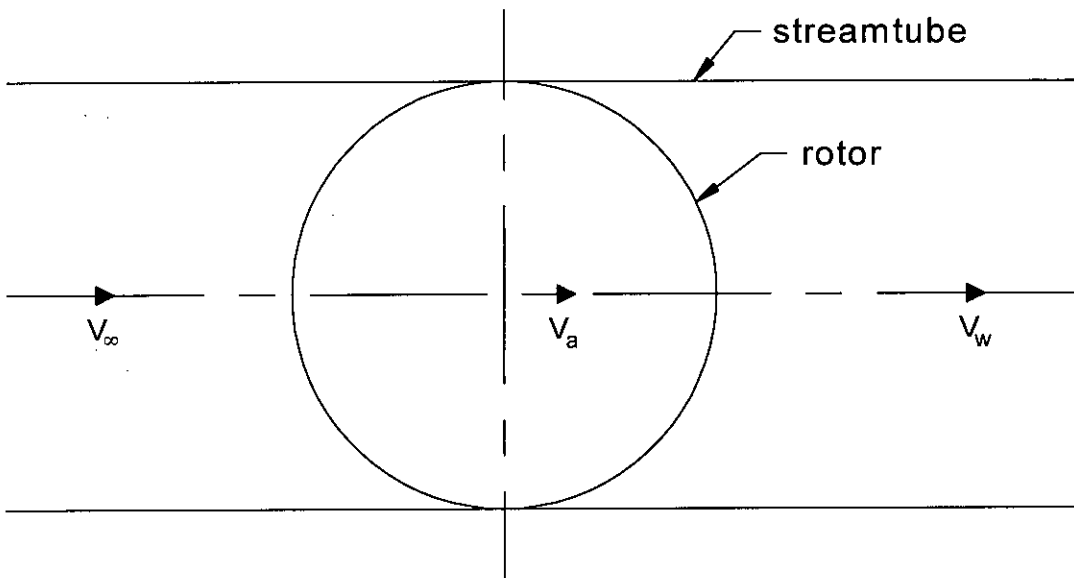


Figure 2.1: Streamtube consisting of the rotor showing the axial flow velocities.

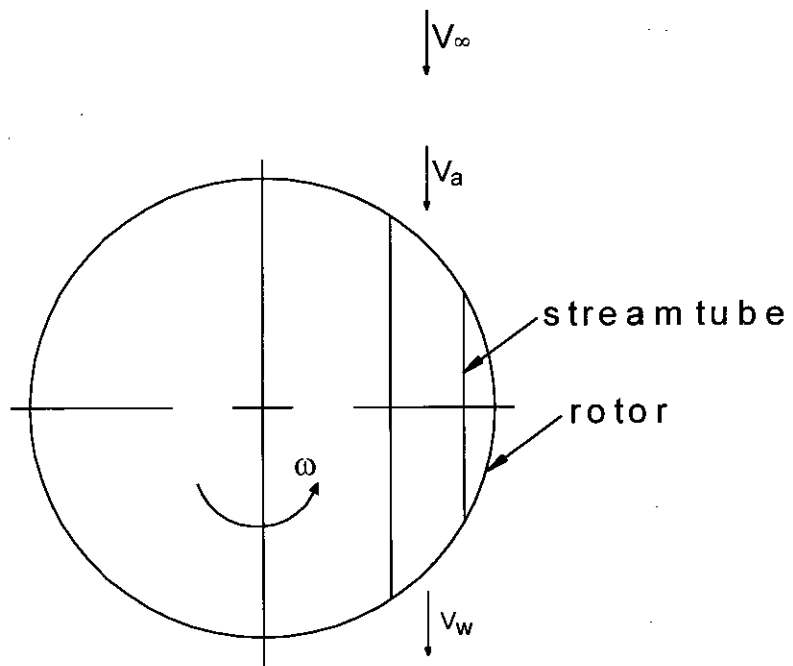


Figure 2.2: Elemental streamtube of a straight-bladed Darrieus wind turbine.

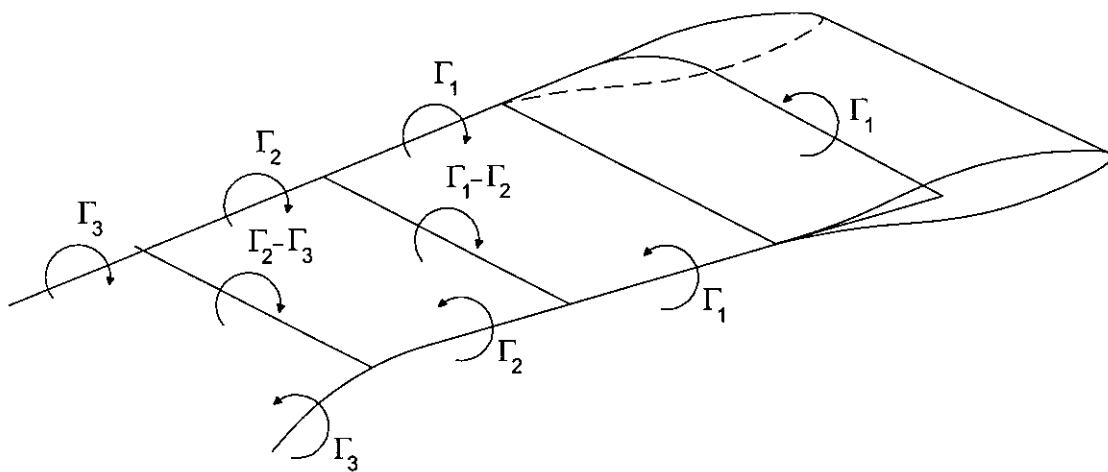


Figure 2.3: Vortex system for a single blade element.

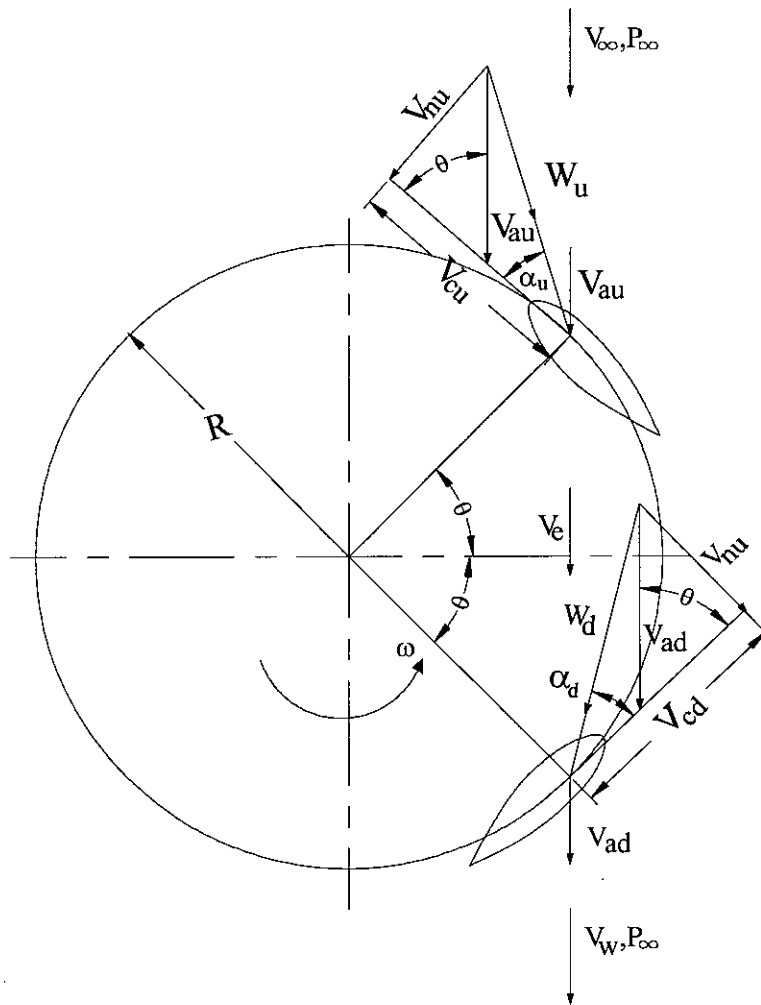


Figure 3.1 : Horizontal section of a straight-bladed Darrieus turbine showing flow velocities

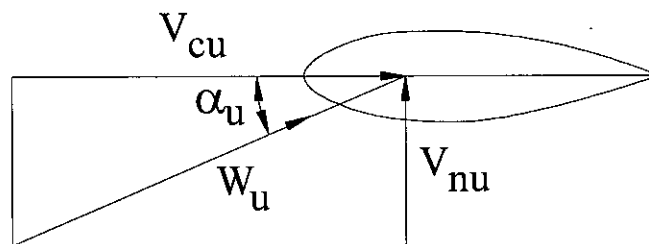


Figure 3.2 : Relative flow velocities on a blade airfoil

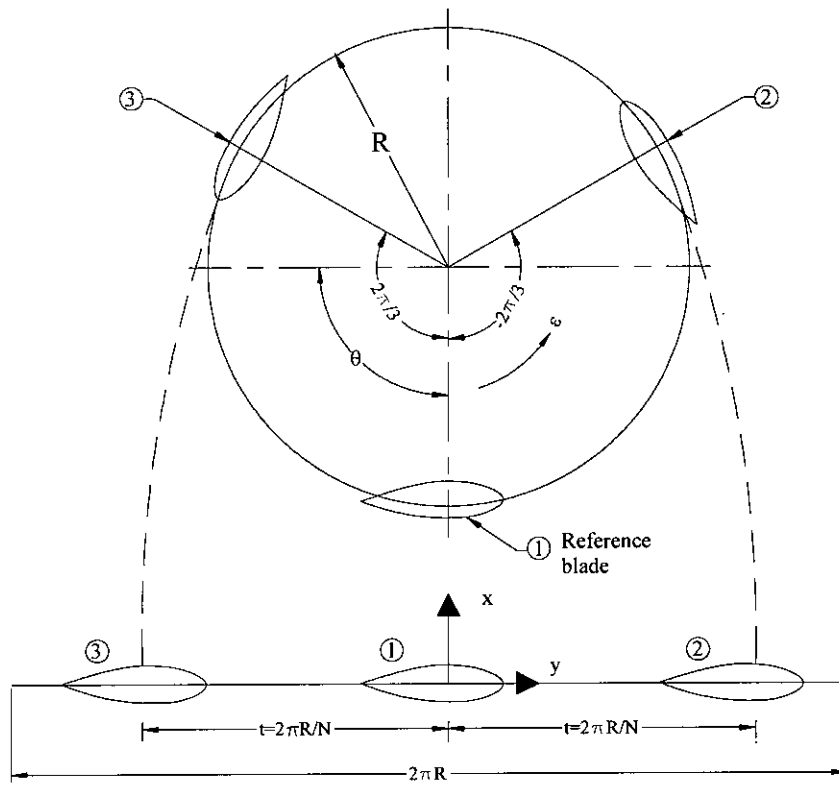


Figure 3.3 : Development of blade into a cascade configuration

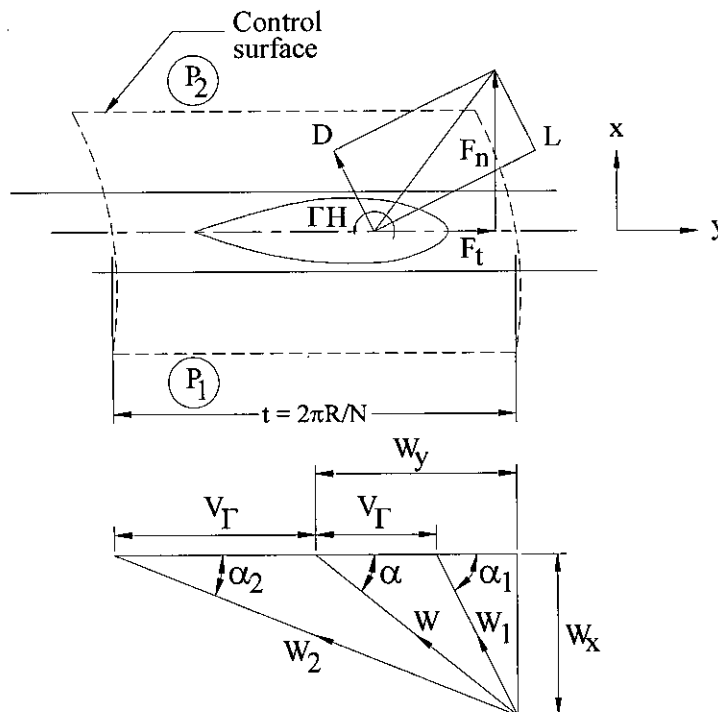


Figure 3.4: Velocity diagram on a blade airfoil

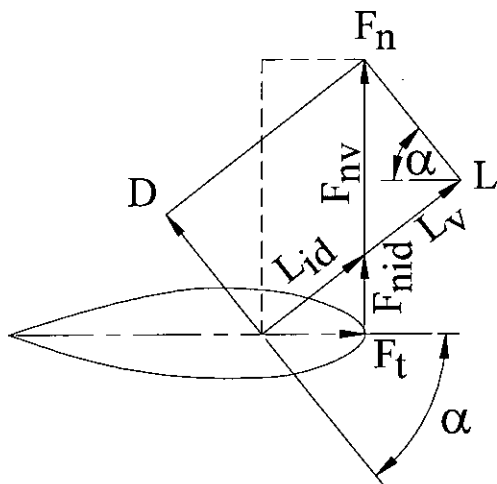


Figure 3.5 : Force diagram on a blade airfoil

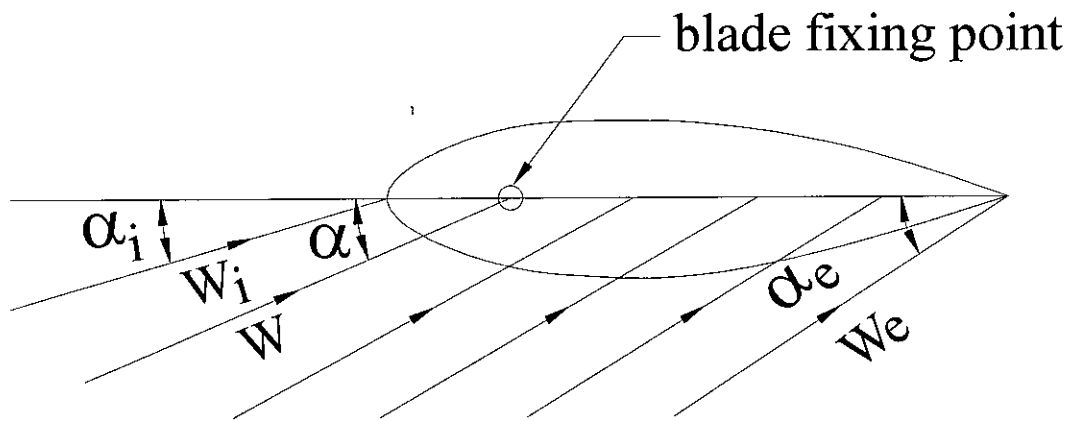


Figure 5.1: Typical variation of relative velocity and angle of attack along chordwise direction

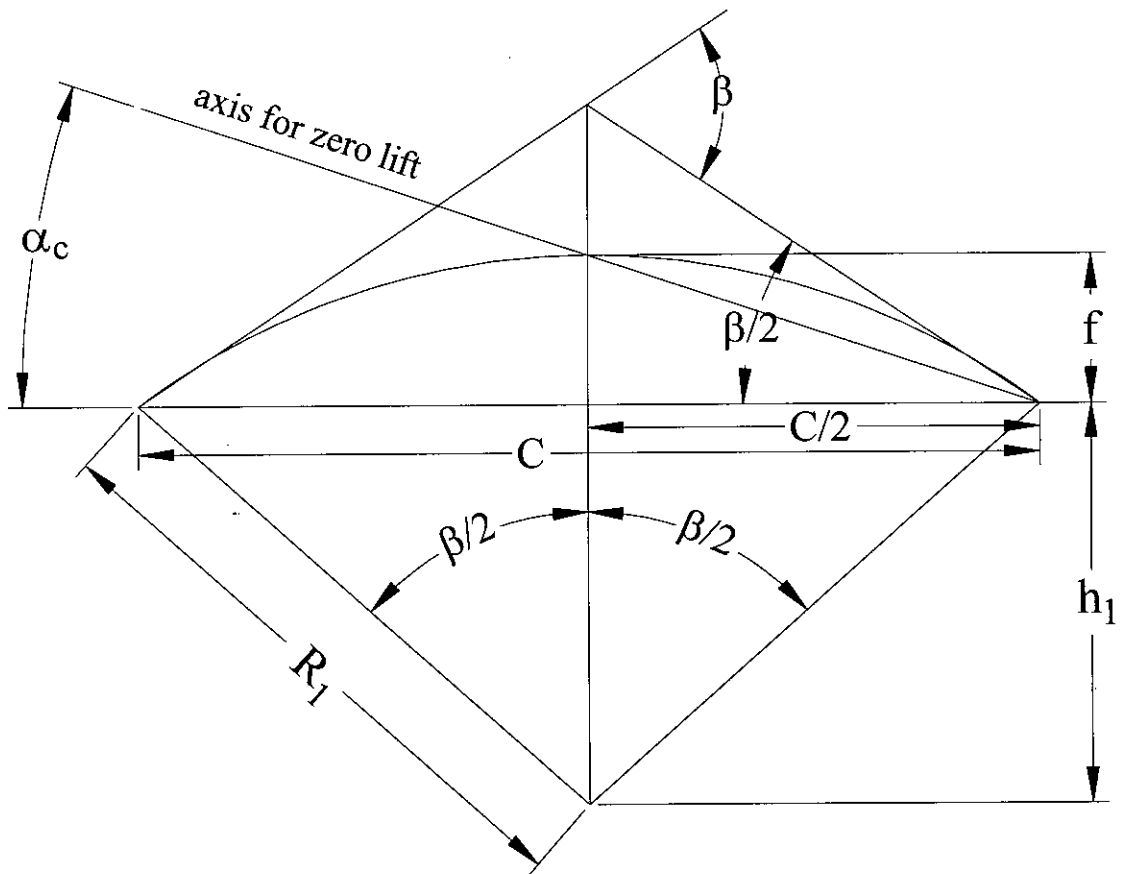


Figure 5.2: Geometry to determine camber of circular arc

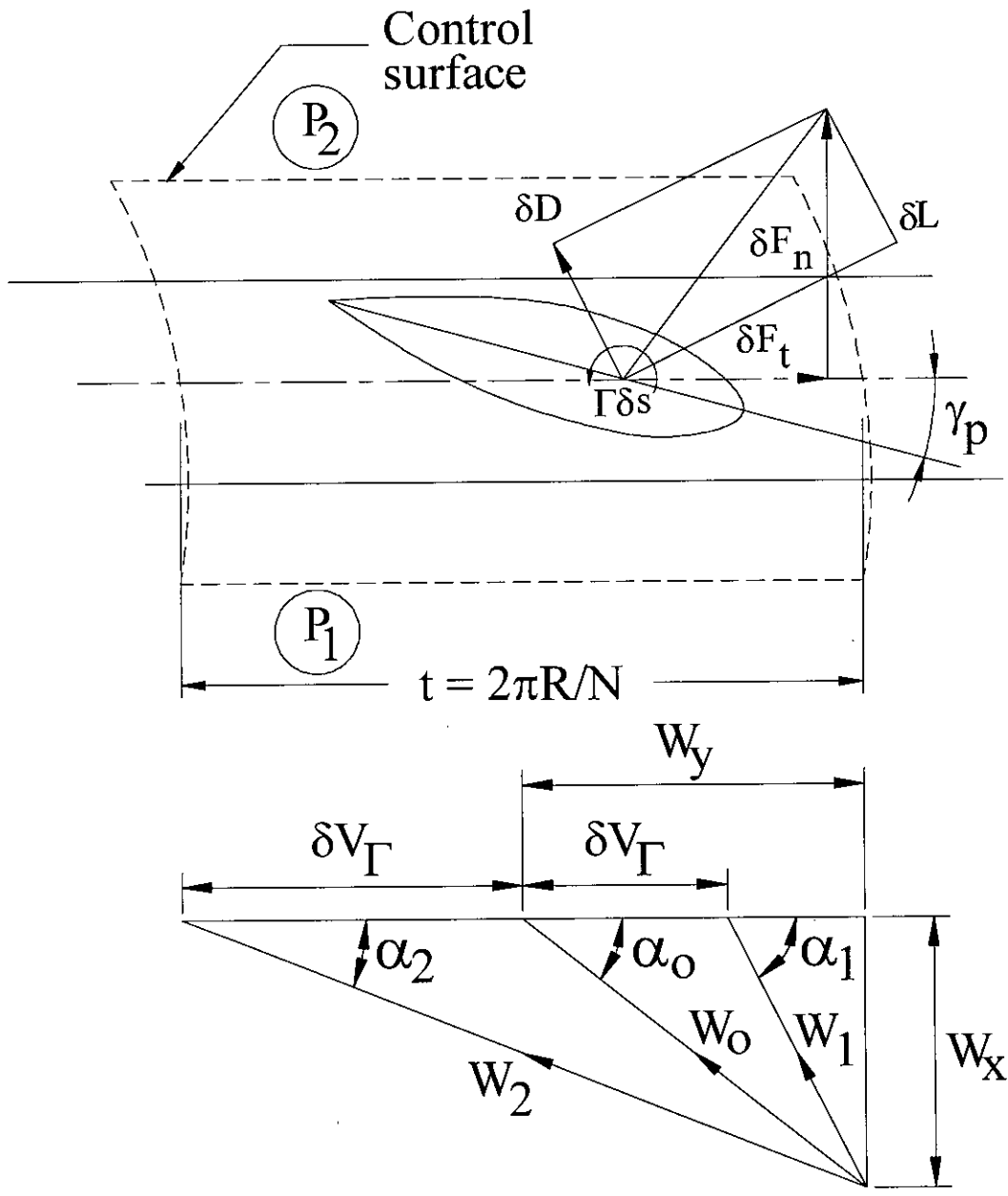


Figure 6.1 : Velocities and forces on blade airfoil with pitching in cascade configuration

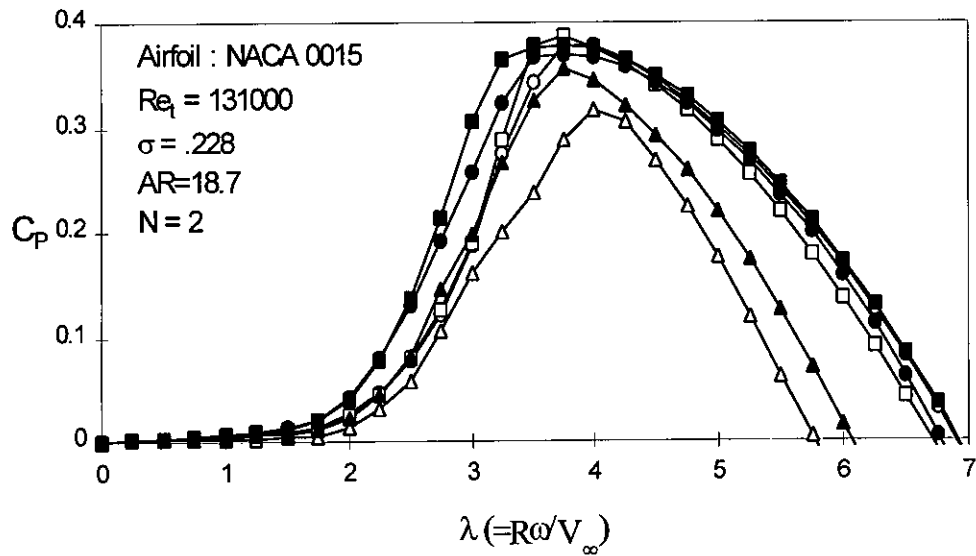


Figure 7.1: Variation of overall power coefficient with tip speed ratios at different fixed blade pitchings.

Symbol : ● ■ ▲ (with dynamic stall & flow curvature)
 ○ □ △ (without dynamic stall & flow curvature)
 Parameters : 0 2 5 (fixed pitch angle in degree)

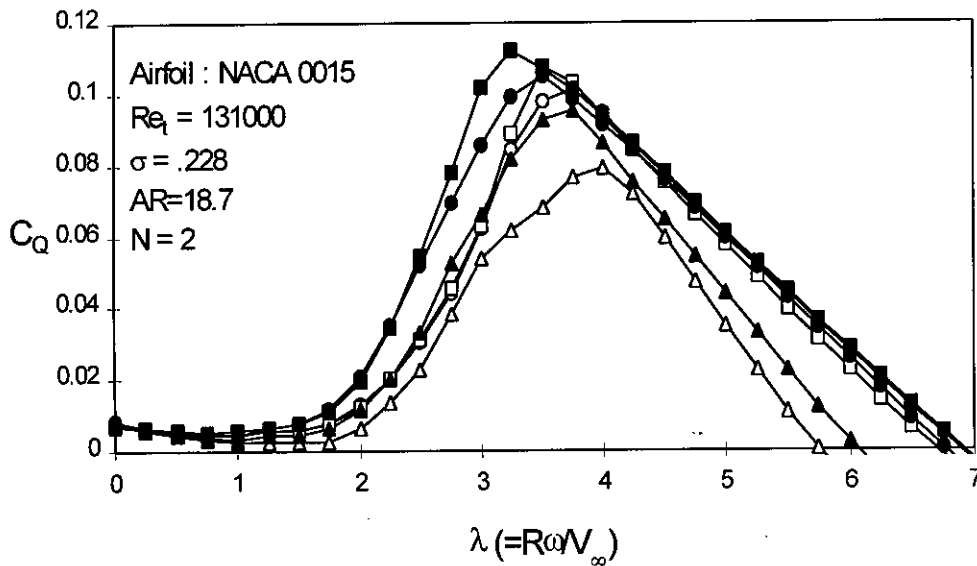


Figure 7.2: Variation of overall torque coefficient with tip speed ratios at different fixed blade pitchings.

Symbol : ● ■ ▲ (with dynamic stall & flow curvature)
 ○ □ △ (without dynamic stall & flow curvature)
 Parameters : 0 2 5 (fixed pitch angle in degree)

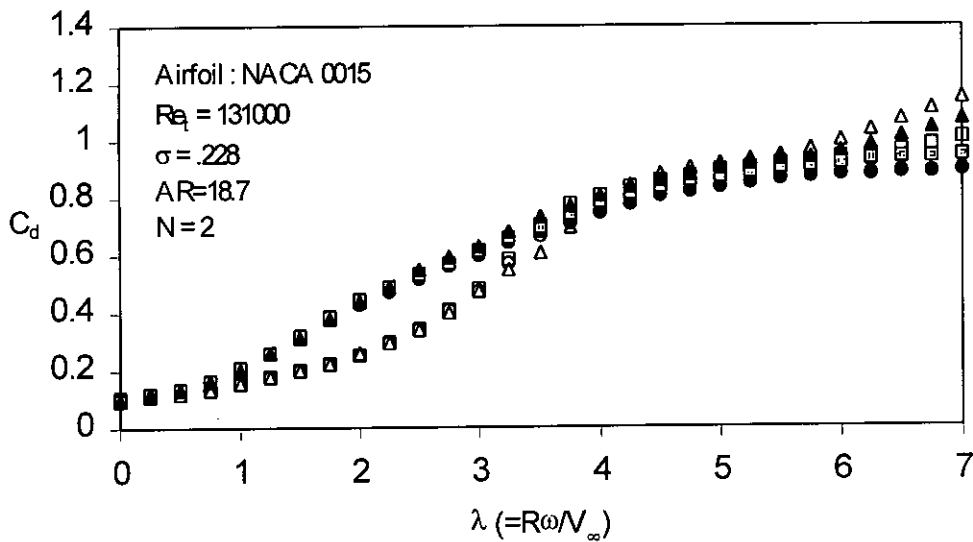


Figure 7.3: Variation of overall drag coefficient with tip speed ratios at different fixed blade pitchings.

Symbol : ● ■ ▲ (with dynamic stall & flow curvature)
 ○ □ △ (without dynamic stall & flow curvature)
 Parameters : 0 2 5 (fixed pitch angle in degree)

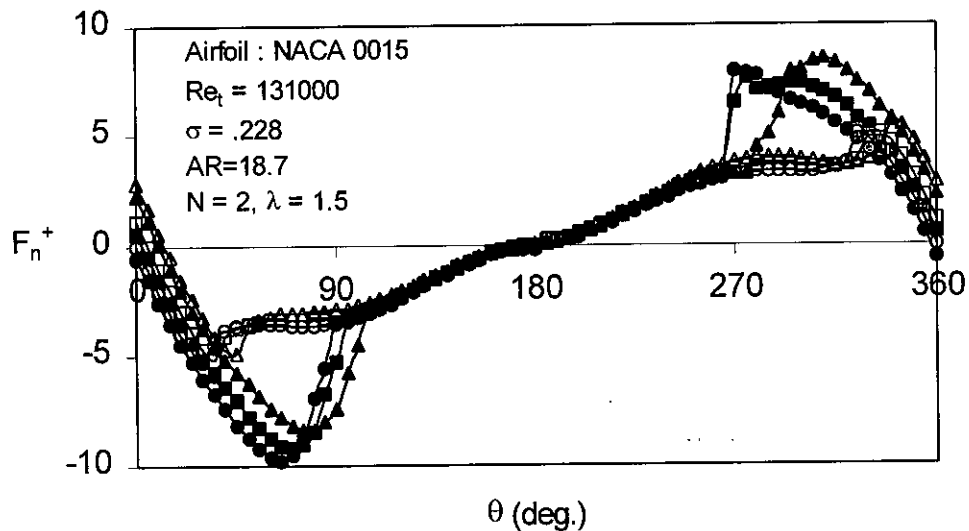


Figure 7.4: Variation of non-dimensional normal forces with azimuth angles at different fixed blade pitchings.

Symbol : ● ■ ▲ (with dynamic stall & flow curvature)
 ○ □ △ (without dynamic stall & flow curvature)
 Parameters : 0 2 5 (fixed pitch angle in degree)

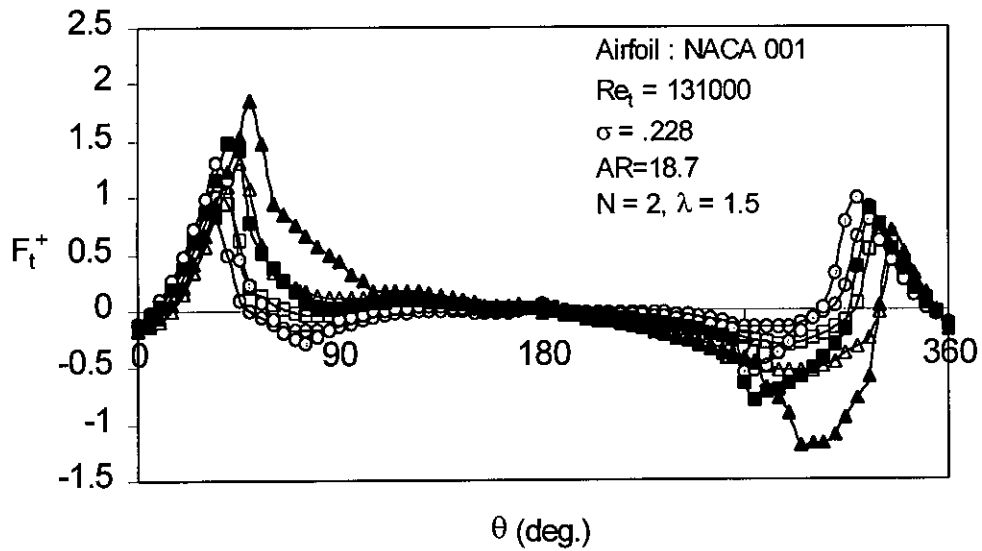


Figure 7.5: Variation of non-dimensional tangential forces with azimuth angles at different fixed blade pitchings.

Symbol : ● ■ ▲ (with dynamic stall & flow curvature)
 ○ □ △ (without dynamic stall & flow curvature)
 Parameters : 0 2 5 (fixed pitch angle in degree)

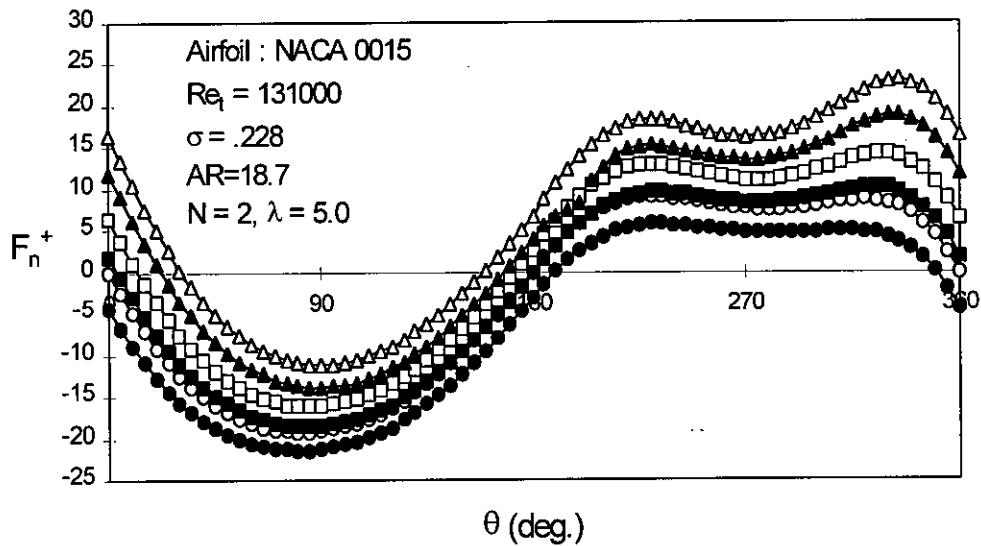


Figure 7.6: Variation of non-dimensional normal forces with azimuth angles at different fixed blade pitchings.

Symbol : ● ■ ▲ (with dynamic stall & flow curvature)
 ○ □ △ (without dynamic stall & flow curvature)
 Parameters : 0 2 5 (fixed pitch angle in degree)

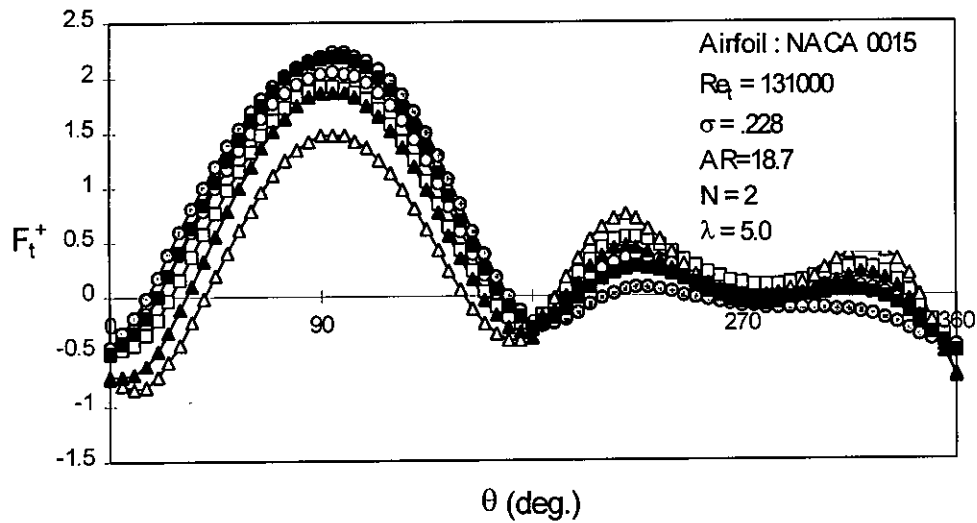


Figure 7.7: Variation of non-dimensional tangential forces with azimuth angles at different fixed blade pitchings.

Symbol : ● ■ ▲ (with dynamic stall & flow curvature)
 ○ □ △ (without dynamic stall & flow curvature)
 Parameters : 0 2 5 (fixed pitch angle in degree)

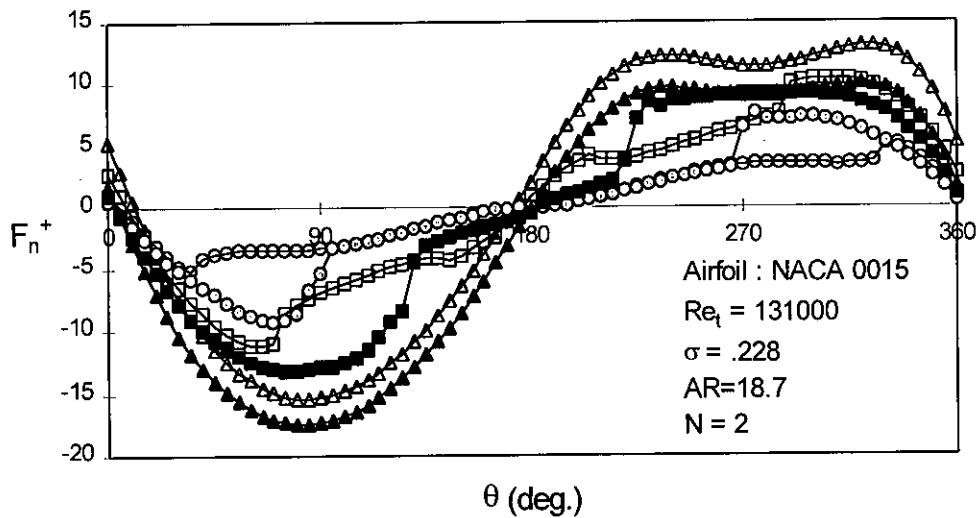


Figure 7.8: Variation of non-dimensional normal forces with azimuth angles at different tip speed ratios for fixed pitch angle 2 degree.

Symbol : ● ■ ▲ (with dynamic stall & flow curvature)
 ○ □ △ (without dynamic stall & flow curvature)
 Parameters : 1.5 3.0 4.5 (tip speed ratio)

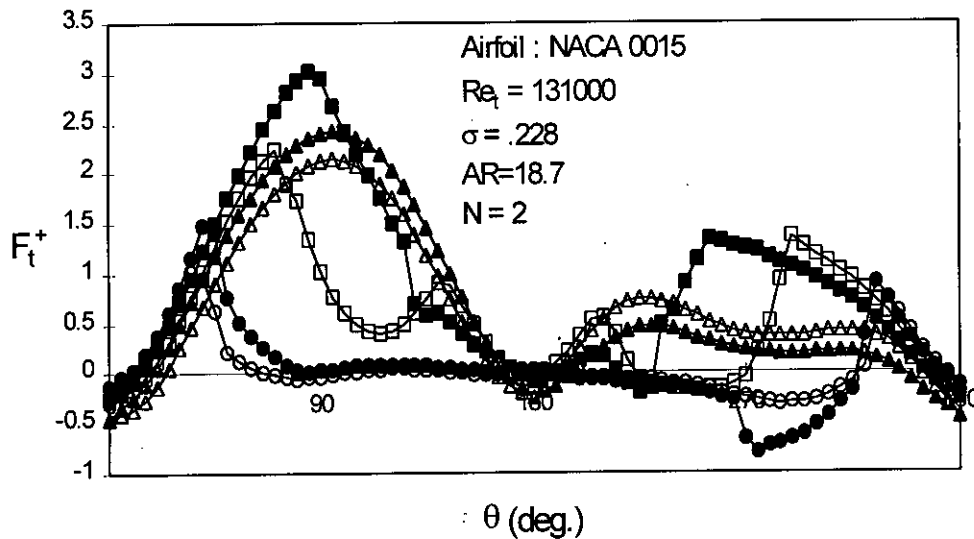


Figure 7.9: Variation of non-dimensional tangential forces with azimuth angles at different tip speed ratios for fixed pitch angle 2 degree.

Symbol : ● ■ ▲ (with dynamic stall & flow curvature)
 ○ □ △ (without dynamic stall & flow curvature)
 Parameters : 1.5 3.0 4.5 (tip speed ratio)

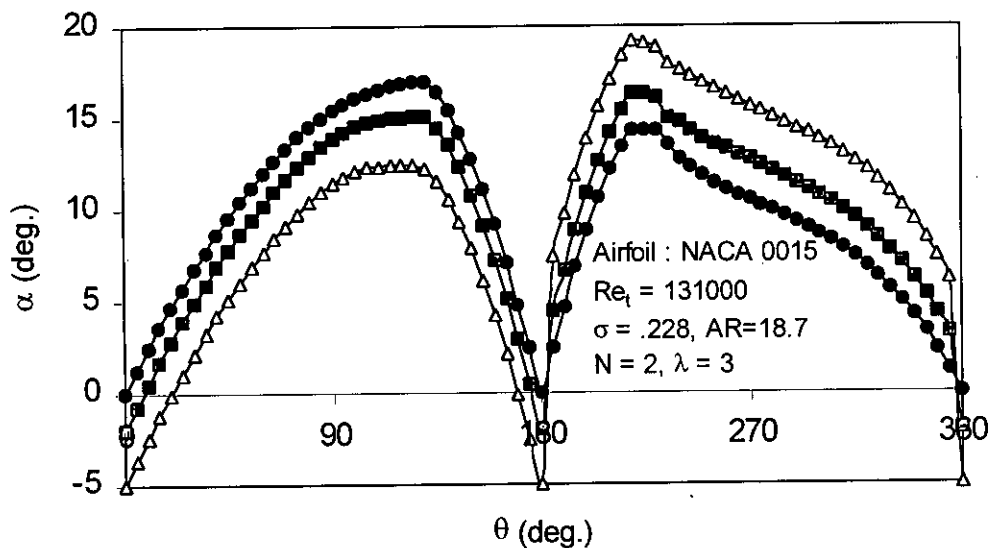


Figure 7.10: Variation of local effective blade angles with azimuth angles at different fixed blade pitchings with dynamic stall and flow curvature effects.

Symbol : ● ■ ▲
 Parameters : 0 2 5 (fixed pitch angle in degree)

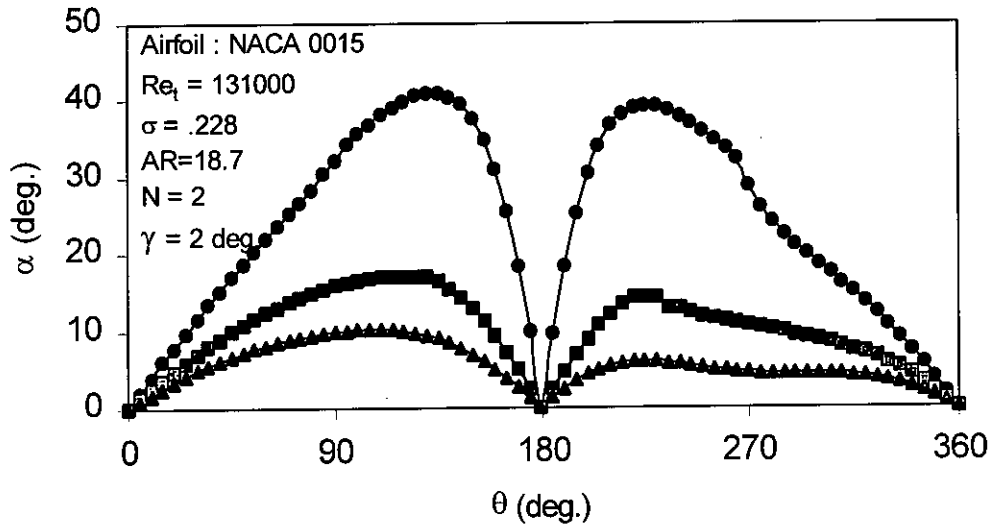


Figure 7.11: Variation of effective blade angles with azimuth angles at different tip speed ratios for fixed pitch angle 2 degree.

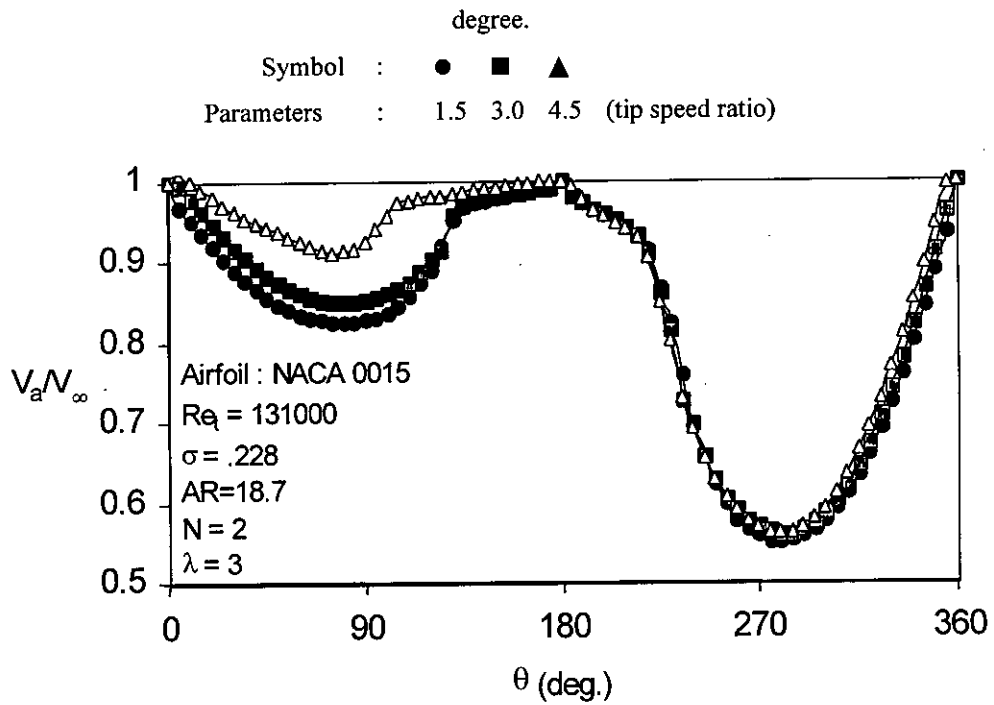


Figure 7.12: Variation of induced velocities with azimuth angles at different fixed blade pitchings with dynamic stall and flow curvature effects.

Symbol : ● ■ ▲
Parameters : 0 2 5 (fixed pitch angle in degree)

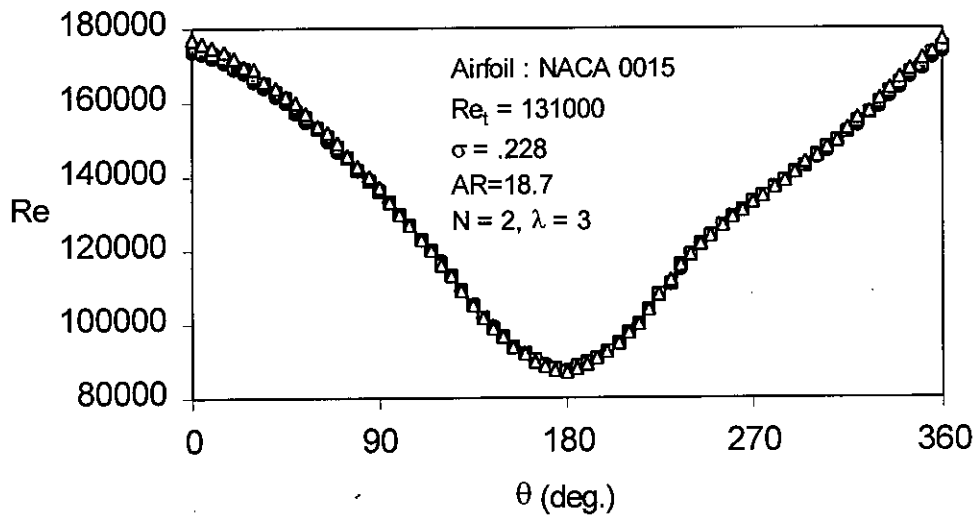


Figure 7.13: Variation of local Reynolds numbers with azimuth angles at different fixed blade pitchings with dynamic stall and flow curvature effects.

Symbol : ● ■ ▲
 Parameters : 0 2 5 (fixed pitch angle in degree)

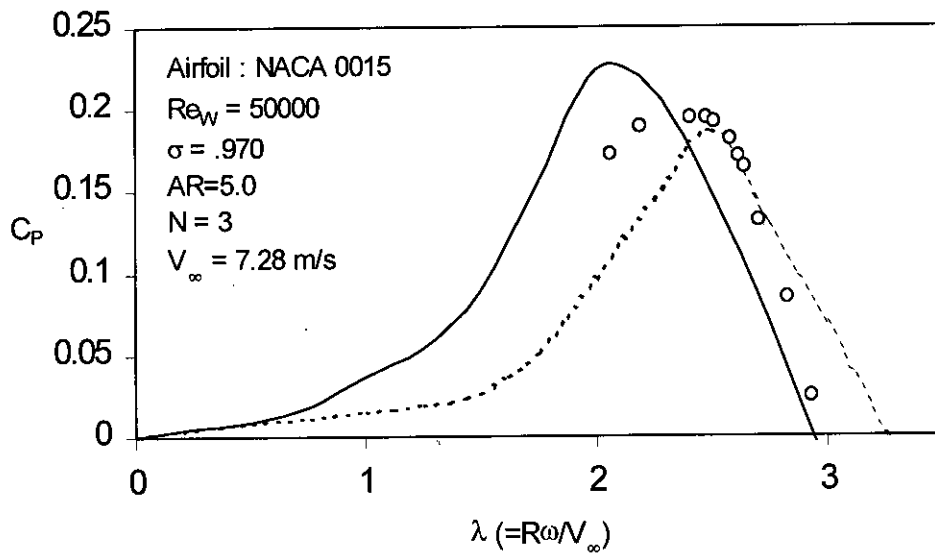


Figure 7.14: Comparison of experimental and calculated overall power coefficients.

———— with dynamic stall and flow curvature
 - - - - - without dynamic stall and flow curvature
 ● experimental (Decleyre et al, 1981)

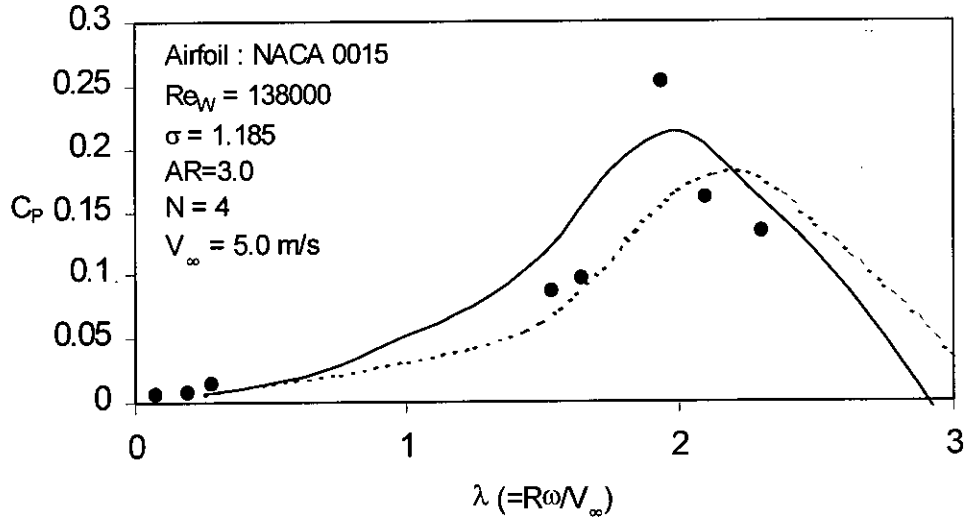


Figure 7.15: Comparison of experimental and calculated overall power coefficients.

- with dynamic stall and flow curvature
- - - - without dynamic stall and flow curvature
- experimental (Mays and Musgrove, 1979)

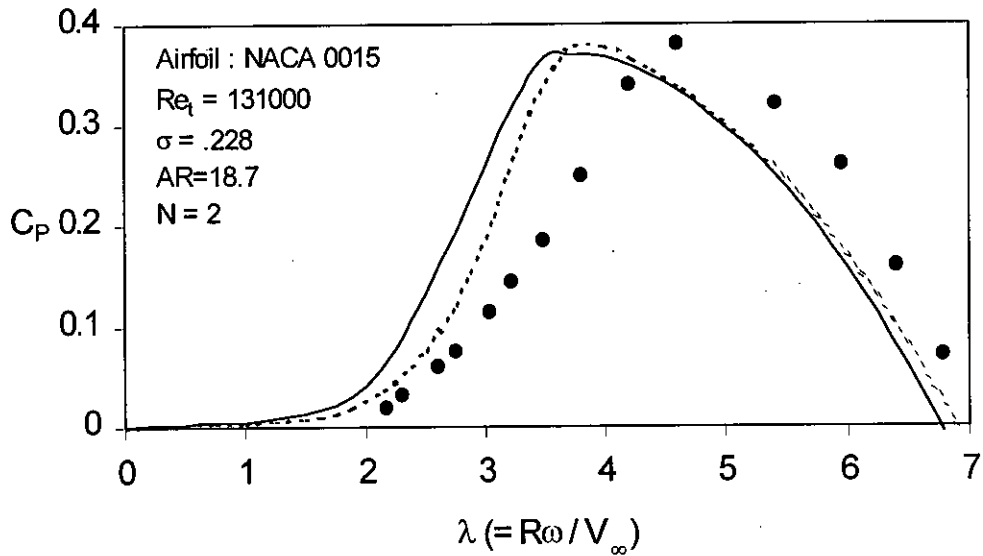


Figure 7.16: Comparison of experimental and calculated overall power coefficients.

- with dynamic stall and flow curvature
- - - - without dynamic stall and flow curvature
- experimental (Migliore et al, 1980)

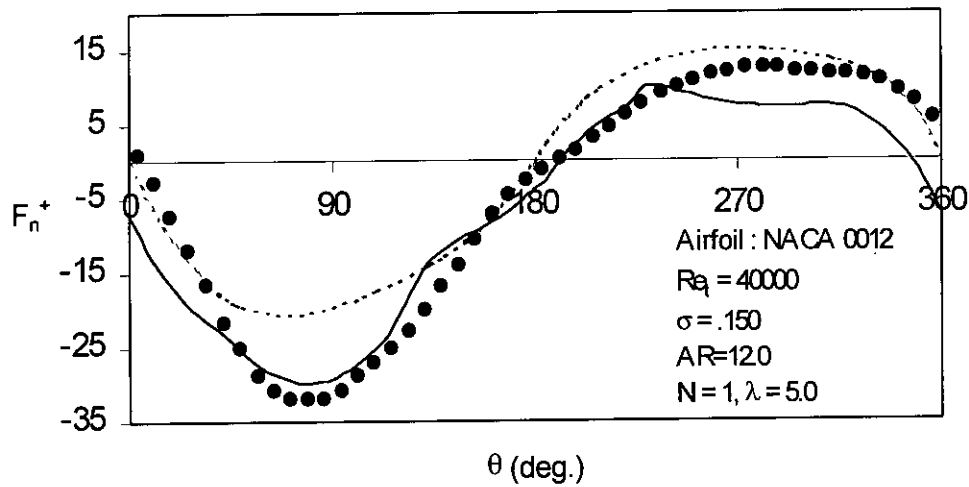


Figure 7.17: Comparison of experimental and calculated non-dimensional normal forces.

- with dynamic stall and flow curvature
- - - without dynamic stall and flow curvature
- experimental (Strickland et al, 1981)

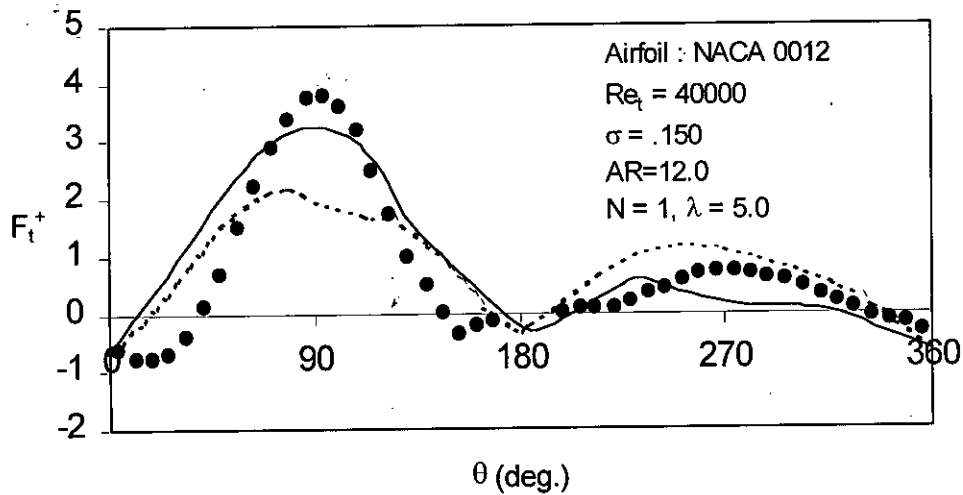


Figure 7.18: Comparison of experimental and calculated non-dimensional tangential forces.

- with dynamic stall and flow curvature
- - - without dynamic stall and flow curvature
- experimental (Strickland et al, 1981)

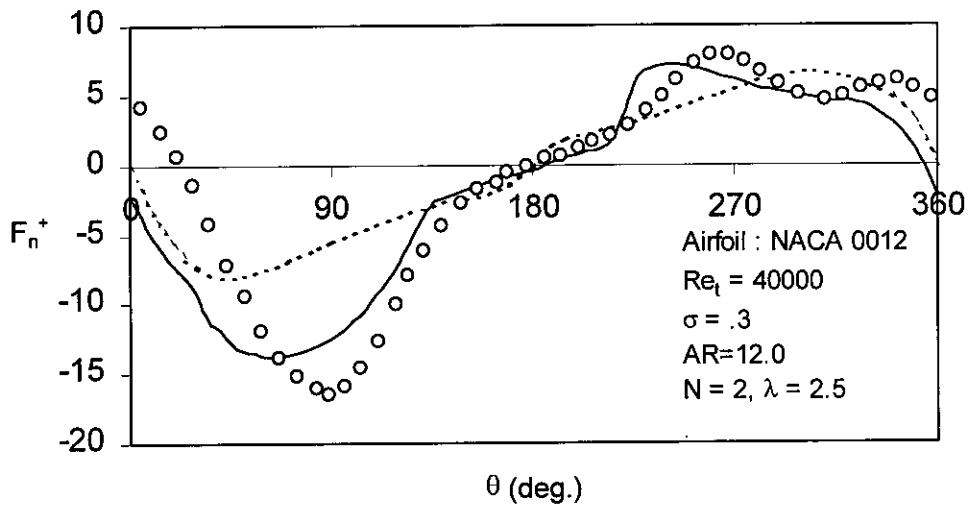


Figure 7.19: Comparison of experimental and calculated non-dimensional normal forces.

- with dynamic stall and flow curvature
- - - without dynamic stall and flow curvature
- experimental (Strickland et al, 1981)

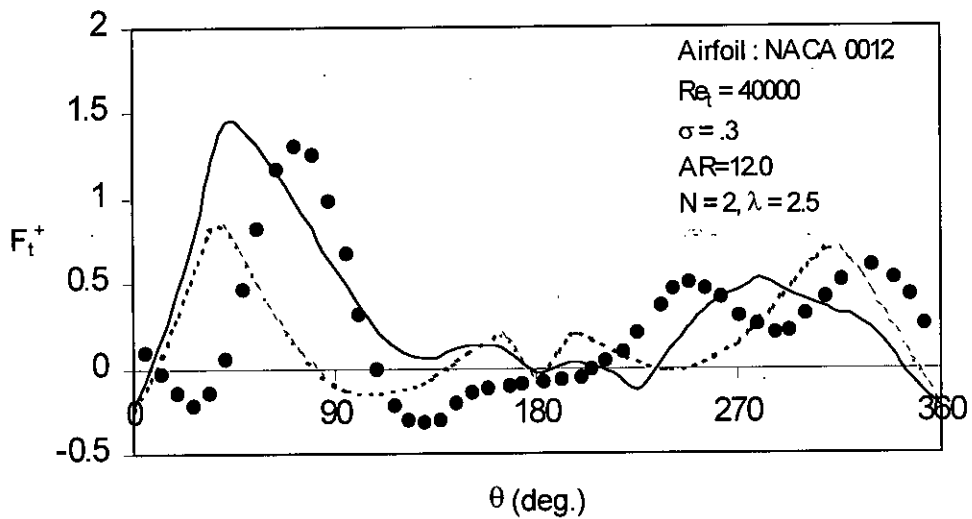


Figure 7.20: Comparison of experimental and calculated non-dimensional tangential forces.

- with dynamic stall and flow curvature
- - - without dynamic stall and flow curvature
- experimental (Strickland et al, 1981)

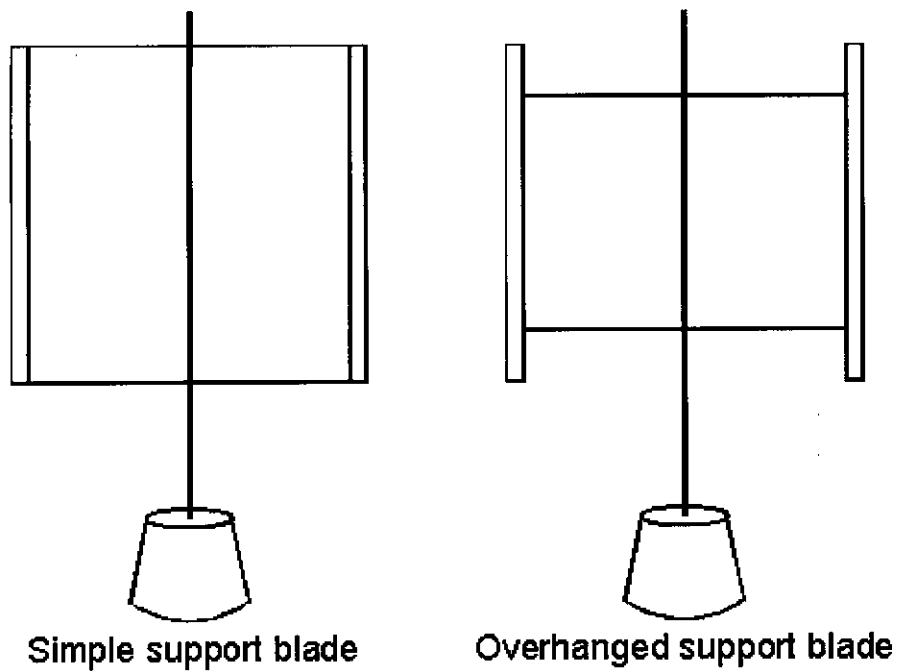


Figure 8.1: Straight-bladed vertical-axis Darrieus wind turbine

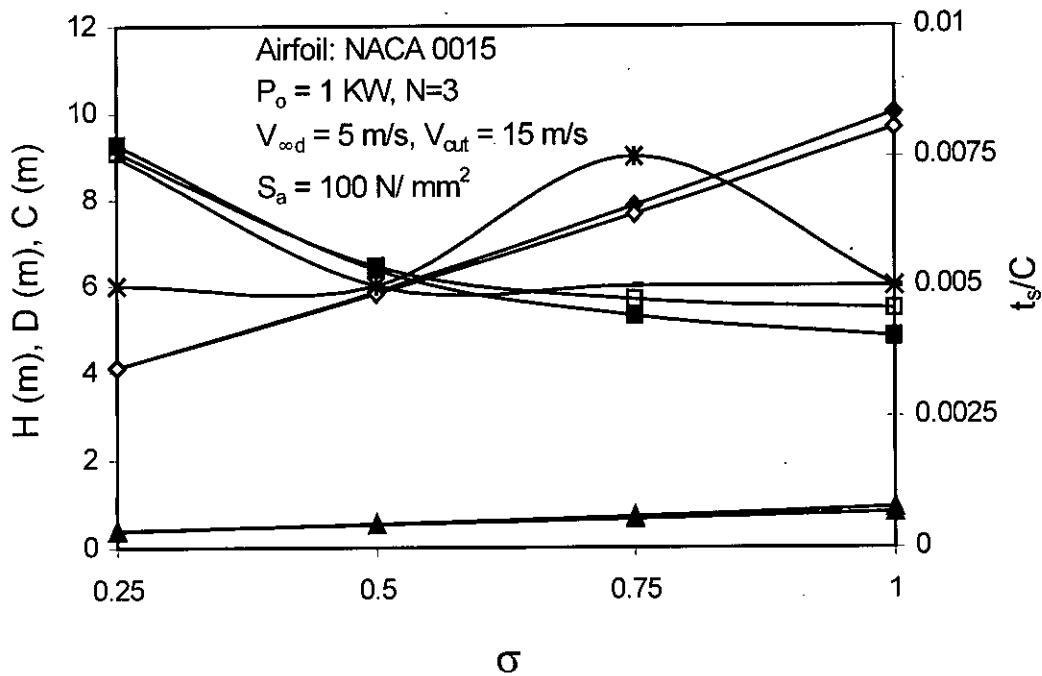


Figure 8.2: Design configurations of 1 kW variable speed straight-bladed VAWT at various solidities

Symbol : ■ ▲ ◆ × (with dynamic stall & flow curvature effect)
 □ △ ◇ + (without dynamic stall & flow curvature effect)
 Parameters : D C H t_s/C

92790

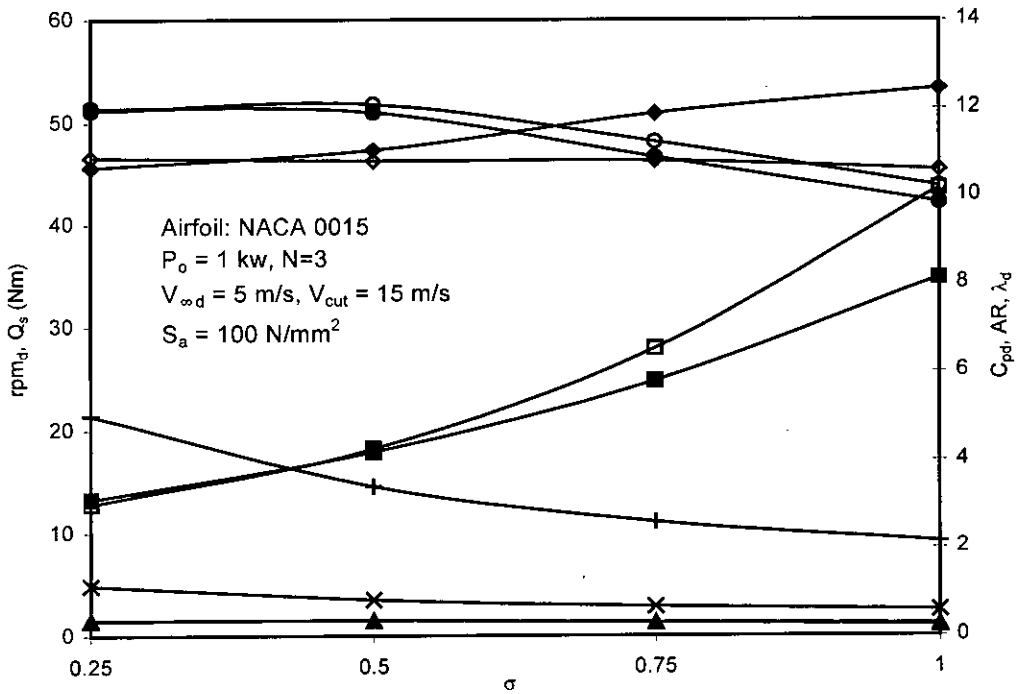


Figure 8.3: Design configurations of 1KW variable speed straight-bladed VAWT at various solidities

Symbol : ■ ▲ ● ◆ + (with dynamic stall & flow curvature)
 □ △ ○ ◇ × (without dynamic stall & flow curvature)
 Parameters : Q_s C_p rpm_d AR λ_d

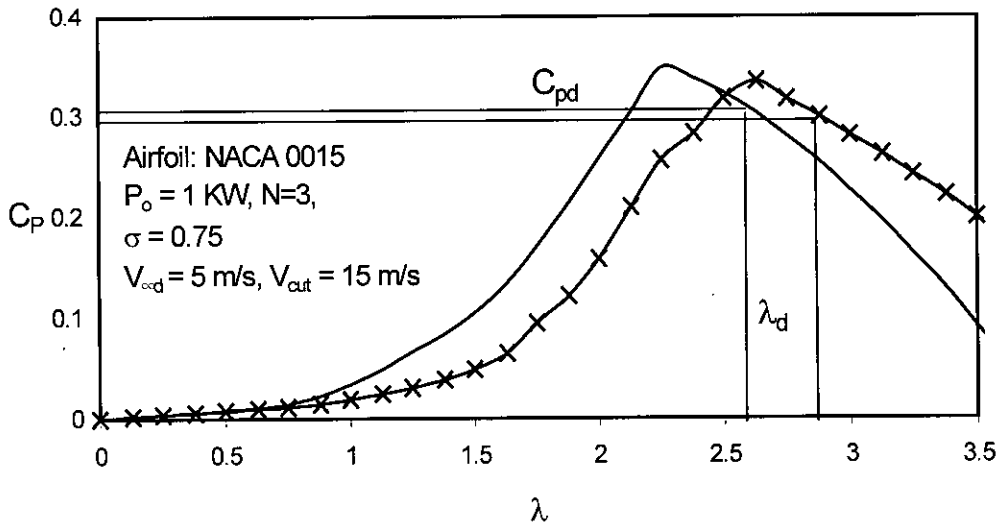


Figure 8.4: Variation of overall power coefficients with tip speed ratio

Symbol : - (with dynamic stall & flow curvature)
 × (without dynamic stall & flow curvature)



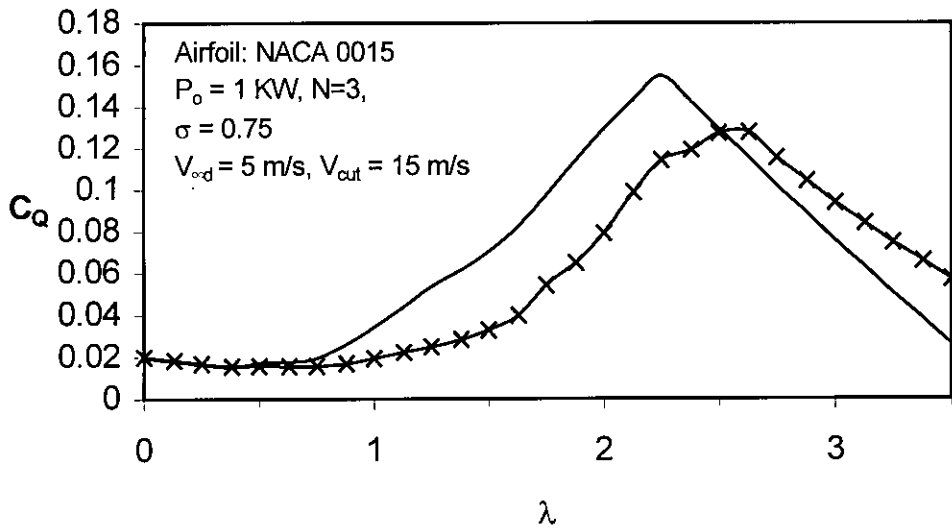


Figure 8.5: Variation of overall torque coefficients with tip speed ratio

Symbol : - (with dynamic stall & flow curvature)
 × (without dynamic stall & flow curvature)

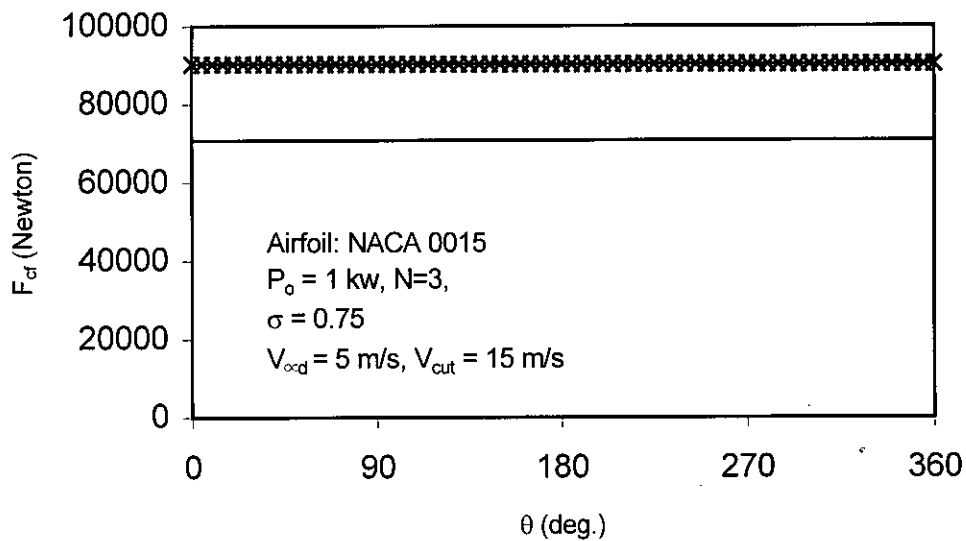


Figure 8.6: Variation of centrifugal force with azimuth angle

Symbol : - (with dynamic stall & flow curvature)
 × (without dynamic stall & flow curvature)

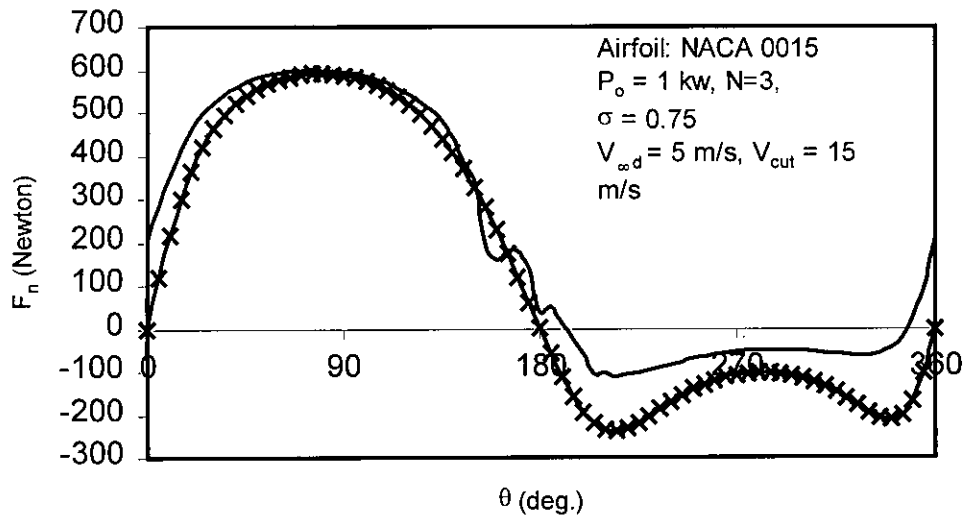


Figure 8.7: Variation of normal force with azimuth angle
 Symbol : - (with dynamic stall & flow curvature)
 × (without dynamic stall & flow curvature)

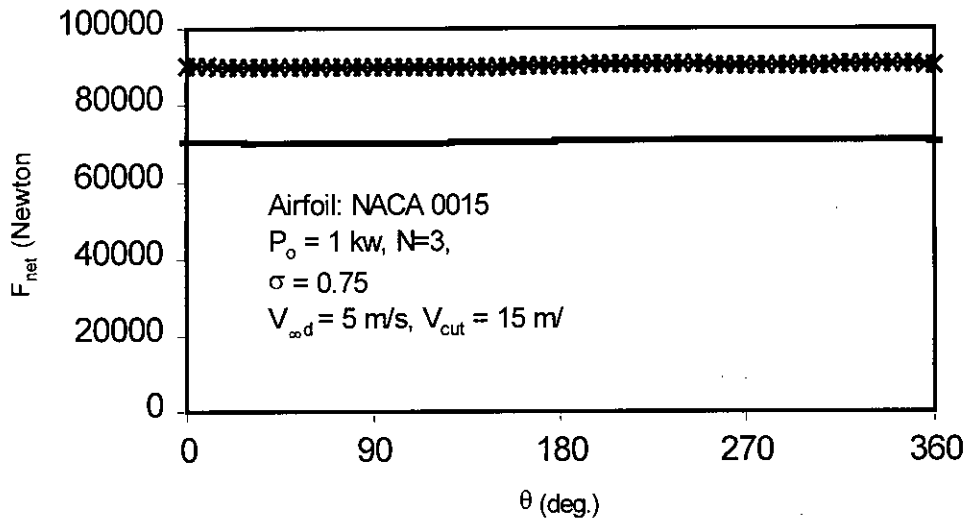


Figure 8.8: Variation of net normal force with azimuth angle
 Symbol : - (with dynamic stall & flow curvature)
 × (without dynamic stall & flow curvature)

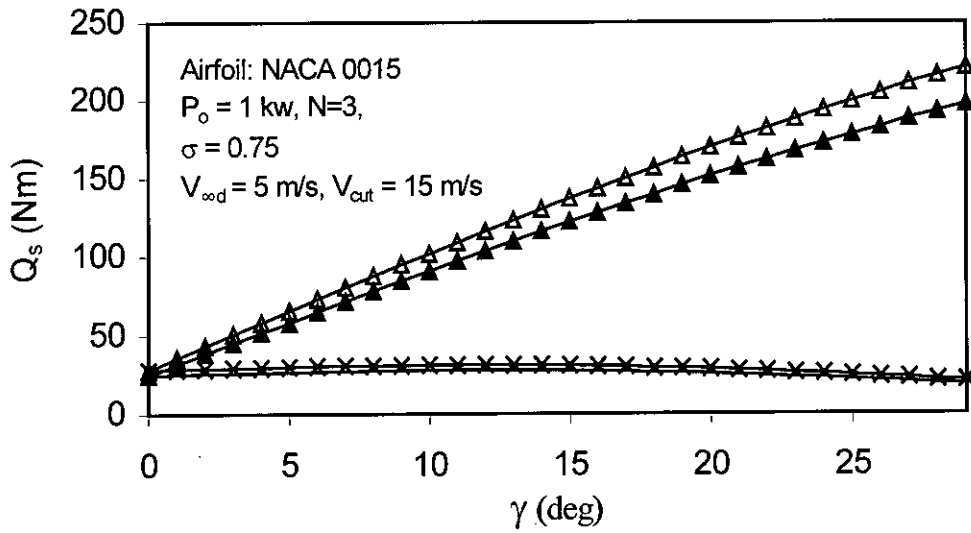


Figure 8.9: Variation of starting torque with blade pitching

Symbol : ▲ - (with dynamic stall & flow curvature effect)
 △ × (with dynamic stall & flow curvature effect)
 Parameters : Variable Fixed

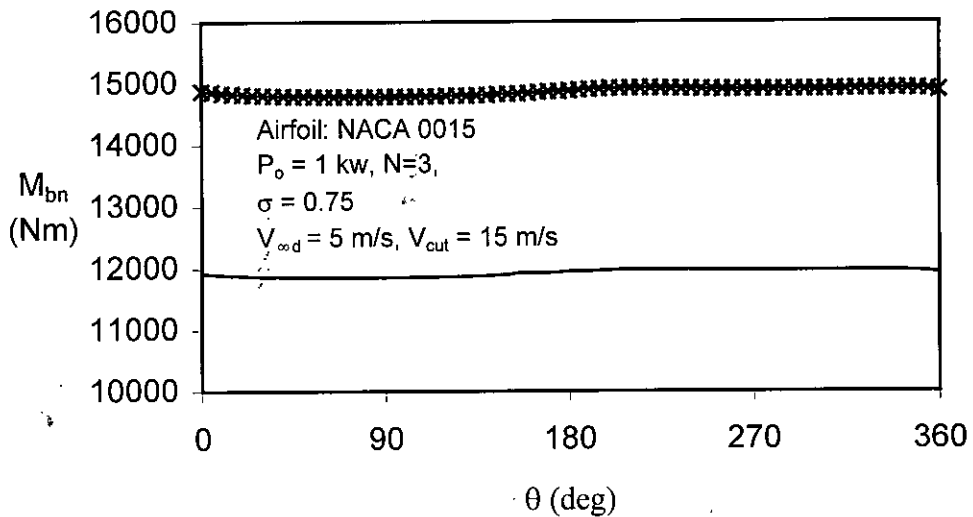


Figure 8.10: Variation of bending moments due to net normal forces with azimuth angle

Symbol : - (with dynamic stall & flow curvature)
 × (without dynamic stall & flow curvature)

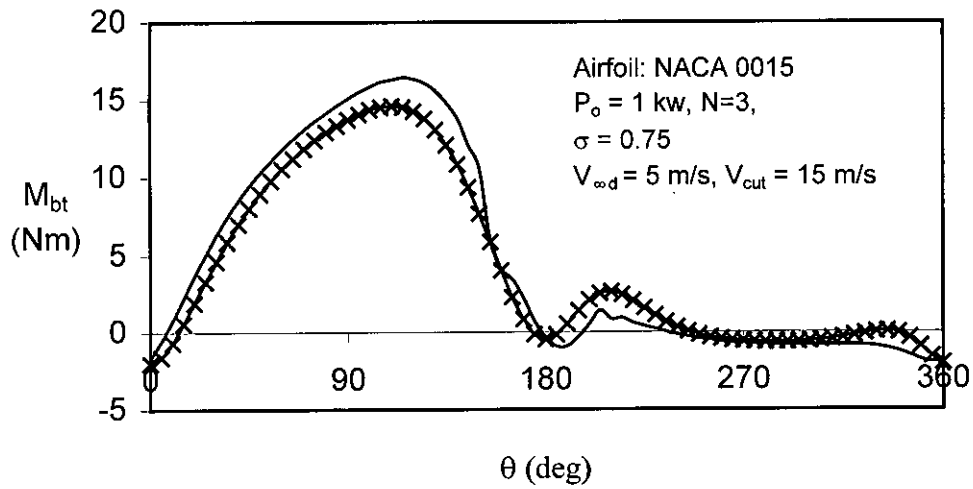


Figure 8.11: Variation of bending moments due to tangential forces with azimuth angle

Symbol : - (with dynamic stall & flow curvature)

× (without dynamic stall & flow curvature)

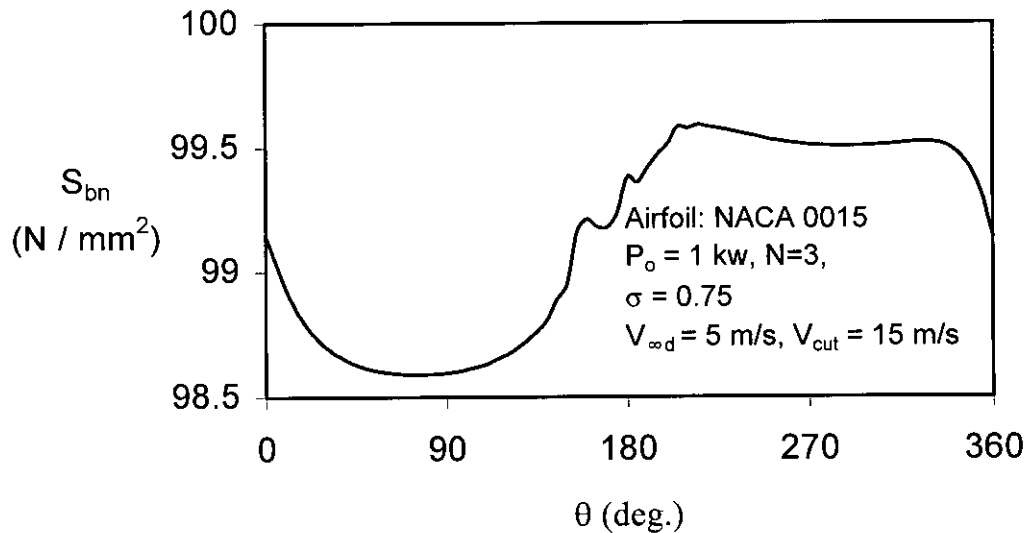


Figure 8.12: Variation of bending stresses due to net normal forces with azimuth angle

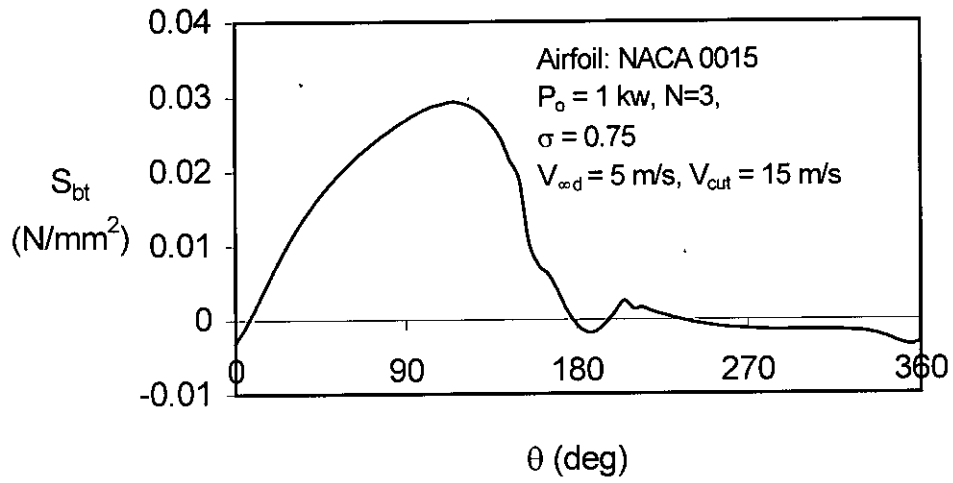


Figure 8.13: Variation of bending stress due to tangential forces with azimuth angle

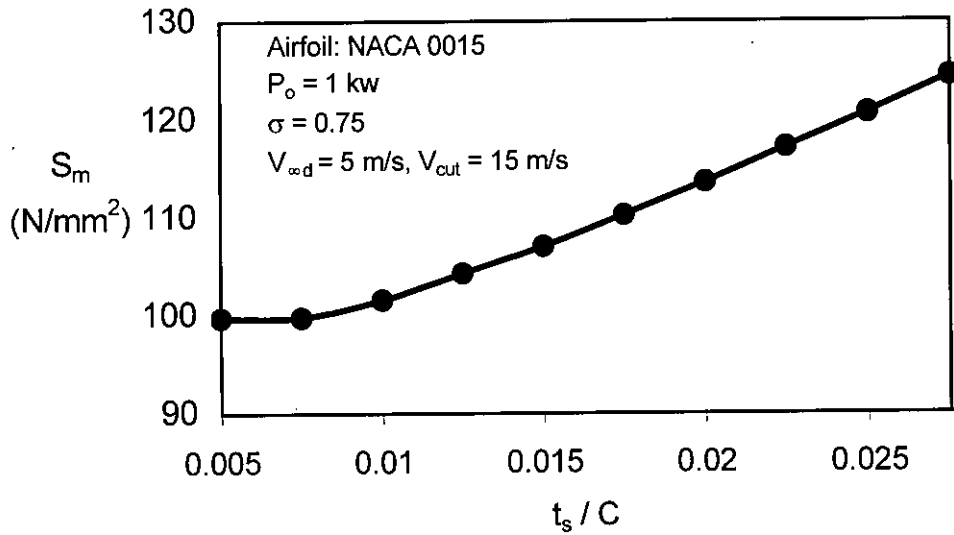


Figure 8.14: Variation of maximum blade stress with blade skin thickness

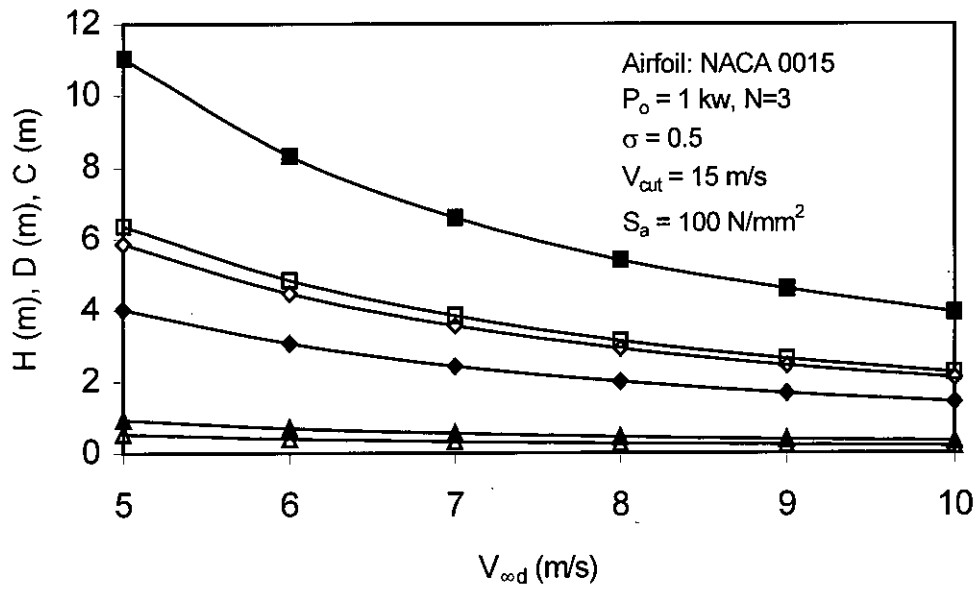


Figure 8.15: Comparison of design configurations of 1 KW variable speed straight-bladed VAWT at various wind velocities

Symbol : ■ ▲ ◆ (simple support)
 □ △ ◇ (overhang support)
 Parameters : D C H

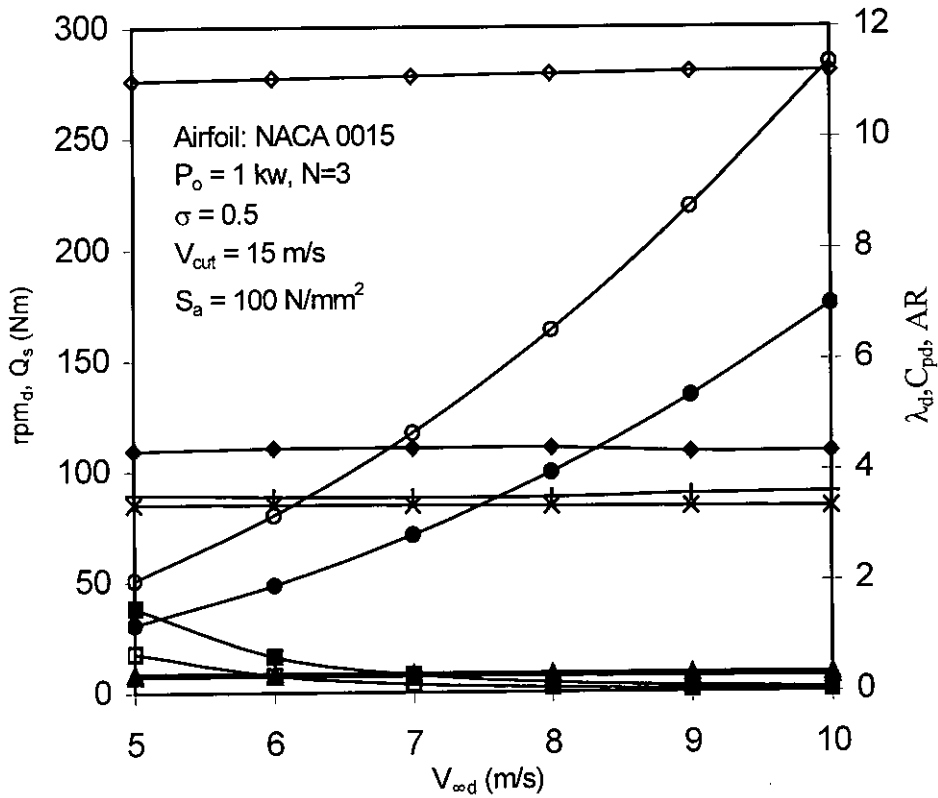


Figure 8.16: Comparison of design configurations of 1KW variable speed straight-bladed VAWT at various wind velocities

Symbol: ■ ▲ ● ◆ + (Simple support)
 □ △ ○ ◇ × (overhang support)
 Parameters: Q_s C_p rpm_d AR λ_d

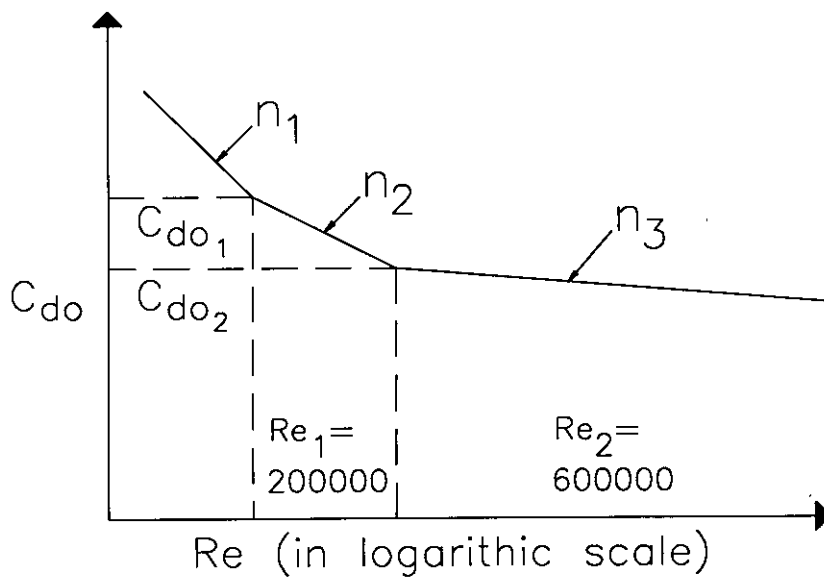


Figure C.1: Zero-lift-drag coefficient as a function of Reynolds number

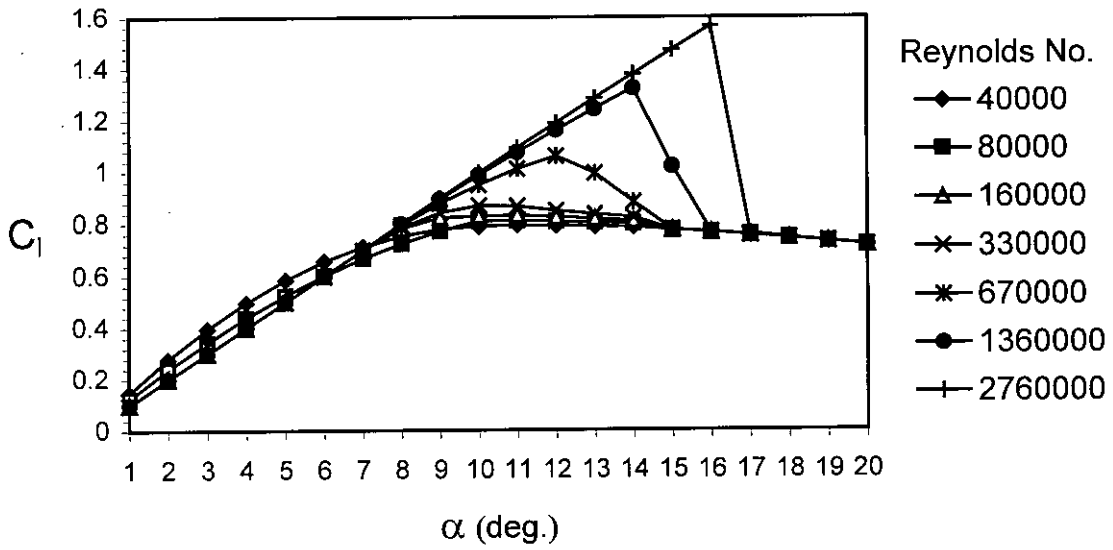


Figure E.1: Variation of lift coefficient with angle of attack at various Reynolds number for the airfoil NACA 0012

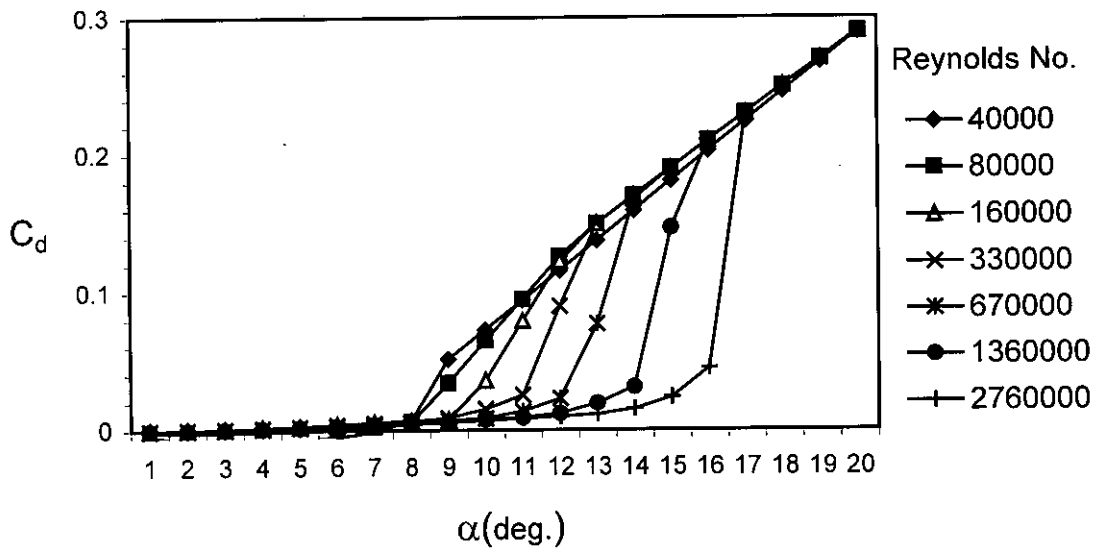


Figure E.2: Variation of drag coefficient with angle of attack at various Reynolds number for the airfoil NACA 0012

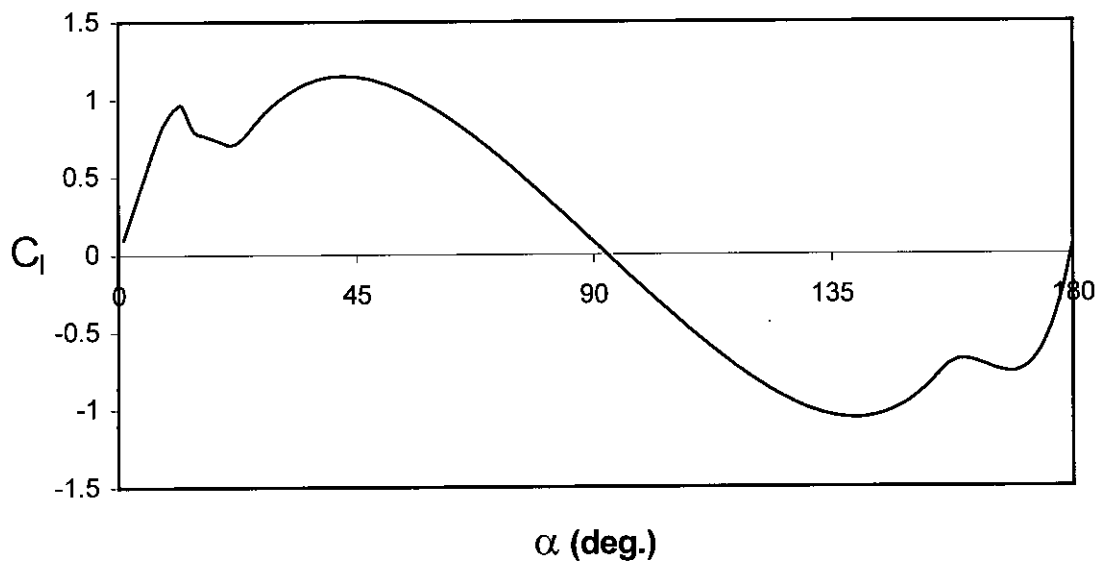


Figure E.3: Variation of lift coefficient with angle of attack at various Reynolds number of 500,000 for the airfoil NACA 0012

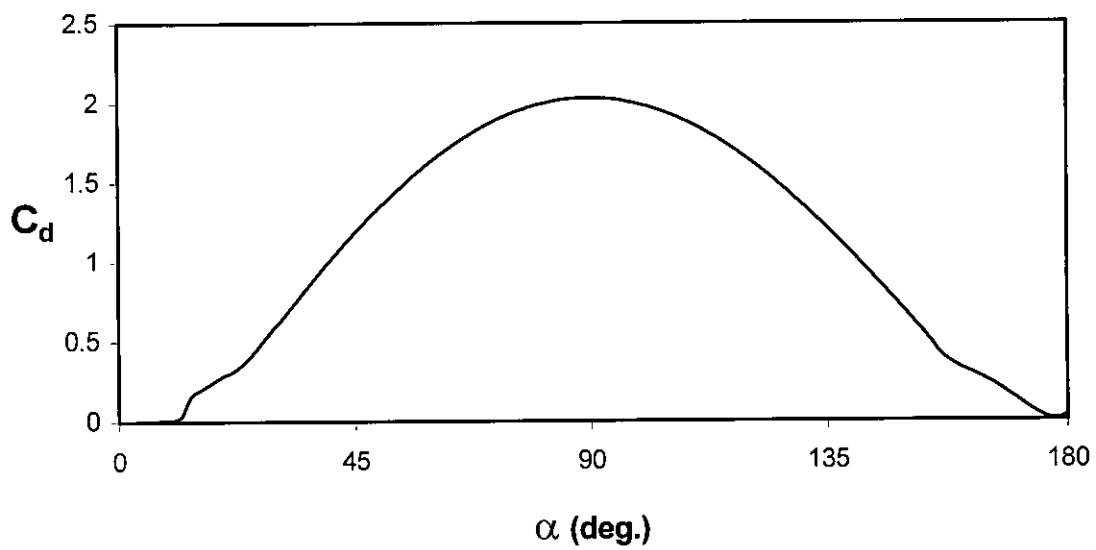


Figure E.4: Variation of drag coefficient with angle of attack at various Reynolds number of 500,000 for the airfoil NACA 0012

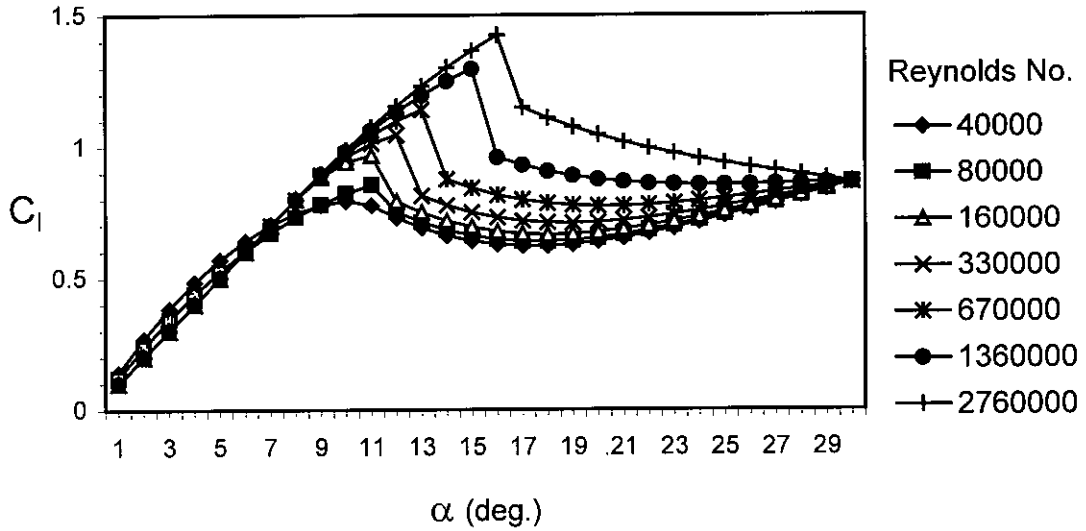


Figure E.5: Variation of lift coefficient with angle of attack at various Reynolds number for the airfoil NACA 0015

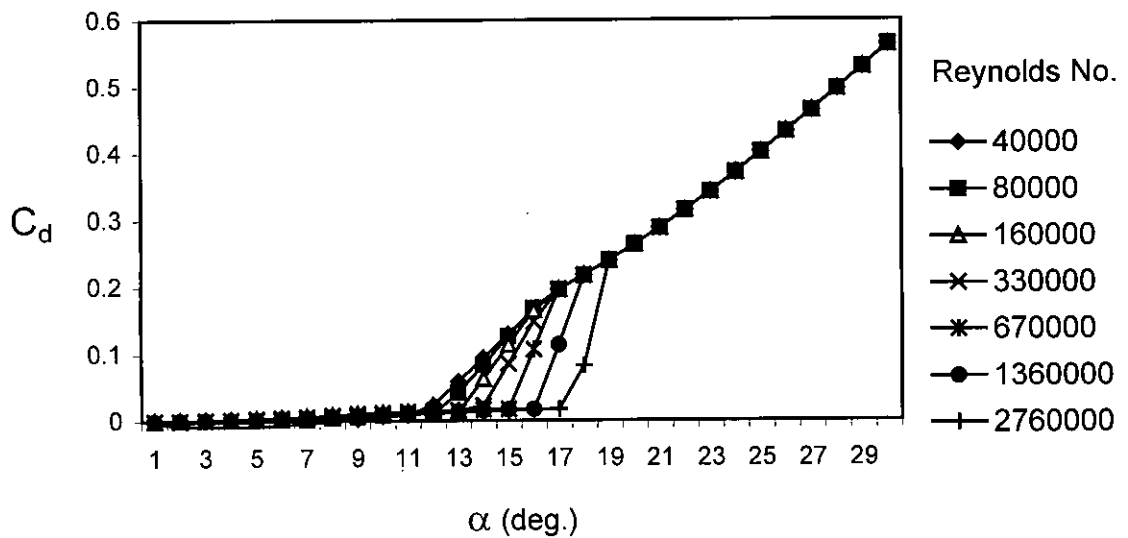


Figure E.6: Variation of drag coefficient with angle of attack at various Reynolds number for the airfoil NACA 0015

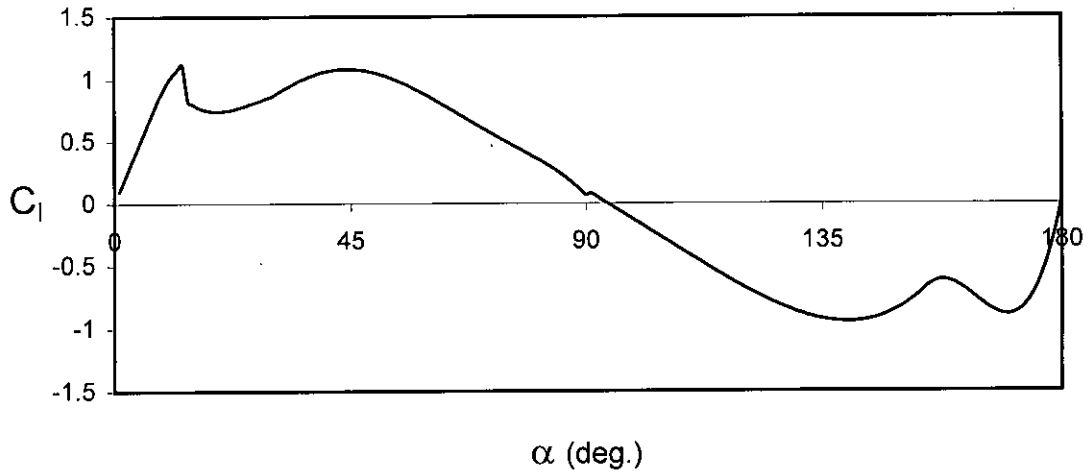


Figure E.7: Variation of lift coefficient with angle of attack at Reynolds number = 500,000 for the airfoil NACA 0015

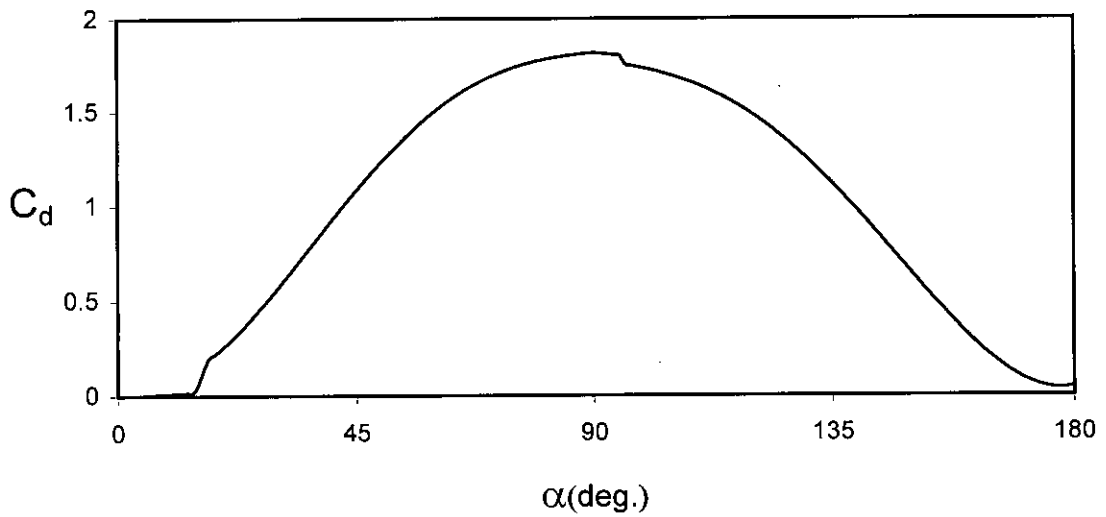


Figure E.8: Variation of drag coefficient with angle of attack at Reynolds number = 500,000 for the airfoil NACA 0015

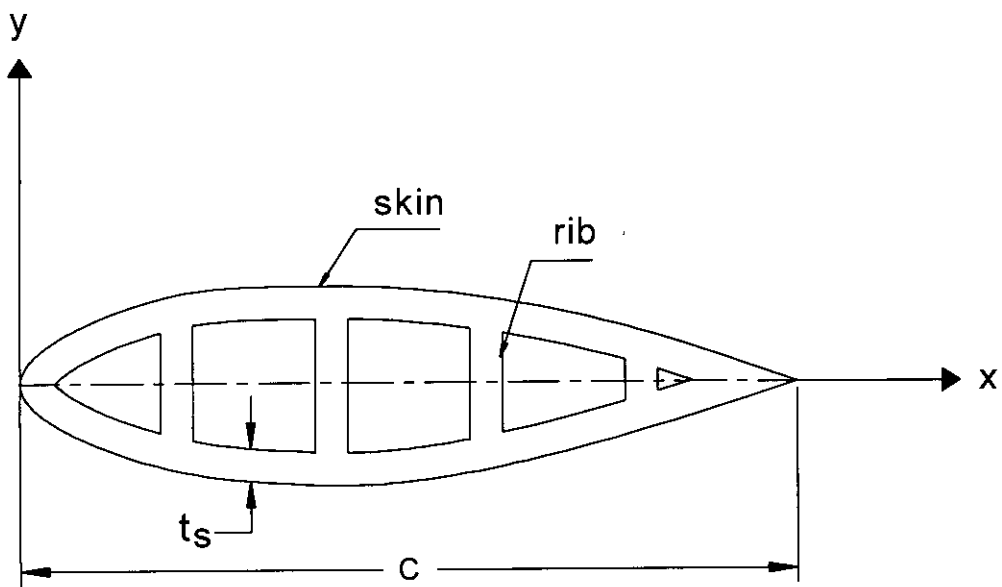


Figure F.1: Blade airfoil cross-section

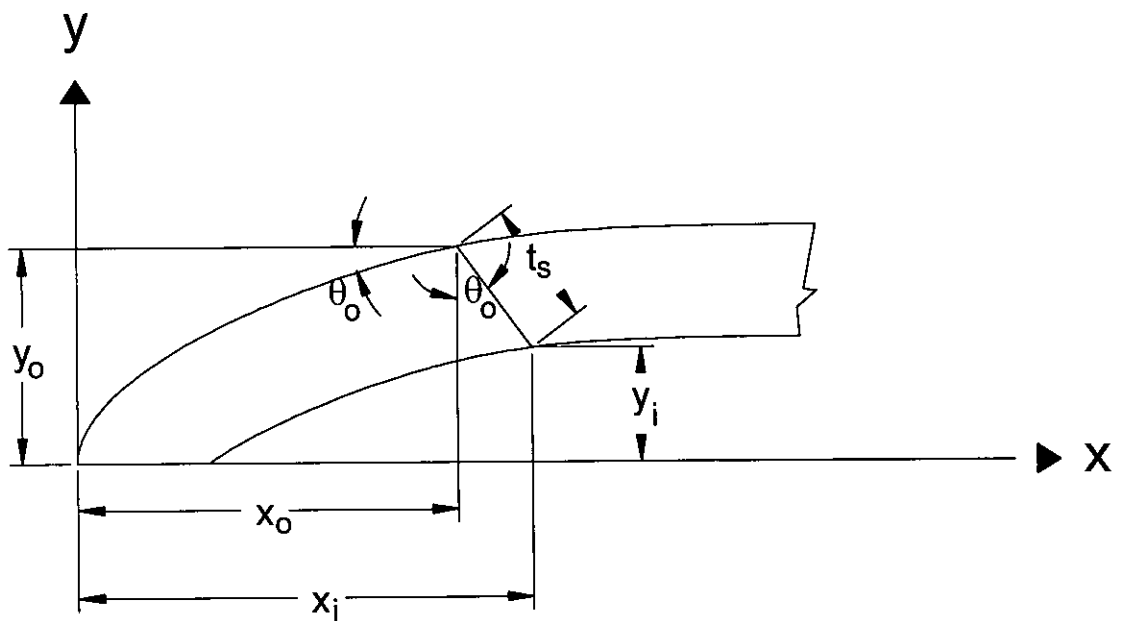


Figure F.2: Geometry of inner and outer faces of blade airfoil.

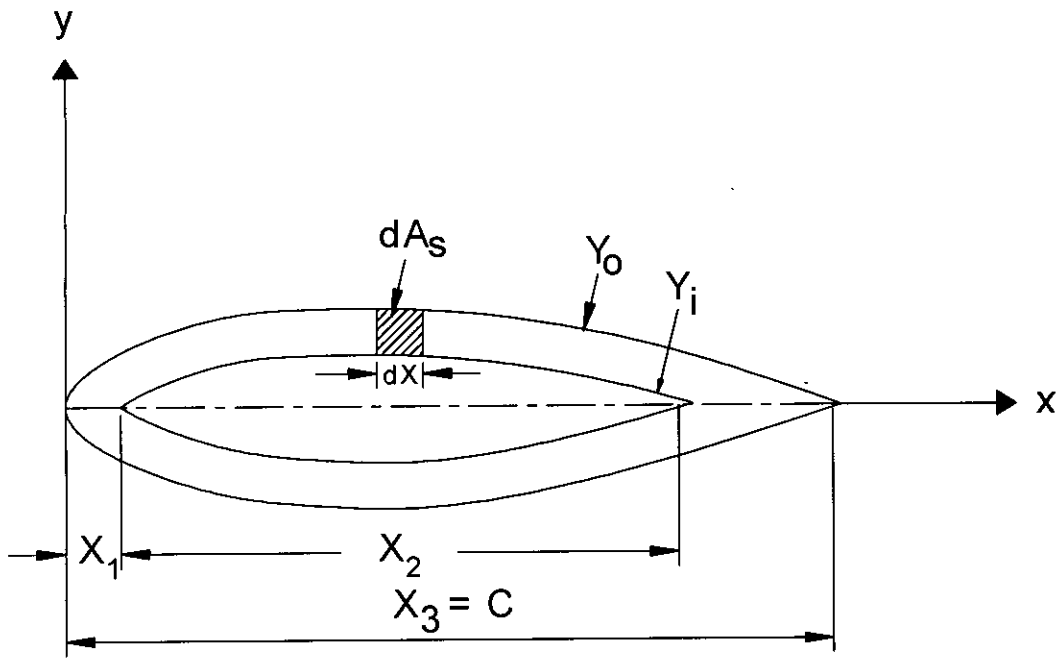


Figure F.3: Geometry of blade airfoil cross-section to find skin area.

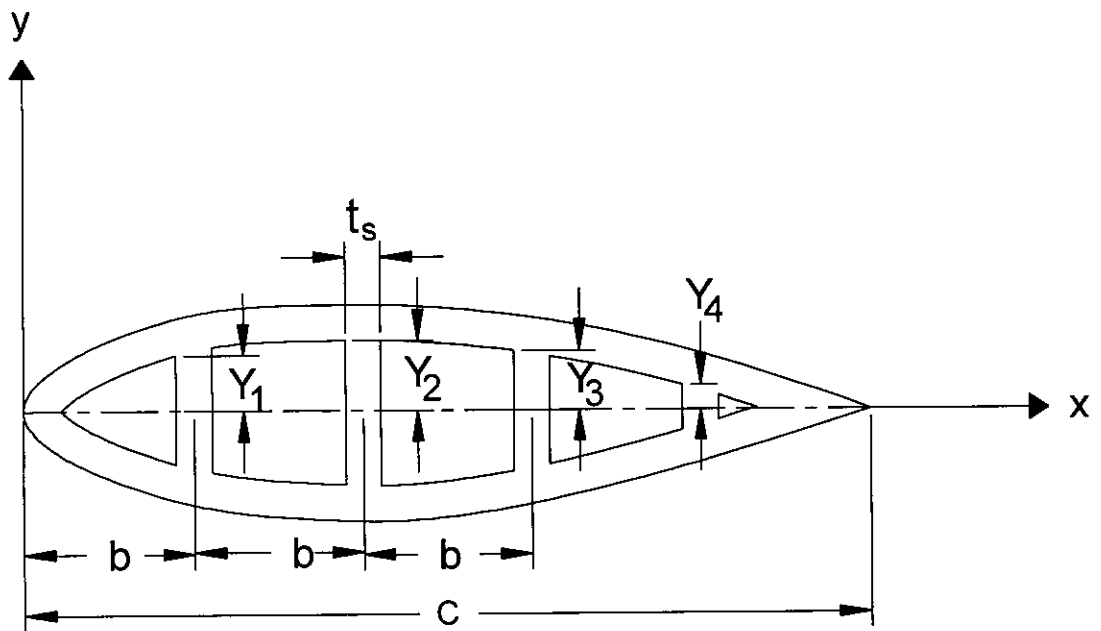


Figure F.4: Geometry to obtain rib area

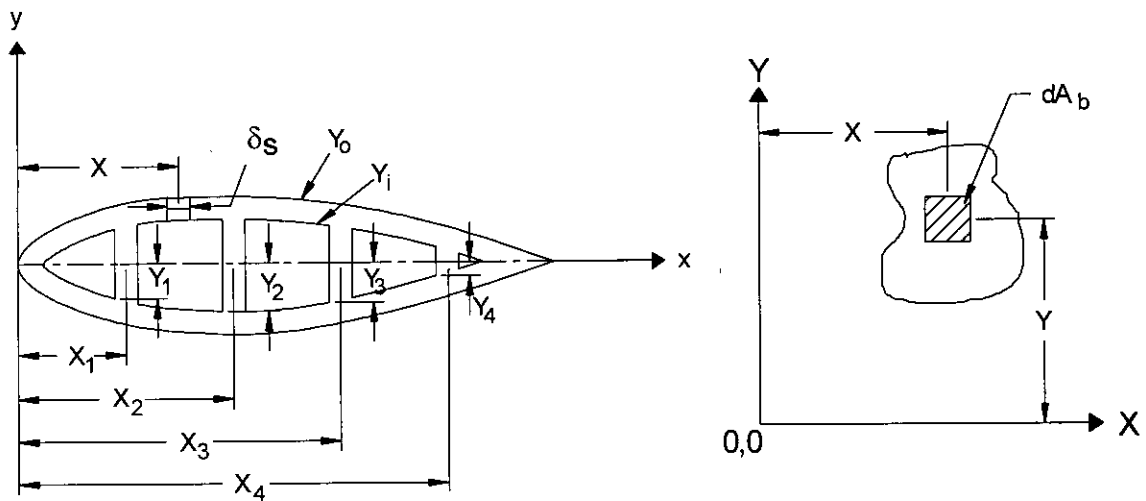


Figure F.5: Geometry to determine centroid and moment of inertia.

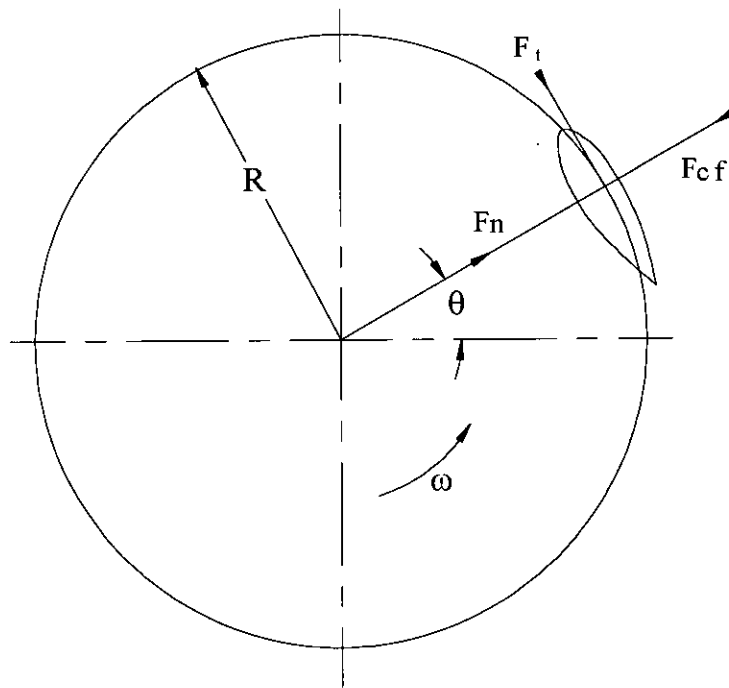


Figure G.1: Horizontal section of a straight-bladed wind turbine showing forces on the turbine blade.

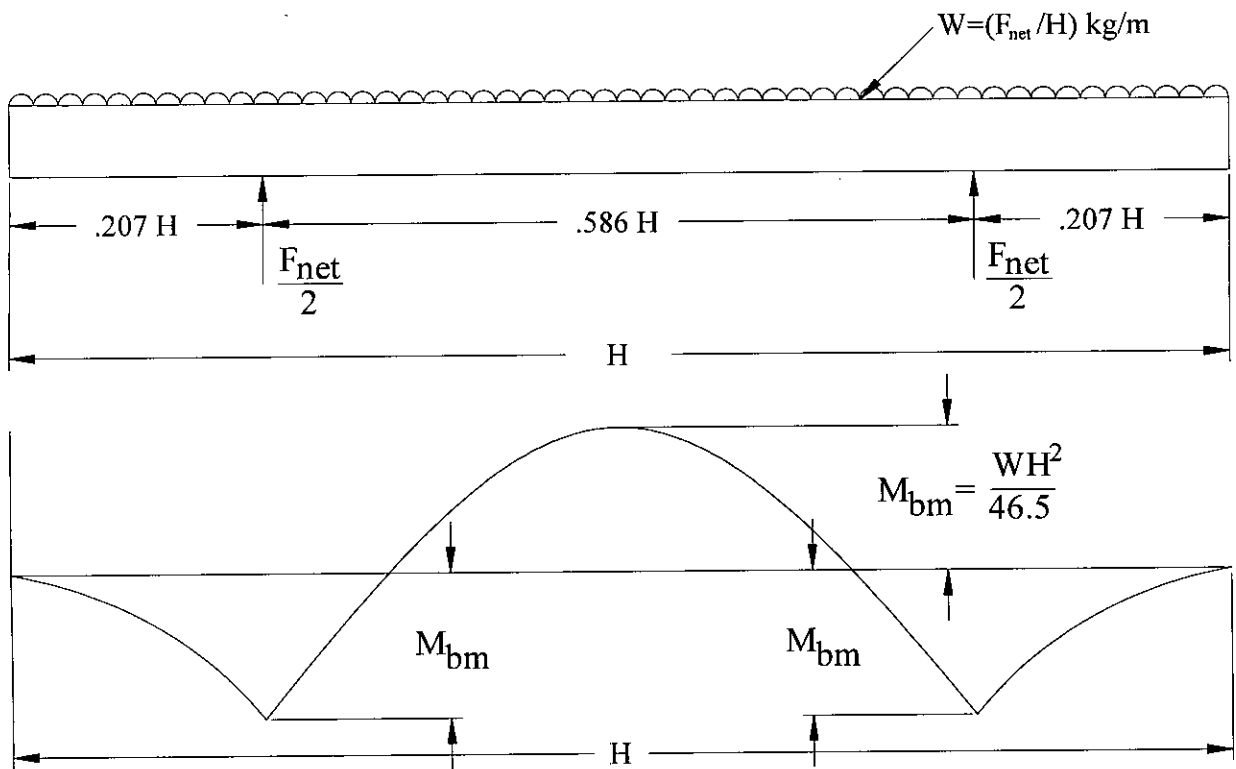
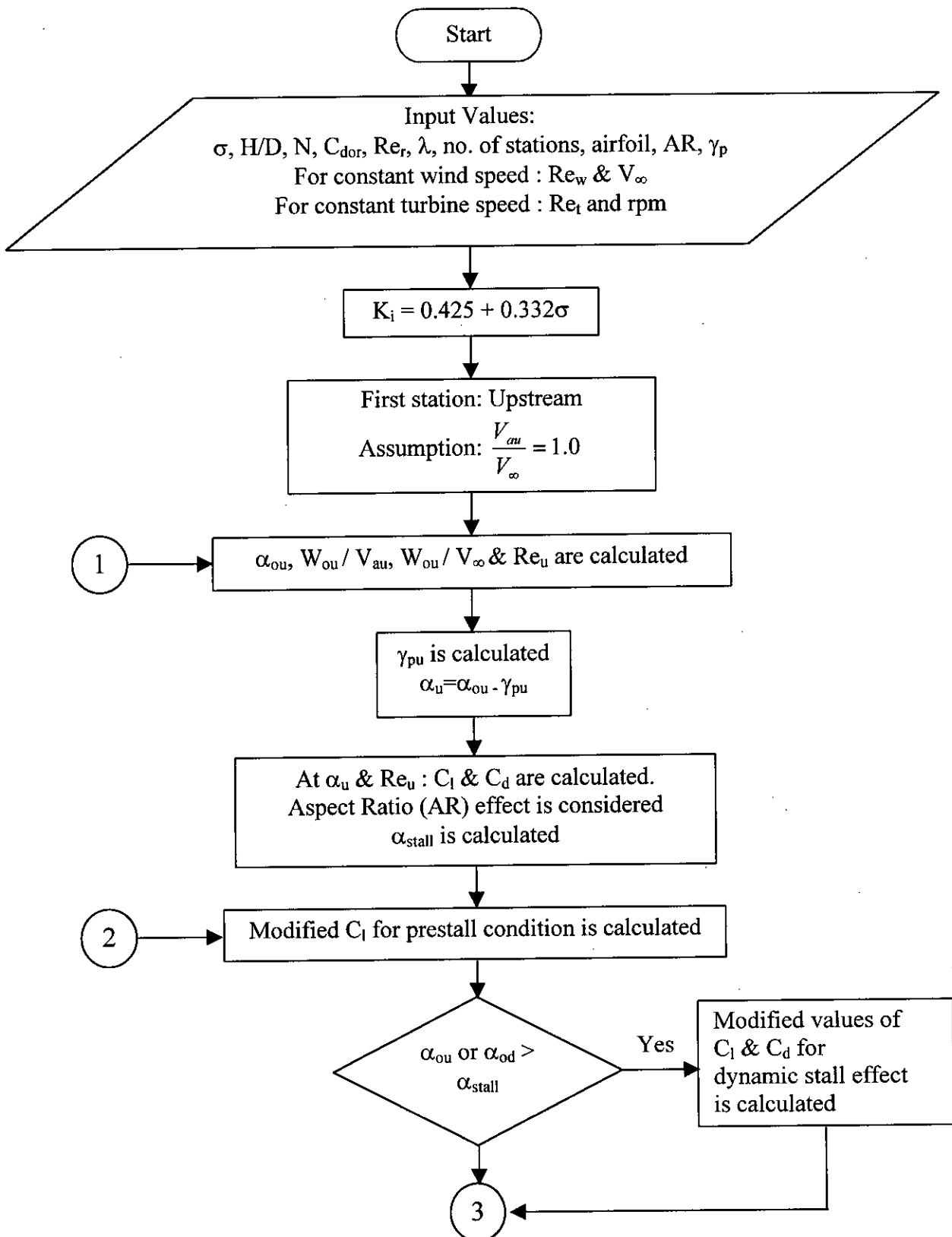
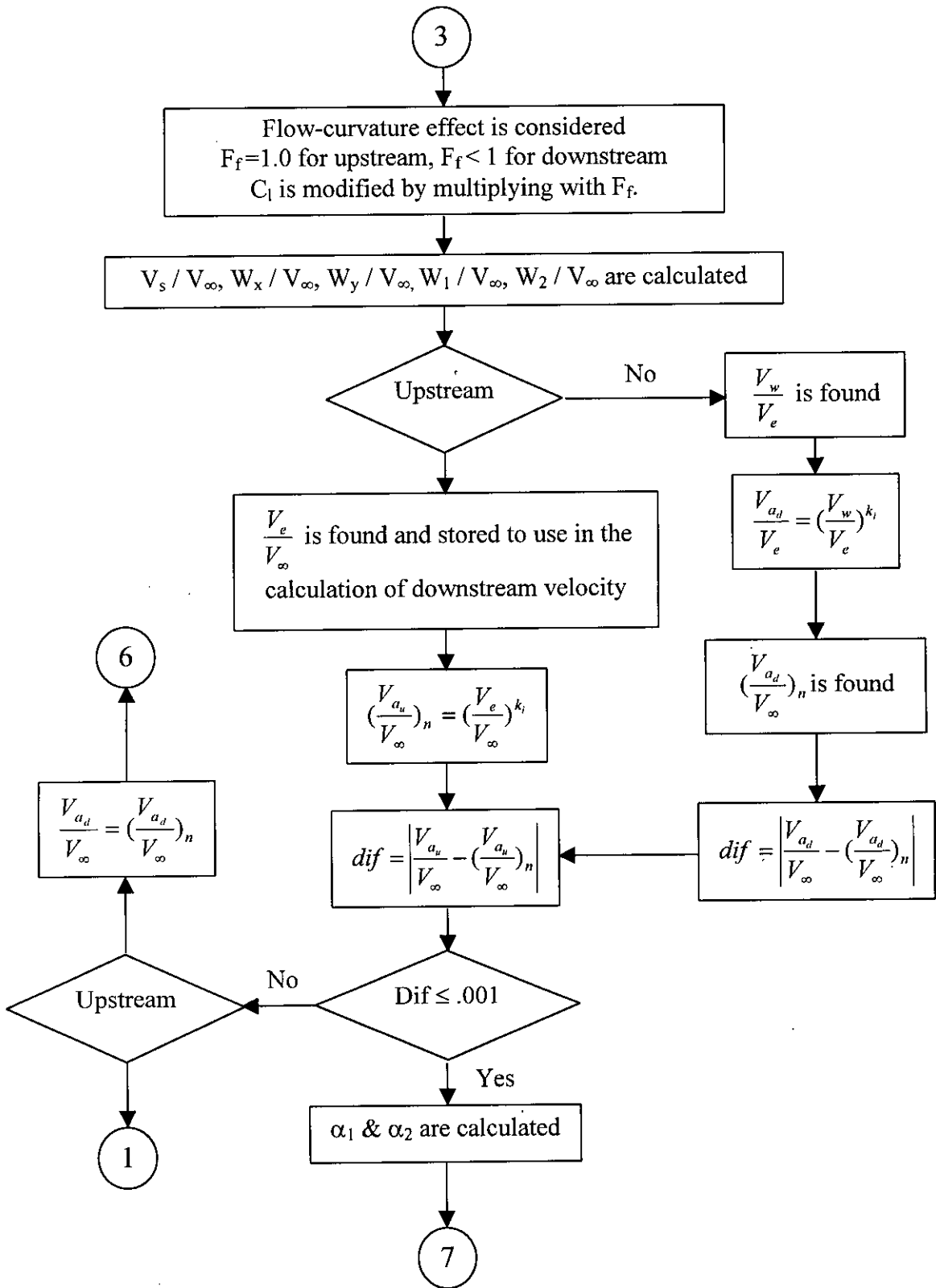


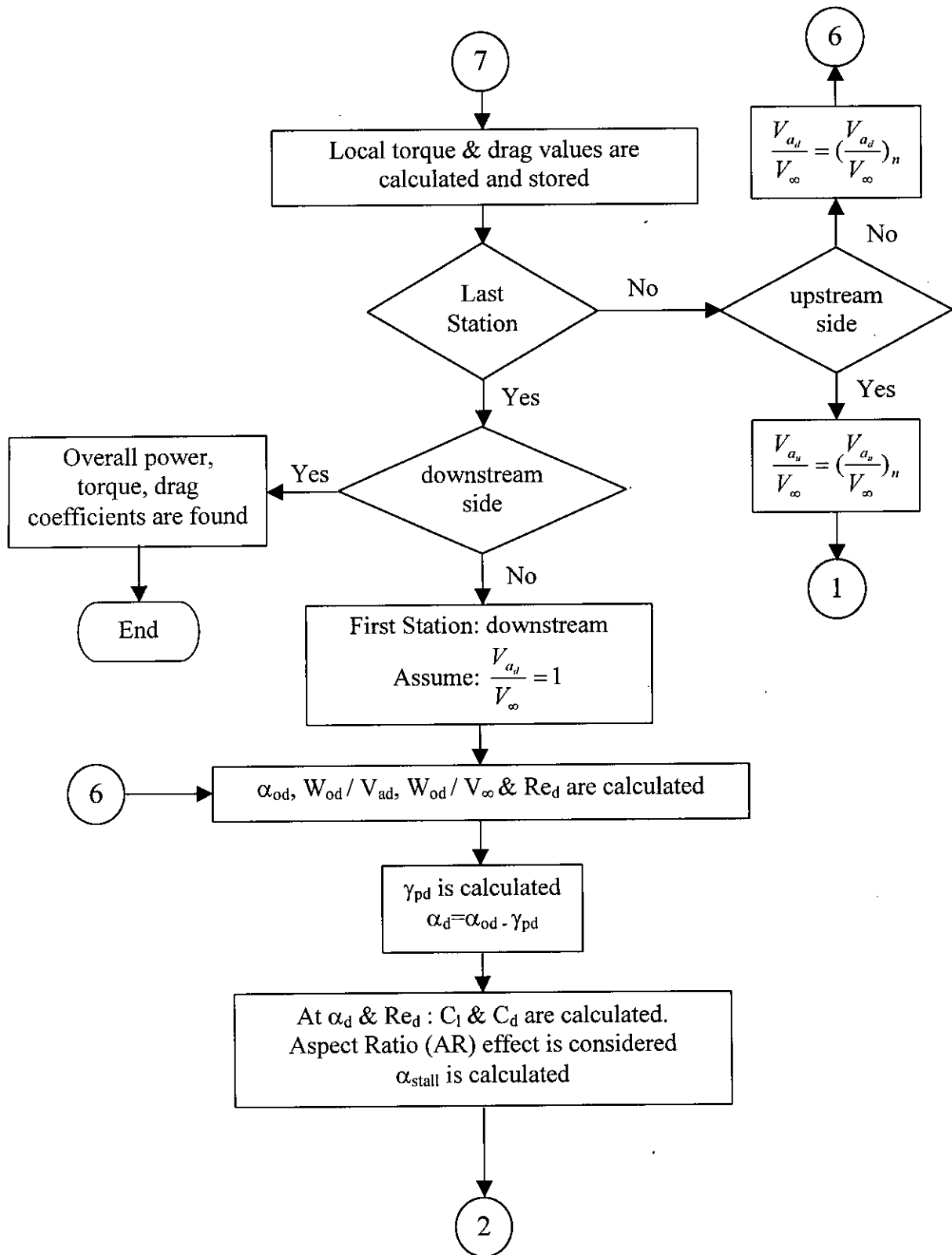
Figure G.2: Bending moment diagram of an overhang supported beam.

APPENDICES

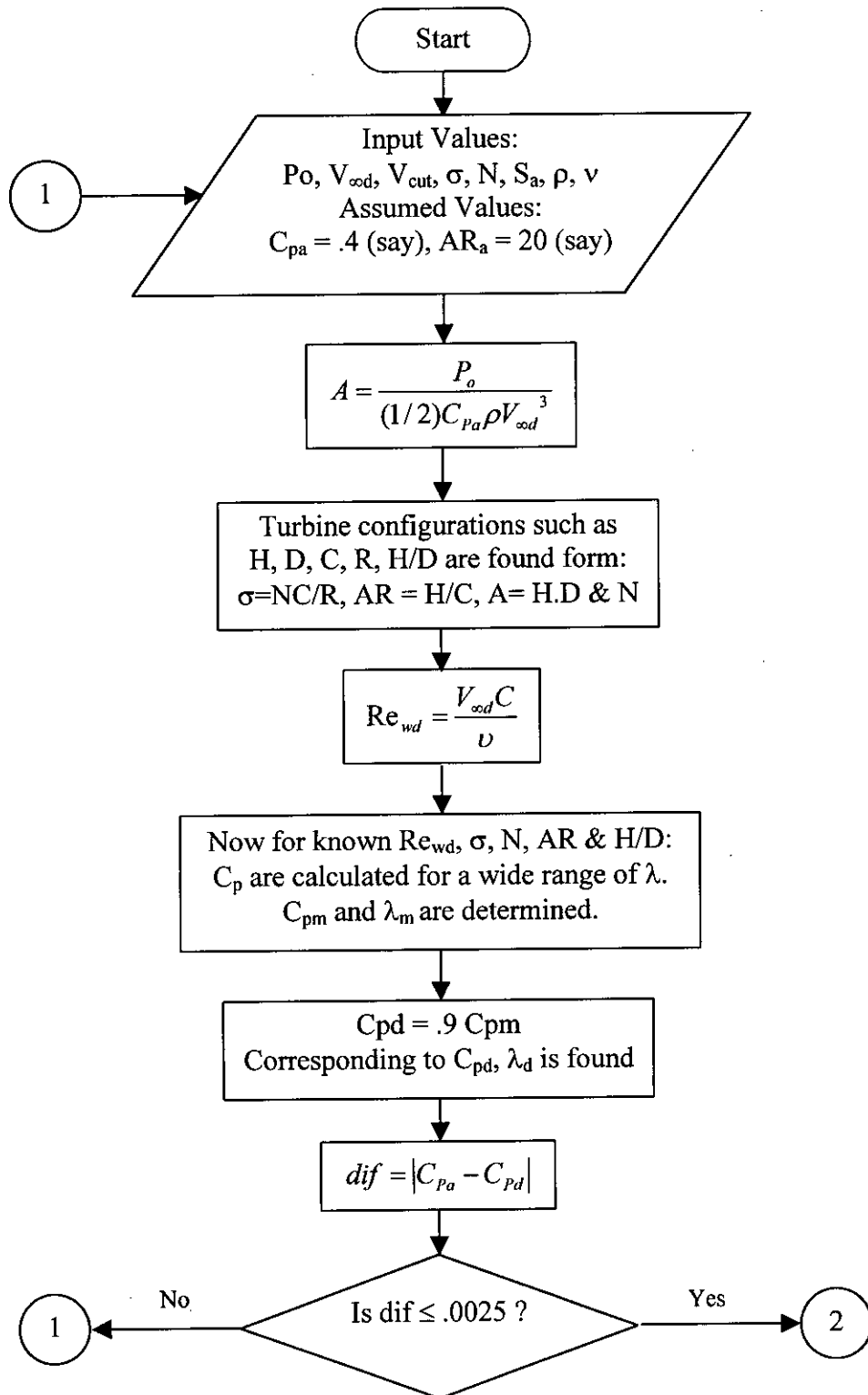
Appendix-A : Flow Diagram of Computational Method

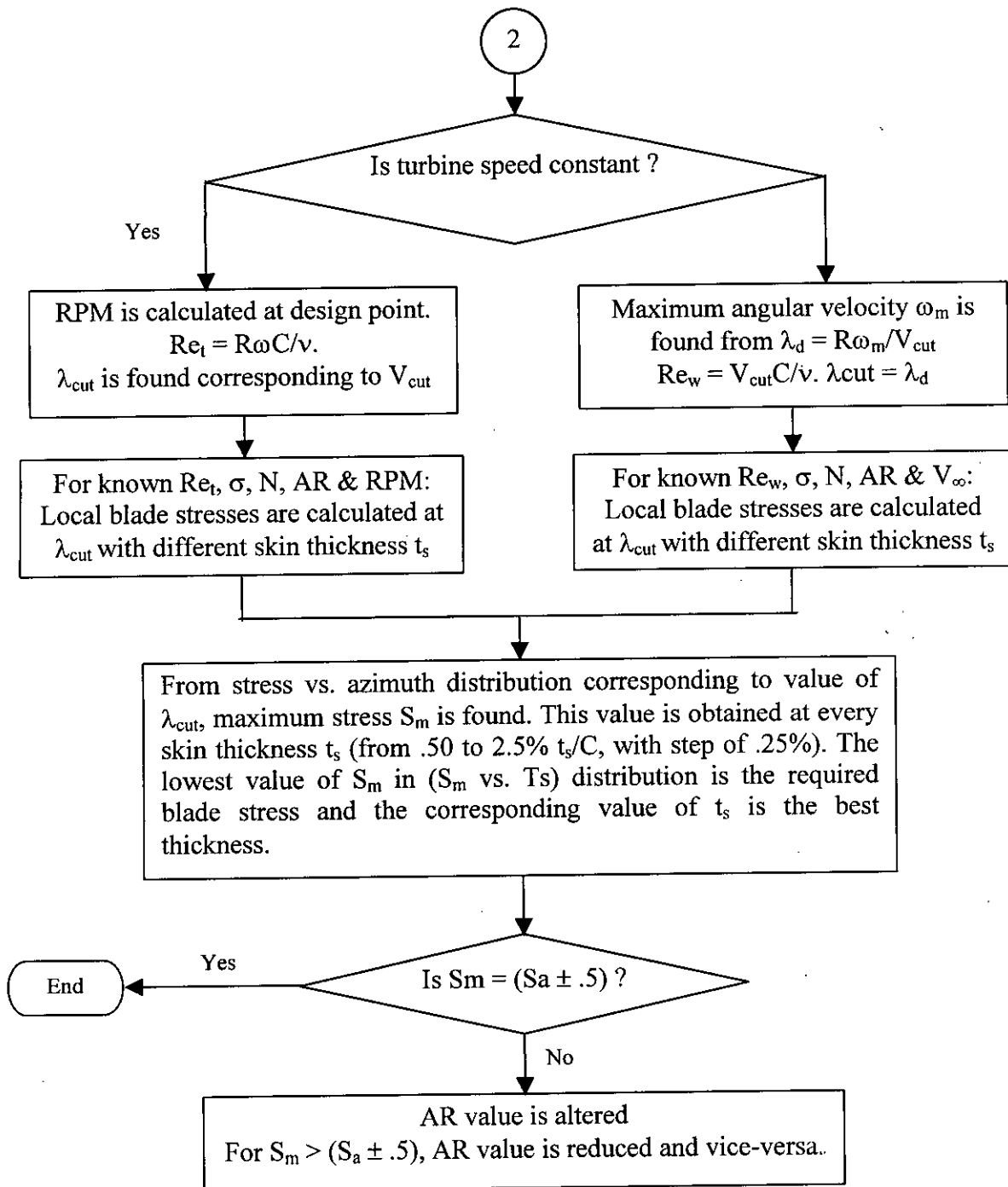






Appendix-B : Flow Diagram of Design Procedure





Appendix-C : Zero-Lift-Drag Coefficient

The aerodynamic efficiency of a vertical axis Darrieus wind turbine is strongly influenced by the value of the zero-lift-drag coefficient. To predict the performance properly it is necessary to consider a reasonable value of the zero-lift-drag coefficient. It is observed that the zero-lift-drag coefficient is a function of the chord-radius ratio in addition to other factors.

The expression of the zero-lift-drag coefficient corrected for the chord-radius ratio is expressed (Hirsch and Mandal, 1984) in the following form,

$$C_{doc} = C_{do} + b[C/R - (C/R)_o] \quad (C.1)$$

where C_{do} is the zero-lift-drag coefficient. The expression of C_{do} (Decleyre et al, 1981) is given in the form,

$$C_{do} = C_{dor} \left(\frac{Re}{Re_r} \right)^n \quad (C.2)$$

where C/R is any chord-radius ratio. $(C/R)_o$ indicates the chord-radius ratio unto which value, the correction of the zero-lift-drag coefficient due to the chord-radius ratio is not necessary. b is a constant. For a straight-bladed Darrieus wind turbine $(C/R)_o=0.180$ and $b=0.047$ at Re_r 500000. Re is the local Reynolds number. C_{dor} and Re_r are respectively the reference zero-lift-drag coefficient and the reference Reynolds number. The value of exponent is given in Table C.1.

Airfoils	Exponent, n		
	$Re < 200000$	$200000 < Re < 600000$	$Re > 600000$
NACA 0012	-.450	-.250	-.100
NACA 0015	-.500	-.300	-.060

Table C.1 : Exponent n for zero-lift-drag coefficient

In Figure C.1, the zero-lift-drag coefficient is shown as a function of Reynolds number. If the reference zero-lift-drag coefficient at any reference Reynolds number can be calculated from the equation (C.2). The calculated values of zero-lift-drag coefficient are based on $C_{dor}=.0074$ at $Re_r = 500000$ for the airfoil NACA 0012 and $C_{dor}=.0078$ at $Re_r = 500000$ for the airfoil NACA 0015, if the experimental value of the zero-lift-drag coefficient for a wind turbine is not specified. The value of C_{dor} taken, is for a perfectly manufactured blade with smooth surface. For the defective blade manufacture and rough blade surface, this value must be changed.

When the reference Reynolds number is given in the middle range (i.e. Re from 200000 to 600000),

$$C_{do_1} = C_{dor} \left(\frac{Re_1}{Re_r} \right)^{n_2} \quad (C.3)$$

$$C_{do_2} = C_{dor} \left(\frac{Re_2}{Re_r} \right)^{n_2} \quad (C.4)$$

where C_{do_1} and C_{do_2} are the zero-lift-drag coefficients corresponding to Re_1 and Re_2 respectively (Figure C.1). n_2 is the exponent. $n_2 = -.250$ for the airfoil NACA 0012 and $n_2 = -.300$ for the airfoil NACA 0015. If given $Re < 200000$,

$$C_{do_1} = C_{dor} \left(\frac{Re_1}{Re_r} \right)^{n_1} \quad (C.5)$$

$$C_{do_2} = C_{do_1} \left(\frac{Re_2}{Re_1} \right)^{n_2} \quad (C.6)$$

where n_1 is the exponent at $Re < 200000$. $n_1 = -.450$ for the airfoil NACA 0012 and $n_1 = -.500$ for the airfoil NACA 0015. If given $Re > 600000$,

$$C_{do_2} = C_{dor} \left(\frac{Re_2}{Re_r} \right)^{n_3} \quad (C.7)$$

$$C_{do_1} = C_{do_2} \left(\frac{Re_1}{Re_2} \right)^{n_2} \quad (C.8)$$

where n_3 is the exponent at $Re < 600000$. $n_3 = -.100$ for the airfoil NACA 0012 and $n_3 = -.060$ for the airfoil NACA 0015. The zero-lift-drag coefficient C_{do} is obtained at any $Re < 200000$, from the following equation,

$$C_{do} = C_{do_1} \left(\frac{Re}{Re_1} \right)^{n_1} \quad (C.9)$$

C_{do} at any Re in the middle range of Reynolds number ($200000 < Re < 600000$) can be obtained from,

$$C_{do} = C_{do_1} \left(\frac{Re}{Re_1} \right)^{n_2} \quad (C.10)$$

At any $Re > 600000$, C_{do} is determined from,

$$C_{do} = C_{do_2} \left(\frac{Re}{Re_2} \right)^{n_3} \quad (C.11)$$

After calculating the value of C_{do} , the corrected value of zero-lift-coefficient C_{doc} due to the chord-radius ratio is determined from the equation (C.1). The total airfoil drag coefficient is obtained from the following form of equation,

$$C_d = C_{doc} + k_c C_l^2 \quad (C.12)$$

where K_c is the constant and C_l is the airfoil lift coefficient. The equation (C.12) is valid upto the stalling angle.

Appendix-D : Finite Aspect Ratio

Two dimensional lift and drag characteristics are normally presented based on the infinite aspect ratio. So, these characteristics cannot be directly used to find the performance of a straight-bladed Darrieus wind turbine whose blades are finite. Hence, corrections for the finite aspect ratio are necessary before going to use those airfoil characteristics for the performance prediction. Since, the finite wing and finite blade of a straight bladed wind turbine are of similar pattern, so, wing theory may be applied for the finite aspect ratio corrections of airfoil characteristics before using them for the performance prediction of straight-bladed Darrieus wind turbine.

For the wing of finite span, there occurs always downwash and power required to induce downwash is expressed in terms of the induced drag. The downwash velocity is created by the presence of tip vortices. The total drag coefficient of a finite wing is given by,

$$C_d = C_{do} + C_{di} \quad (D.1)$$

Where C_{do} is the section drag coefficient for the infinite aspect ratio while C_{di} is the induced drag coefficient. C_{di} is expressed as,

$$C_{di} = \frac{C_l^2}{2\pi AR} \quad (D.2)$$

where AR indicated the aspect ratio of the turbine blade. Introducing the value of C_{di} in the equation (D.1),

$$C_d = C_{do} + \frac{C_l^2}{2\pi AR} \quad (D.3)$$

The angle of attack corrected for the finite aspect ratio effect is obtained as,

$$\alpha = \alpha_o + \alpha_i \quad (D.4)$$

where α_o indicates the angle of attack for the infinite wing and α_i is the induced angle. The expression of the induced angle α_i is,

$$\alpha_i = \frac{C_l}{2\pi AR} \quad (D.5)$$

substituting the equation (D.5) in the equation (D.4), one finds,

$$\alpha = \alpha_o + \frac{C_l}{2\pi AR} \quad (D.6)$$

The above two equations (D.3) and (D.6) are developed on the assumption of uniform distribution of downwash and they are explicitly valid only for the wings possessing an elliptic lift distribution. However, other cases are dealt with considering appropriate correction factors. Letting τ is the correction factor for the induced angle and δ is the correction factor for the induced drag, the expressions of C_d and α become,

$$C_d = C_{do} + \frac{C_l^2}{2\pi AR} (1 + \delta) \quad (D.7)$$

$$\alpha = \alpha_o + \frac{C_l}{2\pi AR} (1 + \tau) \quad (D.8)$$

For a rectangular wing there are two limiting cases. When the chord is large compared with the span, aspect ratio AR approaches zero. In this case Betz finds an elliptical distribution of loading. As the aspect ratio increases to infinity the loading approaches rectangular distribution. The values of τ and δ are obtained from the references (Milne Thompson, 1973) and (Riegels, 1961).

Appendix-E : Airfoil Characteristic

The values of lift and drag characteristics that are used in the present analysis are given in this appendix in the graphical forms. Characteristics of two types of airfoils NACA 0012 and NACA 0015 are taken into consideration which are shown from figures E.1 to E.8.

Appendix-F : Derivation Of Moment Of Inertia Of Blade Airfoil Section

In this appendix, the analysis to find the blade airfoil cross-sectional area, the centered and moment of inertia of the blade airfoil sectional performed. Figure F.1 represents the blade airfoil cross-section that is used in the present design analysis.

The thickness distribution for NACA four-digit sections is given by the following equation [F.1].

$$\pm y = \frac{t_c}{.2} (.2969x^{\frac{1}{2}} - .1260x - .3516x^2 + .2843x^3 - .1015x^4) \quad (F.1)$$

where x , y are in percent of chord. t_c is in fraction of chord. So for blade airfoil NACA 0012, $t_c = .12$ and for blade airfoil NACA 0015, $t_c = .15$.

Equation of Inner Face of Blade Airfoil skin

To distribution the co-ordinates between the outer and the inner faces, subscripts o and i are respectively used. Differentiating equation (F.1) and subscripting x and y by o to indicate the outer face of blade skin, one obtains,

$$\frac{dy_o}{dx_o} = \frac{t_c}{.2} \left(\frac{.14845}{x_o^{\frac{1}{2}}} - .1260 - .7032x_o + .8529x_o^2 - .4060x_o^3 \right) \quad (F.2)$$

Referring to the Figure F.2, the co-ordinates (x_i, y_i) on the inner face of the blade skin are,

$$\begin{aligned} x_i &= x_o + t_s \sin \theta_o \\ y_i &= y_o - t_s \cos \theta_o \end{aligned} \quad (F.3)$$

where t_s is the skin thickness of the blade airfoil. may be expressed as,

$$\theta_o = \tan^{-1} \left(\frac{dy_o}{dx_o} \right) \quad (F.4)$$

x_i , y_i are in per cent of chord. Now the new co-ordinates (X_i, Y_i) are chosen in such a way that $X_i = x_i C$ and $Y_i = y_i C$. In this analysis, the equation of the inner face of the blade skin is obtained in polynomial form the sets of co-ordinates (X_i, Y_i) by the method of curve fit which is given by,

$$Y_i = b_0 + b_1 x_i + b_2 x_i^2 + b_3 x_i^3 + b_4 x_i^4 \quad (F.5)$$

where b_0 , b_1 , b_2 , b_3 and b_4 are the constants.

Area of blade skin

The elemental blade skin area,

$$dA_s = 2(Y_o - Y_i)dX \quad (F.6)$$

Which may be written as,

$$A_s = 2 \int Y_o dX - 2 \int Y_i dX = 2(A_o - A_i) \quad (F.7)$$

$$\text{where, } A_o = \int Y_o dX = c^2 \int y_o dx \quad (F.8)$$

Now subscripting x, y of the equation (F.1) by o to indicate the outer face blade skin and substituting in the equation (F.8) one may find,

$$A_o = 5C^2 t_c \int_0^1 (.2969x_0^{\frac{1}{2}} - .1260x_0 - .3516x_0^2 + .2843x_0^3 - .1015x_0^4) dx_0 \quad (F.9)$$

which may be reduced to,

$$A_o = .34255t_c C^2 \quad (F.10)$$

A_i may be expressed as,

$$A_i = \int Y_i dx \quad (F.11)$$

Now introducing the value of Y_i from the equation (F.5) and integrating between the Limits X_1 and X_2 (Figure F.3) , one obtains,

$$A_i = b_o(x_2 - x_1) + \frac{b_1}{2}(x_2^2 - x_1^2) + \frac{b_2}{3}(x_2^3 - x_1^3) + \frac{b_3}{4}(x_2^4 - x_1^4) + \frac{b_4}{5}(x_2^5 - x_1^5) \quad (F.12)$$

Introducing the values of A_o (F.10) in the equation (F.7), the blade skin area can be determined.

Area of blade Rib

The ribs are assumed to be equally interspaced and the spacing b is considered to be $c/6$. Y_1, Y_2, Y_3, Y_4 are obtained from F.5.

Area of rib

$$A_r = 2t_r(Y_1 + Y_2 + Y_3 + Y_4) \quad (F.13)$$

The total blade sectioned area A_b is ,

$$A_b = (A_s + A_r) \quad (F.14)$$

Mass of the blade per unit length,

$$m_b = \rho_b A_b \quad (F.15)$$

where ρ_b is the density of the blade material.

Centroid of Blade Cross-Section

For the elastic body the neutral axis passes through the centroid of the blade cross-section.

The centroid are defined by,

$$\bar{X} = \frac{\int X dA_b}{A_b} \quad \text{and} \quad \bar{Y} = \frac{\int Y dA_b}{A_b} \quad (F.16)$$

Numerically one may obtain,

$$\int X dA_b = 2\delta_s \sum X(Y_o - Y_i) + 2t_s (X_1 Y_1 + X_2 Y_2 + X_3 Y_3 + X_4 Y_4) \quad (F.17)$$

where δ_s is the thickness of each strip considered in the numerical computation. For symmetric blade \bar{Y} is zero and \bar{X} is on the chord.

Area moment of Inertia

Area moment of inertia about X-axis is defined as,

$$I_x = \int Y^2 dA_b \quad (F.18)$$

while area moment of inertia about Y-axis is defined as,

$$I_y = \int X^2 dA_b \quad (F.19)$$

Moment of inertia of blade section area is found by numerical integration method . Moment of inertia about X-axis may be obtained from,

$$I_x = (I_{sx} + I_{rx}) \quad (F.20)$$

where I_{sx} and I_{rx} are respectively the moments of inertia of blade skin and ribs about the X-axis . Referring to the Figure F.5 , I_{sx} and I_{rx} may be obtained as follows

$$I_{sx} = 2 \sum \left[\delta_s \frac{(Y_o - Y_i)^3}{12} + \delta_s (Y_o - Y_i) \frac{(Y_o - Y_i)^2}{4} \right] \quad (\text{F.21})$$

$$I_{rx} = 2 \frac{t_s}{3} (Y_1^3 + Y_2^3 + Y_3^3 + Y_4^3) \quad (\text{F.22})$$

Now putting the values of I_{sx} (F.21) and I_{rx} (F.22) in the equation (F.20), the moment of inertia about X-axis can be determined. The moment of inertia about Y-axis can be obtained as,

$$I_y = (I_{sy} + I_{ry}) \quad (\text{F.23})$$

Where I_{sy} and I_{ry} are the moments of inertia of the blade skin and ribs respectively about the Y-axis, which may be obtained from,

$$I_{sy} = 2 \sum \left[\frac{(Y_o - Y_i) \delta_s^3}{12} + \delta_s (Y_o - Y_i) X^2 \right] \quad (\text{F.24})$$

$$I_{ry} = \frac{2(Y_1 + Y_2 + Y_3 + Y_4)t_s^3}{12} + 2t_s(Y_1X_1^2 + Y_2X_2^2 + Y_3X_3^2 + Y_4X_4^2) \quad (\text{F.25})$$

Now the centroidal moments of inertia about X-axis and Y-axis are respectively obtained from

$$\begin{aligned} \bar{I}_x &= I_x \\ \bar{I}_y &= I_y - A_b \bar{X}^2 \end{aligned} \quad (\text{F.26})$$

Appendix-G : Derivation of Bending Moment and Bending Stress

Derivation techniques of bending moment and bending stress are given in this appendix. These are done for no blade pitching condition.

Figure G.1 shows the forces developed on the turbine blade. F_n and F_t are respectively the normal and the tangential forces (aerodynamic). F_n and F_t can be obtained from the equation (3.16) and (3.17) respectively, after replacing δs by H . F_{cf} is the centrifugal force. The centrifugal force may be expressed as,

$$F_{cf} = m_b \omega^2 R \quad (G.1)$$

where m_b is the blade mass per unit blade length. ω is the angular velocity and R is the radius of the turbine. The directions of the forces as shown in the Figure G.1, are considered to be positive in this analysis. The net normal force on the turbine blade (in the radially outward direction) can be obtained as,

$$F_{net} = F_{cf} - F_n \quad (G.2)$$

In the present analysis, the blades are considered to be supported like that of a overhang supported beam.

In the Figure G.2, the bending moment diagram of a overhang-supported beam is shown. The forces on the turbine blade are distributed all over the blade length which is also seen from the Figure G.2. The expression of the maximum bending moment can be obtained as,

$$M_{bm} = \frac{wH^2}{46.5} \quad (G.3)$$

where w is the load per unit length of the blade. Introducing the value of $w = F_{net} / H$ in the equation (G.3), one obtains,

$$M_{bm} = \frac{F_{net} H}{46.5} \quad (G.4)$$

where H is the height of the turbine and hence the length of the turbine blade. The maximum bending stress can be found as,

$$S_{bm} = \frac{M_{bm} (t_c C / 2)}{I_x} \quad (G.5)$$

where t_c is the maximum blade thickness as a fraction of chord and C is the chord of the blade airfoil. I_x is the area moment of inertia about the chord of the blade airfoil. From the equation (G.4) and (G.5), the expression of the maximum bending stress can be written as,

$$S_{bm} = \frac{F_{net} H C l_c}{93 I_x} \quad (G.6)$$

The effect of tangential force on the blade stress is not encountered in this analysis, because this force is negligible in comparison to the net normal force.

